

BISTABILITY AND NOISE INDUCED TRANSITION IN A HORIZONTAL RIJKE TUBE

A THESIS

submitted by

GOPALAKRISHNAN E. A.

for the award of the degree

of

DOCTOR OF PHILOSOPHY



DEPARTMENT OF AEROSPACE ENGINEERING

INDIAN INSTITUTE OF TECHNOLOGY, MADRAS

JULY 2016

THESIS CERTIFICATE

This is to certify that the thesis titled **BISTABILITY AND NOISE INDUCED TRANSITION IN A HORIZONTAL RIJKE TUBE**, submitted by **GOPALAKRISHNAN E. A.**, to the Indian Institute of Technology, Madras, for the award of the degree of **Doctor of Philosophy**, is a bona fide record of research work done by him under my supervision. The contents of this thesis, in full or in parts, have not been submitted to any other institute or University for the award of any degree or diploma.

Prof. R. I. Sujith
Research Guide
Professor
Department of Aerospace Engineering
IIT Madras

Place: Chennai
Date: 7th July 2016

Whenever we proceed from the known into the unknown we may hope to understand, but we may have to learn at the same time a new meaning of the word 'understanding'.

Werner Heisenberg, Physics and Philosophy: The Revolution in Modern Science

to Sri Mata Amritandamayi Devi (AMMA)

ACKNOWLEDGEMENTS

In Indian philosophy a *Guru* is described as the one who dispels the darkness of ignorance. I was fortunate to have one of such rare *Gurus* as my Ph. D. advisor. I strongly believe that it is nothing other than the grace of my spiritual master which helped me to choose Prof. Sujith as my guide. Although I am not one of the brilliant students that he had, he was benevolent enough to guide me at times of crises. He modified my idea of research and instilled new thoughts which will definitely help me to pursue a career in research. I have no words to thank him for all his help during my Ph. D.

I wish to thank all my doctoral committee members, Prof. Neelima Gupte, Prof. Nandan Kumar Sinha, Prof. Sayana Gupta and Prof. Sameen for their encouragement and help. I am extremely thankful to Prof. K. Bhaskar, Head of the Department, for all the support that I have received from him. I would like to thank Prof. S. R. Chakravarthy and Prof. T. M. Muruganandam for their immense help while I was preparing for my qualifier.

I wish to thank Prof. Arul Lakshminarayanan who taught me the basic concepts of nonlinear dynamics and statistical mechanics. I express my gratitude to Prof. Tangirala from whom I learned the basics of linear time series analysis. I also would like to thank Prof. Job Kurian, Prof. M. Ramakrishna and Prof. P. A. Ramakrishna for their support and help during my Ph. D. I wish to thank Prof. Sunetra Sarkar and Prof. S. T. G. Raghukanth for teaching me the basics of stochastic Runge-Kutta method. I thank Prof. G. Ambika who gave me an opportunity to learn nonlinear time series analysis and Prof. K. P. Harikrishnan for making me understand many of the techniques

used in nonlinear time series analysis. I would like to thank Prof. Partho Dutta for hosting me in IIT Ropar and for teaching me the basics of devising early warning measures for critical transitions. I also thank his Ph. D. student, Ms. Yogita Sharma who helped me to compute the early warning measures.

I have been constantly supported by Mrs. Mekhala, Mrs. Aruna, Mrs. Nirmala, Mr. Kennedy, Mr. Manikandan, Mr. Sankar Kumaraswamy, Mr. John George, Mr. Stephen, Mr. Biju Kumar and Mr. Dayalan during my Ph. D.

I would like to express my heartfelt gratitude to Prof. Wolfgang Polifke who invited me to TU Munich for an exciting summer school and also who supported me throughout my stay in TUM. I also thank Stefan, Malte, Sebastian, Ralf and Camilo who helped me during my stay in TUM. I would like to acknowledge the generous funding by the Institute for Advanced Studies, TUM during my first visit to Germany to attend the *n3l* conference and the financial support provided by SFB-TRR 40 during my second visit to Germany to attend the summer school. I wish to thank Prof. Maria Heckl who gave me valuable inputs during the early years of my Ph. D. I am very much indebted to her for lucidly explaining me her inspirational work on Rijke tube. I thank Prof. Nicolas Noiray for his help and support in understanding the basics of stochastic dynamics and for his specific inputs in understanding Fokker-Planck equation. I also would like to thank Prof. Elena Surovyatkina who helped me to understand the bistability and hysteresis found in dynamical systems.

I would like to acknowledge the funding provided by Ministry of Human Resource Development, Govt. of India during my Ph. D. and also the generous funding provided by IIT Madras for attending the *European Fluid Mechanics Conference* held at Denmark. I wish to thank Office of

Naval Research Global (ONRG) for funding my Ph. D. I would like to specially thank Dr. Ramesh Kolar (ONRG) who encouraged and inspired me during all the review meetings.

It will be unfair, if I do not thank Prof. Sarith. P. Sathian and Prof. Balaji Sreenivasan who motivated me to do a Ph. D. and who helped me stay focused on my path when I was tempted to quit. I will always be grateful to them for their selfless support. I also wish to thank my M-Tech thesis advisor Prof. Ajith Kumar for inspiring me to do a Ph. D.

I would like to thank Lipika who built the Rijke tube setup and the excellent structural design helped me observe many interesting dynamics. I have no words to thank Koushik who provided many valuable insights to me during my Ph. D. His simple yet elegant model of Rijke tube helped me replicate many of the interesting dynamics found in experiments. I wish to thank all my seniors, Sathesh, Priya, Lipika, Vivek, Gireesh Sir, Vinu for their constant help and support during the early days of my Ph. D. I am sure that without their support I would not have gathered the courage to pursue my Ph. D.

I thank all my colleagues, Unni, Meena, Rana Sir, Abin, Samadhan, Manikandan (GTRE), Mukund, Sirshendu, Mridula, Nitin, Akhil, Vishnu (Agni), Tony, Akshay, Sreelekha, Aanveeksha, Pavitra, Rama, Manikantan, Syam, Hashir, Dileep, Dileesh and Thilagaraj for their immense encouragement and support during my Ph. D. I am always indebted to them for the unconditional help that I have received. I thank Dileesh for helping me during my experiments and for providing me a wonderful schematic of my experimental set-up. I thank Meena for her support during my JFM submission. She helped me improve my article significantly. I cannot forget the help that I have received from Unni, Nitin, Dileesh and Syam when I was ill during the final phase of my Ph. D. I specially thank Tony for all the help that he provided during the preparation of my thesis and

my journal articles. I thank Akshay for teaching me lot of intricate concepts in nonlinear dynamics with at most patience.

One of the most precious companionship that I developed during my Ph. D is with Vineeth Nair. I thank him wholeheartedly for all the moral support and technical help that he provided during my Ph. D. He always amazed me with his prophetic intelligence combined with unbelievable modesty. I learned a lot from Nair. I am sure that he will ever remain as my inspiration throughout my scientific journey.

I am sure that I would not have completed my Ph. D. without the support that I received from my family. I thank my mother Vasantha, my sisters Sreevidya and Sudha, my brother Rajesh and my brothers-in-law Kumar and Hareesh who supported me during the course of my Ph. D. I specifically thank my mother who sacrificed most of her comforts and allowed me to pursue my dream irrespective of her difficulties. I also would like to acknowledge the help that I received from my niece Aishwarya and Sruti and my nephew Sairam in the form of intriguing questions about science and research.

Above all, I offer my gratitude at the lotus feet of my spiritual master Sri Mata Amritanandamayi Devi whom I affectionately call as *Amma* who gave me the inner courage and strength and who uplifted me from all the difficulties during my Ph. D.

ABSTRACT

KEYWORDS: Bifurcations, Bistability; Subcritical Hopf bifurcation; Noise induced transitions; Fokker-Planck equation; Stochastic bifurcations; Critical slowing down; Early warning signals; Horizontal Rijke tube.

Thermoacoustic instability hampers the development of gas turbine engines, solid rocket motors, industrial burners and various other engineering systems where the prime source of energy is derived from combustion. The instability occurs when the pressure fluctuations inherently present in a confinement are in phase with the heat release rate fluctuations of a heat source present in the same confinement. The physical reasons of the origin of this instability need to be understood in order to implement effective control strategies. Systems which are susceptible to thermoacoustic instability are often too intricate to conduct a detailed investigation. This creates the need for a prototypical system which is simple enough to investigate, yet retains the essential dynamical features of the original system. A horizontal Rijke tube with a mesh type electrical heater is often chosen as a model system in literature.

The present study aims to investigate the bifurcation characteristics of a horizontal Rijke tube with special focus on the region of bistability. The influence of system parameters such as heater power and heater location on the bistable characteristics of this prototypical thermoacoustic system is investigated. A study on the region of bistability is essential as bistability demarcates a subcritical Hopf bifurcation from a supercritical Hopf bifurcation.

As any thermoacoustic system undergoing a subcritical Hopf bifurcation can be triggered to the state of oscillations even when the system is stable by fluctuations of the order of background

noise, the effect of noise on the bistable nature also needs to be investigated. The change in the width of the bistable zone with Strouhal number and noise intensity is studied in the current thesis. Both experimental and modelling approaches are employed to achieve the objectives. Experiments are performed in a horizontal Rijke tube and the acoustic pressure signals are recorded with the help of a piezoelectric transducer. A simple mathematical model which resembles a nonlinear bistable oscillator is used in the present study. The model, although simple, retains the essential features of a thermoacoustic system such as nonlinearity in heat release rate and time delay. The effect of noise is captured in the model by using additive Gaussian white noise.

Often, the transitions found in thermoacoustic systems are sudden and catastrophic which creates the need to develop effective early warning measures. The current thesis aims to develop precursors based on the theory of critical slowing down and to test the viability of these early warning measures in the presence of noise.

Bifurcation experiments performed in a horizontal Rijke tube reveal that the transition to thermoacoustic instability happens via a subcritical Hopf bifurcation for the conditions used in the present study. Moreover, a reduction in the non-dimensional width of the bistable zone is observed with increase in the value of Strouhal number. The study also reveals the existence of a power law relationship between the non-dimensional width of the bistable zone and the Strouhal number. From this study, it is clear that the non-dimensional width of the bistable zone remains almost independent of the bifurcation parameter used.

The width of the bistable zone decreases also with increase in noise intensity. This is observed in results from experiments and from the mathematical model. The rate of decrease of the non-dimensional bistable zone with noise intensity is found to be linear and independent of Strouhal

number. Bistable zone becomes completely indiscernible in the presence of high intensity noise. The need to track the evolution in the distribution of the acoustic pressure rather than the absolute value of the acoustic pressure in the presence of high intensity noise is brought out in this study. Stochastic bifurcation formalism is used to describe the transition in the presence of high intensity noise and to this end the associated Fokker-Planck equation is derived.

The present thesis establishes that early waning measures based on the theory of critical slowing are robust precursors to predict impending transitions in a prototypical thermoacoustic system. A significant increase in the value of these early warning measures are observed well before the transition to thermoacoustic instability. The effectiveness of the precursors based on critical slowing down in the presence of noise to predict a subcritical Hopf bifurcation is clearly brought out in this study.

In summary, the current investigation reveals the dependence of the bistable nature of a prototypical thermoacoustic system on system parameters and noise present in the system. The reduction and suppression of the bistable nature with system parameters and with noise are quantified. Finally, precursors based on critical slowing down are employed to predict the impending transitions in a horizontal Rijke tube.

TABLE OF CONTENTS

ACKNOWLEDGEMENTS	i
ABSTRACT	v
LIST OF FIGURES	xiii
ABBREVIATIONS	xix
NOTATION	xxi
1 INTRODUCTION	1
1.1 Causes and control of thermoacoustic instability	2
1.2 Laboratory scale combustors to study thermoacoustic instability	5
1.3 Prototypical thermoacoustic systems.....	6
1.4 Dynamical system approach.....	11
1.4.1 Supercritical and subcritical Hopf bifurcations.....	11
1.4.2 Bifurcations in thermoacoustic systems	13
1.5 Effect of noise in thermoacoustic systems.....	15
1.5.1 Noise induced triggering in thermoacoustic systems.....	16
1.6 Precursors for transitions in thermoacoustic systems.....	19
1.7 Summary of the state of the art.....	23
1.8 Objectives of the thesis	24
1.9 Overview of the thesis	25
2 TOOLS FROM DYNAMICAL SYSTEM THEORY	29
2.1 Bifurcations in a dynamical system	29
2.1.1 Saddle-node bifurcation	30
2.1.2 Hopf bifurcation	31

2.2 Phase space reconstruction	33
2.2.1 Optimum time delay	34
2.2.2 Minimal embedding dimension	35
2.3 Concluding remarks	39
3 EXPERIMENTAL SET-UP	41
3.1 Experimental set-up	41
4 THEORETICAL MODEL	45
4.1 Conservation equations of momentum and energy.....	46
4.2 Non-dimensional equations	48
4.3 Stochastic delay differential equations	52
5 INFLUENCE OF SYSTEM PARAMETERS ON THE BISTABLE CHARACTERISTICS OF A HORIZONTAL RIJKE TUBE	55
5.1 Effect of heater power on bistable characteristics	55
5.2 Effect of heater location on bistable characteristics	61
5.3 Variation of width of the bistable zone with Strouhal number	70
5.4 Concluding remarks.....	72
6 EFFECT OF NOISE ON THE BISTABLE CHARACTERISTICS OF A HORIZONTAL RIJKE TUBE	75
6.1 Reduction in the width of the bistable zone in the presence of external noise	73
6.2 Suppression of bistable zone in the presence of high amplitude noise.....	80
6.4 Concluding remarks.....	85
7 STOCHASTIC BIFURCATION OBSERVED IN A HORIZONTAL RIJKE TUBE	87
7.1 Background	87
7.2 Fokker-Planck equation for a prototypical thermoacoustic system	90
7.3 Concluding remarks	95

8 EARLY WARNING MEASURES FOR CRITICAL TRANSITIONS IN A HORIZONTAL RIJKE TUBE	97
8.1 Early warning indicators based on critical slowing down	97
8.2 Early warning measures for a subcritical Hopf bifurcation in a Rijke tube	99
8.3 Robustness of early warning indicators in the presence of noise	102
8.4 Concluding remarks	108
9 CONCLUSIONS	111
A Stochastic Runge-Kutta method applied to a general stochastic differential equation	115
B Methods to calculate lag-1 autocorrelation and variance	119

LIST OF FIGURES

1.1 Bifurcation characteristics of a measure M when a control parameter μ is varied. (a) Supercritical bifurcation. (b) Subcritical bifurcation. In supercritical bifurcation, as the control parameter reaches the value of zero, low amplitude stable limit cycle oscillations are born. Unlike the supercritical bifurcation, large amplitude oscillatory solutions are present right at the onset of instability in the case of a subcritical bifurcation. The system is bistable in the hysteresis region $BCEF$ and the stability of the system is dependent on the initial conditions in this region. ● – Stable oscillatory solutions. ○ – Unstable oscillatory solutions. The figures are obtained from the normal form equations of Hopf bifurcation.....	12
2.1 The variation of $I(\hat{\tau})$ with $\hat{\tau}$ for acoustic pressure time series corresponding to limit cycle oscillations observed in horizontal Rijke tube. The time delay corresponding to the first minima of AMI is considered as the optimal time delay.....	35
2.2 The variation of $E_1(d)$ and $E_2(d)$ with d for acoustic pressure time series corresponding to limit cycle oscillations observed in horizontal Rijke tube. It can be seen that $E_1(d)$ saturates around $d = 11$. Hence, the minimal embedding dimension is taken as 12.....	38
2.3 The reconstructed phase portrait of acoustic pressure time series corresponding to limit cycle oscillations observed in horizontal Rijke tube. It can be seen that the topological structure in the phase space is an isolated closed trajectory which represents a limit cycle.....	38
3.1 Schematic of the experimental setup. A blower is used to provide the mean flow and a flow meter is used to measure the flow rate. A DC power supply unit is used to heat the wire mesh. The acoustic pressure is measured using piezoelectric transducers and the temperature is measured with the help of K- type thermocouple. A traverse mechanism is used to change the location of the electrical heater.	42
4.1 Schematic of the Rijke tube setup considered for numerical modelling. The thickness of the heater wire is negligible compared to the acoustic length scale L	46
5.1 Experimental bifurcation diagram displaying the values of acoustic pressure P measured at $x = 30$ cm for a quasi-steady variation in the power supplied to heater K . The system undergoes a subcritical Hopf bifurcation at $K = 337$ W and a fold bifurcation at $K = 307$ W. $BCDF$ represents the hysteresis region where the system is in a bistable state. The heater is located at $x_f = L/4$. Mass flow rate $\dot{m} = 2.34$ g/s. ▲ - Increasing K , ▽-Decreasing K	57
5.2 (a) The amplitude spectrum of the pressure time series showing distinct peaks indicating limit cycle oscillations. The bin size used is 0.3 Hz (b) Phase portrait reconstructed from pressure time series depicting an isolated closed orbit in the phase space. Heater power $K = 339$ W. Heater is located at $x_f = L/4$. Mass flow rate $\dot{m} = 2.34$ g/s	59

5.3 (a) Experimental bifurcation plot for mass flow rate $\dot{m} = 1.25$ g/s. The heater power is varied with a step size of 2 W. The hysteresis zone is not observable in this case, however there is a sudden jump in the value of acoustic pressure during the transition (b) Experimental bifurcation plot for mass flow rate $\dot{m} = 1.25$ g/s. The heater power is varied with step size of 0.5 W. The hysteresis zone is observable with this fine variation in the control parameter. (c) Experimental bifurcation plot for mass flow rate $\dot{m} = 2.34$ g/s. The heater power is varied with a step size of 2 W. The hysteresis is clearly observable. The heater is located at $x_f = L/4$. ▲-Increasing K , ∇ -Decreasing K	60
5.4 Experimental bifurcation diagram displaying the values of acoustic pressure at $x = 30$ cm for a quasi-steady variation in the heater location x_f . Subcritical Hopf bifurcation happens at $x_f = 19$ cm during the forward path and at $x_f = 29$ cm during the reverse path. Hysteresis zone near the second Hopf point is observable with coarse variation in heater location and the hysteresis zone near the first Hopf point is shown only with fine variation in heater location (see inset). The heater power $K = 423$ W. Mass flow rate $\dot{m} = 2.34$ g/s. ▲- Increasing x_f , ∇ - Decreasing x_f	62
5.5 (a) The amplitude spectrum of the pressure time series showing distinct peaks indicating limit cycle oscillations. The bin size used is 0.3 Hz (b) Phase portrait reconstructed from pressure time series depicting an isolated closed orbit in the phase space. Heater is located at $x_f = 19$ cm. Heater power $K = 423$ W. Mass flow rate $\dot{m} = 2.34$ g/s	63
5.6 (a) The amplitude spectrum of the pressure time series showing distinct peaks indicating limit cycle oscillations. The bin size used is 0.3 Hz (b) Phase portrait reconstructed from pressure time series depicting an isolated closed orbit in the phase space. Heater is located at $x_f = 29$ cm. Heater power $K = 423$ W. Mass flow rate $\dot{m} = 2.34$ g/s	64
5.7 Experimental bifurcation diagrams displaying the variation of acoustic pressure P at $x = 30$ cm with a quasi-steady variation of heater location x_f (a) for mass flow rate $\dot{m} = 1.25$ g/s and (b) for mass flow rate $\dot{m} = 2.34$ g/s. The hysteresis zone is not observable for $\dot{m} = 1.25$ g/s whereas the hysteresis zone is observable for $\dot{m} = 2.34$ g/s. The heater power $K = 423$ W. ▲-Increasing x_f , ∇ -Decreasing x_f	65
5.8 Experimental bifurcation diagram displaying the values of acoustic pressure at $x = 30$ cm versus the location of the heater (a) near the first Hopf point and (b) near the second Hopf point. Heater location is varied in fine steps of 1 mm. With this fine variation in heater location, the hysteresis zones at first and second Hopf points become observable. The heater power $K = 423$ W. Mass flow rate $\dot{m} = 1.25$ g/s. ▲- Increasing x_f ; ∇ - Decreasing x_f	66
5.9 Experimental bifurcation diagram displaying the variation of acoustic pressure P at $x = 30$ cm for a quasi-steady variation in the heater location x_f for a mass flow rate of $\dot{m} = 2.97$ g/s. Two distinct regions of instability can be seen. The bifurcations that happen in both region-1 and region-2 are subcritical Hopf bifurcations confirmed by the presence of hysteresis zones. The heater power $K = 482$ W. ▲-Increasing x_f ; ∇ - Decreasing x_f	67
5.10 (a) The amplitude spectrum of the pressure time series showing distinct peak indicating limit cycle oscillations. The bin size used is 0.3 Hz (b) Phase portrait reconstructed from pressure	

time series depicting an isolated closed orbit in the phase space. Heater is located at $x_f = 8$ cm. Heater power $K = 482$ W. Mass flow rate $\dot{m} = 2.97$ g/s	68
5.11 Variation of peak pressure P at $x = 30$ cm for a quasi-steady variation of the heater location x_f (a) during the forward path (b) during the return path showing the presence of period-2 oscillations for a mass flow rate $\dot{m} = 2.97$ g/s. $K = 482$ W. \blacktriangle -Increasing x_f . ∇ - Decreasing x_f	69
5.12 (a) The amplitude spectrum of the pressure time series showing distinct peaks at f and $f/2$, where f is 352.8 Hz, indicating period-2 oscillations. The bin size used is 0.3 Hz (b) Phase portrait reconstructed from pressure time series depicting a double loop in the phase space. Heater is located at $x_f = 10$ cm. Heater power $K = 482$ W. Mass flow rate $\dot{m} = 2.97$ g/s	70
5.13 Variation of non-dimensional hysteresis width χ with Strouhal number St shown in (a) Linear scale and in (b) Log-Log scale. It can be seen that the non-dimensional hysteresis widths are same for heater power and heater location for a range of Strouhal numbers and there exists a power law relation. ■-Heater power, ○-Heater location	72
6.1 (a) Bifurcation diagram, obtained from experiments, depicting the variation of the median value of the peak acoustic pressure P with heater power K for mass flow rate $\dot{m} = 2.34$ g/s. Here, the transition to instability occurs via a subcritical Hopf bifurcation at the heater power $K = 380$ W. (b) The amplitude spectrum of the pressure time series, showing distinct peaks indicating limit cycle oscillations. The bin size used is 0.3 Hz (c) Phase portrait reconstructed from pressure time series depicting an isolated closed orbit in the phase space. The experiment is conducted in the absence of external noise. \blacktriangle - Forward path; ∇ - Reverse path	76
6.2 (a) Bifurcation diagram, obtained from experiments, depicting the variation of the median value of the peak acoustic pressure P with heater power K , for a mass flow rate of $\dot{m} = 2.34$ g/s. Here, the transition to instability happens via a subcritical Hopf bifurcation at the heater power $K = 382$ W. (b) The amplitude spectrum of pressure time series, showing sharp peaks indicating limit cycle oscillations. (c) Phase portrait reconstructed from pressure time series, depicting an isolated closed orbit in the phase space. The experiment is performed in the presence of external noise of amplitude 10.5 Pa. \blacktriangle - Forward path; ∇ Reverse path	77
6.3 Variation of non-dimensional hysteresis width ($\chi - \chi_0$) calculated from experimental and numerical results with non-dimensional noise intensity β for different mass flow rates \dot{m} and for different time lags τ . The width of the hysteresis zone decreases with increase in noise intensity in both experiments and in numerical simulations. The rate of decrease is constant for all mass flow rates and for all time lags. Nevertheless, for the noise levels mentioned here, the transition remains subcritical both in experiments and in numerical simulation. ●- $\dot{m} = 2.19$ g/s, ■- $\dot{m} = 2.34$ g/s, \blacktriangle - $\dot{m} = 2.50$ g/s, ♦- $\dot{m} = 2.97$ g/s. ○- $\tau = 0.2$, □ - $\tau = 0.175$, Δ - $\tau = 0.15$, ◇- $\tau = 0.125$	79

6.4 Bifurcation diagrams, obtained from experiments (<i>a-d</i>) and from numerical model (<i>e-h</i>) depicting the variation of median value of peak non-dimensional acoustic pressure p with normalized non-dimensional heater power \tilde{k} (normalized by the value of heater power at the Hopf point in the absence of noise) for different values noise intensities. Here, β refers to the non-dimensional noise intensity. We can observe a change in the nature of transition and suppression of bistable region as the intensity of the external noise increases in experimental results. Although the pressure amplitudes differ in magnitude, a qualitatively similar behavior is observed in the case of numerical model. Note that the ordinates are different.	
▲ - Increasing \tilde{k} ; ∇ Decreasing \tilde{k}	81
6.5 Histogram of pressure time series at the onset of instability for experimental (<i>a-d</i>) and numerical (<i>e-h</i>) results for various values of noise amplitude. Here, β refers to the non-dimensional noise intensity. N represents the number of data points in the pressure time series with a non-dimensional pressure p . ψ^2 represents the variance of the pressure time series. We can see an increase in the spread of the distribution with increase in external noise amplitude, both in case of experimental and numerical results. The increase in the spread is confirmed by the increasing value of variance with increase in noise amplitude. The experimental and numerical results differ in magnitude; however, we intend a qualitative comparison rather than a quantitative one. Note that the abscissas are different by an order of magnitude	84
7.1 The regimes of unimodal and bimodal probability distribution in the (μ, I) plane, where μ is the control parameter and I is the intensity of the noise. Regions I and III correspond to the parameter regimes where the amplitude distribution is unimodal whereas region II corresponds to the parameter regime of bimodal amplitude distribution. The boundaries of the regions represent the locus of points where phenomenological bifurcation occurs. It can also be observed that above a noise intensity P-bifurcations are not observed	94
8.1 Early warning signals for a subcritical bifurcation in a prototypical thermo-acoustic system using pressure time series generated from the experiments (a) Time series of acoustic pressure depicting transition from one stable to an alternate stable state. The control parameter is increased every 20 seconds. The system undergoes a critical transition from a non-oscillatory state to an oscillatory state via a subcritical Hopf bifurcation (b) Plot depicting the change in lag-1 autocorrelation as the system approaches the critical transition. (c) Plot depicting the change in variance as the system approaches the critical transition. The lag-1 autocorrelation and variance are calculated using a moving window of half the size of the time series. The black horizontal arrow represents the length of the moving window. We observe a clear increase in variance, well before the transition, whereas the autocorrelation shows a decrease. The thick black line indicates the time stamp up to which the data is used to generate the early warning indicators. Although, no external noise added to the system, the inherent fluctuations in the system correspond to a non-dimensional noise intensity $\beta = 0.02$	100
8.2 Early warning signals for a subcritical bifurcation in a prototypical thermo-acoustic system using pressure time series generated from the numerical model (a) Time series of acoustic pressure depicting the transition from one stable to an alternate stable state. The control	

parameter is increased at every time step. The system undergoes a critical transition from a non-oscillatory state to an oscillatory state via a subcritical Hopf bifurcation (b) Plot depicting the change in variance as the system approaches the critical transition. (c) Plot depicting the change in lag-1 autocorrelation as the system approaches the critical transition. A clear increase in variance well before the transition can be observed. The non-dimensional noise intensity is maintained as $\beta = 0.02$ to match with the experimental conditions 101

- 8.3 Early warning signals for a subcritical bifurcation in a prototypical thermo-acoustic system in the presence of external fluctuations using pressure time series generated from the experiments (a) Time series of acoustic pressure depicting transition from one stable to an alternate stable state. The control parameter is increased every 20 seconds. The system undergoes a critical transition from a non-oscillatory state to an oscillatory state via a subcritical Hopf bifurcation (b) Plot depicting the change in variance as the system approaches the critical transition. (c) Plot depicting the change in lag-1 autocorrelation as the system approaches the critical transition. A clear increase in variance can be observed well before the transition. The thick black line indicates the time stamp up to which the data is used to generate the early warning signals. External noise is added to the system such that the non-dimensional noise intensity is $\beta = 0.05$ 103
- 8.4 Early warning signals for a subcritical bifurcation in a prototypical thermo-acoustic system in the presence of external fluctuations using pressure time series generated from the experiments (a) Time series of acoustic pressure depicting transition from one stable to an alternate stable state. The control parameter is increased every 20 seconds. The system undergoes a critical transition from a non-oscillatory state to an oscillatory state via a subcritical Hopf bifurcation (b) Plot depicting the change in variance as the system approaches the critical transition. (c) Plot depicting the change in lag-1 autocorrelation as the system approaches the critical transition. A clear increase in variance as well as autocorrelation can be observed well before the transition. External noise is added to the system such that the non-dimensional noise intensity is $\beta = 0.1$ 104
- 8.5 Early warning signals for a subcritical bifurcation in a prototypical thermo-acoustic system in the presence of external fluctuations using pressure time series generated from the experiments (a) Time series of acoustic pressure depicting transition from one stable to an alternate stable state. The control parameter is increased every 20 seconds. The system undergoes a critical transition from a non-oscillatory state to an oscillatory state via a subcritical Hopf bifurcation (b) Plot depicting the change in variance as the system approaches the critical transition. (c) Plot depicting the change in lag-1 autocorrelation as the system approaches the critical transition. A clear increase in variance as well as autocorrelation can be observed well before the transition. External noise is added to the system such that the non-dimensional noise intensity is $\beta = 0.2$ 105
- 8.6 Early warning signals for a subcritical bifurcation in a prototypical thermo-acoustic system using pressure time series generated from the numerical model (a) Time series of acoustic pressure depicting the transition from one stable to an alternate stable state. The control parameter is increased at every time step. The system undergoes a critical transition from a non-oscillatory state to an oscillatory state via a subcritical Hopf bifurcation (b) Plot depicting the change in variance as the system approaches the critical transition. (c) Plot

depicting the change in lag-1 autocorrelation as the system approaches the critical transition. A clear increase in variance well before the transition can be observed. The non-dimensional noise intensity is maintained as $\beta = 0.05$ to match with the experimental conditions.....106

- 8.7 Early warning signals for a subcritical bifurcation in a prototypical thermo-acoustic system using pressure time series generated from the numerical model (a) Time series of acoustic pressure depicting the transition from one stable to an alternate stable state. The control parameter is increased at every time step. The system undergoes a critical transition from a non-oscillatory state to an oscillatory state via a subcritical Hopf bifurcation (b) Plot depicting the change in variance as the system approaches the critical transition. (c) Plot depicting the change in lag-1 autocorrelation as the system approaches the critical transition. A clear increase in variance well before the transition can be observed. The non-dimensional noise intensity is maintained as $\beta = 0.1$ to match with the experimental conditions.....107
- 8.8 Early warning signals for a subcritical bifurcation in a prototypical thermo-acoustic system in the presence of high intensity additive noise using pressure time series generated from the numerical model (a) Time series of acoustic pressure depicting the transition from one stable to an alternate stable state. The control parameter is increased in every time step. The system undergoes a critical transition from a non-oscillatory state to an oscillatory state via a subcritical Hopf bifurcation (b) Plot depicting the change in variance as the system approaches the critical transition. (c) Plot depicting the change in lag-1 autocorrelation as the system approaches the critical transition. A clear increase both in autocorrelation and in variance can be observed well before the transition. The thick black line indicates the time stamp up to which the data is used to generate the early warning measures. The non-dimensional noise intensity $\beta = 0.2$ to match with the experimental conditions.....108

ABBREVIATIONS

CFD	Computational Fluid Dynamics
DMD	Dynamic Mode Decomposition
PDE	Partial Differential Equation
ODE	Ordinary Differential Equation
SDE	Stochastic Differential Equation
P-bifurcation	Phenomenological bifurcation
F-P equation	Fokker-Planck equation

NOTATION

μ	Control parameter
M	Measure
α	Cold decay rate
K	Heater power
x_f	Heater location
P	Median of the peak acoustic pressure
χ	Width of the bistable zone
χ_0	Width of the bistable zone in the absence of external noise
μ_H	Value of the control parameter at the Hopf point
μ_f	Value of the control parameter at the fold point
β	Non-dimensional noise intensity
\dot{m}	Mass flow rate
u'	Non-dimensional acoustic velocity
p'	Non-dimensional acoustic pressure
M_a	Mach number
γ	Ratio of specific heats
\dot{Q}'	Non-dimensional heat release rate fluctuation
k	Non-dimensional heater power
L_w	Length of the heater wire
d_w	Diameter of the heater wire
T_w	Temperature of the heater wire
\bar{p}	Mean pressure
\bar{T}	Mean temperature
$\bar{\rho}$	Mean density
u_0	Mean velocity

S	Cross-sectional area of the duct
λ	Heat conductivity of the medium
C_V	Specific heat at constant volume of the medium
t	Time
τ	Time delay between acoustic velocity and heat release rate
$u'_f(t - \tau)$	The acoustic velocity at the heater location at a time $(t - \tau)$
η	Time varying co-efficient of acoustic velocity
$\dot{\eta}$	Time varying co-efficient of acoustic pressure
ω_j	Non-dimensional angular frequency of the j^{th} acoustic mode
N	Number of Galerkin modes
ζ	Damping co-efficient
c_1	Acoustic damping constant
c_2	Acoustic damping constant
σ	Strength of the additive noise
Δt	Time step used in the numerical simulation
$\xi(t)$	Gaussian white noise with zero mean and variance proportional to $(\Delta t)^{1/2}$
L	Length of the horizontal Rijke tube
S_t	Strouhal number
c_0	Speed of sound in air at mean temperature
A	Cross-sectional area of the horizontal Rijke tube
\tilde{k}	Non-dimensional heater power normalized by μ_H
Δp	Width of the bin used in histogram of p
$W(t)$	Wiener process
I	Intensity of additive noise used in the numerical model
$p(a, t)$	Transition probability density function
C	Normalization constant

CHAPTER 1

INTRODUCTION

Combustion of fossil fuels provide more than 80% of the global energy supply. Land based gas turbine engines, jet engines used for aviation, and rocket engines fall into the category of combustion dependent power generating systems. One of the major hassles in the development of energy efficient power generating systems is the phenomenon of combustion instability or thermoacoustic instability. In a combustion system, power is generated by the burning of fuel inside a chamber. The chamber or the duct often acts as an acoustic resonator and the inherent acoustic fluctuations of the duct are amplified in the presence of the heat source. The inherent fluctuations present in the acoustic field of the confinement perturb the heat release rate from the heat source and these perturbations in the heat release rate, in turn, affect the acoustic field. The amplification of the acoustic field happens when the heat release rate fluctuations are in phase with the inherent acoustic pressure perturbations (Rayleigh, 1878). Thus, the positive feedback between the acoustic field and the heat source results in thermoacoustic instability.

Acoustic oscillations grow in amplitude by extracting energy from the heat source; however the saturation of acoustic oscillations occur due to the inherent nonlinearities present in the system. If the frequency of these acoustic oscillations match with the natural frequency of the chamber, resonance results which leads to structural damage. Thermoacoustic oscillations can also cause the damage of guidance and control systems in rockets and missiles (McManus *et al.*, 1993; Lieuwen, 2012).

Moreover, these high amplitude oscillations are often observed when we operate at very lean fuel air ratios. Operating at rich fuel air ratios is also not desirable as it results in increased emissions. So combustion instability acts as an impediment to proceed towards emission-free combustion. These self-sustained high amplitude pressure oscillations also result in plane crashes due to engine failure and operational failure of space rockets (Fisher & Rahman, 2009). Thus combustion instability causes billions of dollars of revenue loss for the power generating industry (McManus *et al.*, 1993; Lieuwen, 2012). Hence, it is highly pertinent to understand the mechanisms that lead to thermoacoustic instability.

1.1 Causes and control of thermoacoustic instability

Thermoacoustic instability is the result of complex nonlinear interactions between the inherent acoustic waves of the confinement, unsteady heat release rate from the heat source and the hydrodynamics of the associated flow. Many different mechanisms are identified which can lead to the onset of large amplitude, self-sustained acoustic oscillations.

A combustion process in a practical combustor involves many different time scales such as the evaporation time scale of the liquid fuel, convection time scale, acoustic time scale and chemical time scale. If there exists a parity of any of these timescales it can result in the onset of thermoacoustic instability (Polifke, 2004).

The presence of large scale coherent structures in the flow also can lead to combustion instabilities (Zinn & Lieuwen, 2005). These coherent structures are a result of different flame holding mechanisms such as a V-gutter in an afterburner or a bluff body in a turbulent combustor. The

large scale structures present in the flow force the heat release to become periodic. This flow-flame interaction eventually leads to the onset of thermoacoustic instability.

In the case of premixed burners, equivalence ratio fluctuations act as the source of combustion instability. The fluctuations in the equivalence ratio can lead to unsteady heat release rate. The flame with the unsteady heat release rate act as a potential source of sound (Lieuwen *et al.*, 2001). The acoustic waves generated from the unsteady heat source can further perturb the equivalence ratio and a positive feedback develops which results in thermoacoustic instability (Lieuwen *et al.*, 2001).

The inherent flow fluctuations present in a turbulent combustor can also eventually lead to thermoacoustic instability. The fluctuations in the turbulent flow alter the flame dynamics and the perturbations in the flame enhance the inherent acoustic fluctuations which in turn influences the turbulent fluctuations. Thus the feedback between heat release rate and acoustics mediated by the turbulent flow results in combustion instability.

Another important mechanism that is responsible for the onset of large amplitude oscillations is the presence of entropy waves (Marble & Candel, 1977). The entropy waves originate as temperature fluctuations generated by the unsteady heat release rate. If these entropy waves are accelerated as it can happen in the combustor exit or turbine inlet, they generate acoustic waves. The acoustic waves generated from entropy waves are termed as indirect combustion noise and the interaction of indirect combustion noise with the heat source can cause the onset of combustion instability (Bake *et al.*, 2009; Goh & Morgans, 2013).

In short, many different mechanisms can result in the onset of large amplitude, self-sustained thermoacoustic oscillations and these oscillations can result in structural damage and reduced

performance. Hence, mitigation or control of these oscillations is highly necessary. Various control techniques are adopted to mitigate thermoacoustic instability in combustors. Some of the control techniques focus on the hardware changes of the combustor and are passive in nature. Many active control measures are also developed to control thermoacoustic oscillations.

The passive control measures include, but are not limited to the changes in the structural design of the combustor, the use of Helmholtz resonators, changes in fuel injection distribution pattern and the use of acoustic liners. Passive strategies focus on either dissipating the acoustic energy or avoiding the onset of oscillations by design modifications such as the changes in the dimension of combustors to avoid the possible resonant modes. Passive strategies do not involve any dynamic change in the system parameters and have limited viability. On the other hand active control strategies focus on perturbing the system parameters so as to prevent the growth of the detrimental thermoacoustic oscillations. The system parameters are modified by implementing an actuator. The typical actuator units used in combustion systems are acoustic drivers to generate acoustic waves or servo valves to control the flow rates (McManus *et al.*, 1993). However, it may be difficult to employ the acoustic actuators for full-scale combustors. Another important mechanism for implementing active control is secondary fuel injection. Instead of controlling the acoustic field directly, secondary fuel injection controls the heat release rate by appropriately timing the injection through the pilot injector (Hantschk *et al.*, 1996; Zinn & Neumeier, 1997).

In order to effectively implement the control strategies, a complete understanding of thermoacoustic oscillations are necessary. Controlled experiments are essential to understand the physics of thermoacoustic oscillations. Many different laboratory scale combustion systems are used to perform controlled experimental studies.

1.2 Laboratory scale combustors to study thermoacoustic instabilities

Different types of combustor configurations were used in order to study the phenomenon of combustion instability. Both laminar and turbulent configurations are employed for understanding the dynamics of thermoacoustic instabilities. Similarly, premixed, partially premixed and non-premixed configurations were also used by various researchers (Lieuwen & Zinn, 1998; Venkataraman *et al.*, 1999; Lieuwen, 2003; Kabiraj & Sujith, 2012; Jegadeesan & Sujith, 2013; Nair & Sujith, 2014).

One of the prevalent experimental setups employed to investigate thermoacoustic instability is ducted flames. The experimental setup consists of an optically accessible duct in which the flame will be held. The fuel – air mixture can be premixed, partially premixed or non-premixed. Both laminar and turbulent versions of ducted flames are used to understand the dynamics of thermoacoustic oscillations (Birbaud *et al.*, 2008; Karimi *et al.*, 2009; Kabiraj, 2012; Jegadeesan, 2012).

Apart from ducted flames, many model gas turbine combustors are also employed for investigating the physics of combustion instability. These combustors differ with each other in terms of the flame holding mechanism employed. The flame holding devices in these combustors can be a bluff body, a back ward facing step or a swirler. Depending upon the Reynolds number of the mean flow, these combustors can be laminar or turbulent (McManus & Bowman, 1991; Venkataraman *et al.*, 1999; Zahringer *et al.*, 2003; Shanbhogue *et al.*, 2009; Komarek & Polifke, 2010; Lieuwen, 2012; Nair, 2014; Thampi, 2015).

Although, these model combustors reveal the dynamics associated with combustion instability, performing controlled experiments in these combustors is not an easy task. Moreover, repeatability of the results is also difficult to achieve. These difficulties can be bypassed by employing a canonical system which retains the essential features of thermoacoustic systems, but simple enough for detailed analysis.

1.3 Prototypical thermoacoustic systems

A horizontal Rijke tube, a horizontal duct with a concentrated heat source, is a prototypical system often chosen to study the intricacies of thermoacoustic instabilities in the past (Matveev, 2003; Balasubramanian & Sujith, 2008; Subramanian *et al.*, 2010; Juniper, 2011; Mariappan, 2011). The heat source in a Rijke tube can be a flame or an electrically heated wire mesh. In a traditional vertical Rijke tube, the mean flow is set up by buoyancy. The vertical configuration avoids the need of an external means to create the mean flow. However, the flow rate will be dependent on the heat release rate and hence it is not possible to control the flow rate independently. In contrast, in a horizontal Rijke tube, the mean flow has to be established by external means and hence can be controlled independently.

Rijke tube derives its name from its inventor who first observed sustained acoustic oscillations when a heated wire gauze was placed in a glass tube open at both ends (Rijke, 1859). Although Rijke provided an explanation for the observed acoustic oscillations, it was proved to be incorrect. Thereafter, there were many studies investigating the reason for Rijke oscillations (Lehman, 1937; Pflaum, 1909; Rayleigh, 1878). Pflaum (1909) wrongly concluded that the oscillations were caused by wire vibrations induced by gas flow. Flow reversal was suggested as the reason for Rijke oscillations by Lehman (1937). However, his experimental results never confirmed the necessity

for flow reversal. The most appropriate explanation consistent with the experimental observations was given by Rayleigh (1878).

There were many attempts to model the Rijke oscillations. Neuringer & Hudson (1952) proposed a model which was able to explain the absence of oscillations when the heater was located in the second half of the Rijke tube. They linked the establishment of oscillations to the turbulent heat transfer and proposed the idea of ‘negative velocity gradient’ heaters. A heat driven wave equation was derived by Putnam & Dennis (1954) and they verified the validity of Rayleigh criteria. Using fundamental principles of fluid mechanics, Merk (1957) developed a mathematical model for thermoacoustic systems by assuming constant temperature and a concentrated heat source and introduced the concept of transfer functions in the Rijke tube analysis.

The major purpose of the experimental studies conducted in Rijke tube was to determine the stability boundaries for different system parameters. Some of the important experimental studies are those performed by Saito (1965), Collyer & Ayres (1972), Katto & Sajiki (1977) and by Madarame (1981). However, none of them reported the order in which various parameters were varied. Further, experimental uncertainties were also not mentioned.

Saito (1965) investigated the onset of Rijke oscillations both by performing experiments and by theoretical analysis. He concluded that the onset of oscillations depends upon the phase between the acoustic velocity and the acoustic pressure at the heater location. Hence, he concluded that the heater must be located at the upstream half of the duct for the onset of thermoacoustic oscillations.

Collyer & Ayres (1972) demonstrated the Rayleigh criterion with the help of experiments where they used two electrical heaters in a Rijke tube. They showed that a heater located at $3l/4$ from the upstream end can suppress the first mode oscillations caused by a heater located at $l/4$. Further,

they were able to excite second mode and third mode by suitably positioning the heaters. In short, the experimental results of Collyer & Ayres (1972) were in agreement with the Rayleigh criterion.

Katto & Sajiki (1977) studied the onset of thermoacoustic oscillations in an open-open duct with an electric heater. They calculated the critical heater power required for the onset of oscillations for different flow rates. They also studied the effect of varying the heater location and changing the length of the duct. Different types of electrical heaters were also tested by Katto & Sajiki (1977). They concluded that the thermoacoustic system remains in the non-oscillatory state for high as well as low mass flow rates for a given heater power. They also reported that the critical heater power required is minimum when the heater is located at $l/4$ from the upstream end where l represents the length of the duct.

Madarame (1981) also developed a model to predict the growth rate based on mean flow velocity and heater temperature. However, Madarame (1981) made no attempt to explain the limit cycle oscillations observed in his experiments. A limit cycle oscillation is one in which the amplitude of oscillation is limited by nonlinear saturation mechanisms. Madarame (1981) provided the experimental evidence for the existence of regions in Rijke tube where both first and second mode are excitable. He showed experimentally that both modes can be excited if the heater is located $l/8$ from the upstream end.

Bayely (1986) developed a model of Rijke oscillations where the heat transfer from the heater was related to the acoustic velocity. He observed saturation of the acoustic pressure amplitude and attributed the same to the nonlinearities. Further, he reported the possibility of observing hysteresis.

In a pioneering study, Heckl (1985) explored the nature of thermoacoustic oscillations in a Rijke tube and also implemented control strategies. Heckl (1985) adopted a control volume approach and the balance of acoustic energy to identify the nature of oscillations in the Rijke tube. Using the non-linear theory, Heckl (1985) predicted the amplitude of limit cycle oscillations. Further, Heckl (1988) initiated the efforts to implement active control to suppress the Rijke oscillations. In a subsequent work by Heckl (1990), the nonlinear effects in a Rijke tube were studied experimentally and a model for predicting the limiting amplitude was proposed. The reasons for the presence of a limiting amplitude were explained by comparing nonlinear driving and damping terms. A major contribution by Heckl (1990) is the use of modified King's law to model the heat release rate from a heated wire.

Instability in a Rijke tube was studied by Hantschk & Vortmeyer (1999) with the help of a commercially available CFD code (Fluent 4.4.4). Experimental results were matching with the simulation. However the comparison was done only for one experimental condition.

In another important work by Matveev (2003), the stability boundaries for three characteristic heater positions $L/8$, $L/4$ and $5L/8$ were determined by considering heater power as the bifurcation parameter. The stability margins for different mass flow rates were determined experimentally. An important observation was the variation of hysteresis width with mass flow rates. The hysteresis width was found to increase with increase in mass flow rate. A linear acoustic theory was proposed by Matveev (2003) to predict the onset of oscillations. He also proposed a simple theory to model the nonlinear thermoacoustic oscillations. Matveev (2003) studied limit cycle characteristics extensively for different modes of excitation and identified the unstable domains of operation of a Rijke tube.

Selimefendigil & Polifke (2011) employed a lower order model in frequency domain to predict the occurrence of limit cycle oscillations in a Rijke tube model which represents a heated cylinder in pulsating cross flow. Further Selimefendigil *et al.* (2011) developed a system identification technique and performed non-modal stability analysis of the Rijke tube model.

One of the noteworthy formalism on the stability analysis of thermoacoustic systems, with special focus on Rijke tube, is the Green's function approach introduced by Heckl and co-workers (Heckl & Howe, 2007; Heckl & Kosztin, 2013; Bigongiari & Heckl, 2014; Bigongiari & Heckl, 2015, Bigongiari & Heckl, 2016). Heckl & Howe (2007), performed stability analysis of Rijke tube by employing the Green's function approach. They predicted the growth rate of the oscillations in terms of the properties of the heat release rate model. The stability of a dump combustor with a generic heat release law was investigated by Heckl & Kosztin (2013) using Green's function approach. They derived the governing equation for the single mode in a dump combustor. They analyzed the effects of acoustic properties of the resonant chamber, the coupling between the acoustics and the heat release rate and a tunable termination of the inlet chamber. Bigongiari & Heckl (2014), prescribed a new model to describe the coupling between heat driven modes in a Rijke tube. They derived the characteristic equation for the complex eigenfrequencies using the Green's function approach. Their model was able to predict the linear stability boundaries for different resonant modes. Further, Bigongiari & Heckl (2015), described the hysteresis and oscillations observed in a Rijke tube by employing Green's function approach. Their model was able to predict the hysteresis characteristics of the Rijke tube and the influence of system parameters on the observed hysteresis. Recently Bigongiari & Heckl (2016) employed a tailored Green's function which they calculated analytically to predict the salient nonlinear features of

thermoacoustic feedback such as limit cycle oscillations, bistability and hysteresis. Their model also explained the frequency shift in the acoustic modes.

1.4 Dynamical system approach

In many of the investigations performed in thermoacoustic systems, the presence of limit cycle and hysteresis are reported. The phenomena such as limit cycle and the presence of hysteresis region are specific characteristics of a nonlinear system. Hence, it is clear that thermoacoustic systems are nonlinear in nature.

Nonlinear systems exhibit a sudden change in their qualitative behavior for an infinitesimal change in any of the system parameters termed bifurcation in the dynamical systems theory. If this change takes the system from a non-oscillatory state to an oscillatory state, it is called a Hopf bifurcation (Hilborn, 2000; Strogatz, 2000). Hopf bifurcation can be of two types, supercritical and subcritical.

1.4.1 Supercritical and subcritical Hopf bifurcations

In a supercritical Hopf bifurcation, the system remains in the non-oscillatory state until the control parameter reaches the critical value. Once the value of the control parameter crosses the critical value, the non-oscillatory state becomes unstable and the system goes to the oscillatory state. This change is marked by the presence of a low amplitude stable limit cycle. The parameter value at which the system loses its stability; i.e. when the non-oscillatory state becomes unstable, is called the Hopf point (Point B in figure 1(a, b)).

In the case of a subcritical bifurcation, the system experiences large amplitude oscillations right at the onset of instability. Moreover, while changing the operating conditions along the reverse path, the control parameter needs to be varied to a value significantly beyond the critical value to bring

the system back to the non-oscillatory state. The parameter value at which the system regains its stability when the control parameter is varied along the reverse path (Point E in figure 1(b)), is called the fold point (Hilborn, 2000; Strogatz, 2000; Subramanian *et al.*, 2010). The existence of a fold point along with the Hopf point results in the presence of a hysteresis region (Region BCEF in figure 1(b)).

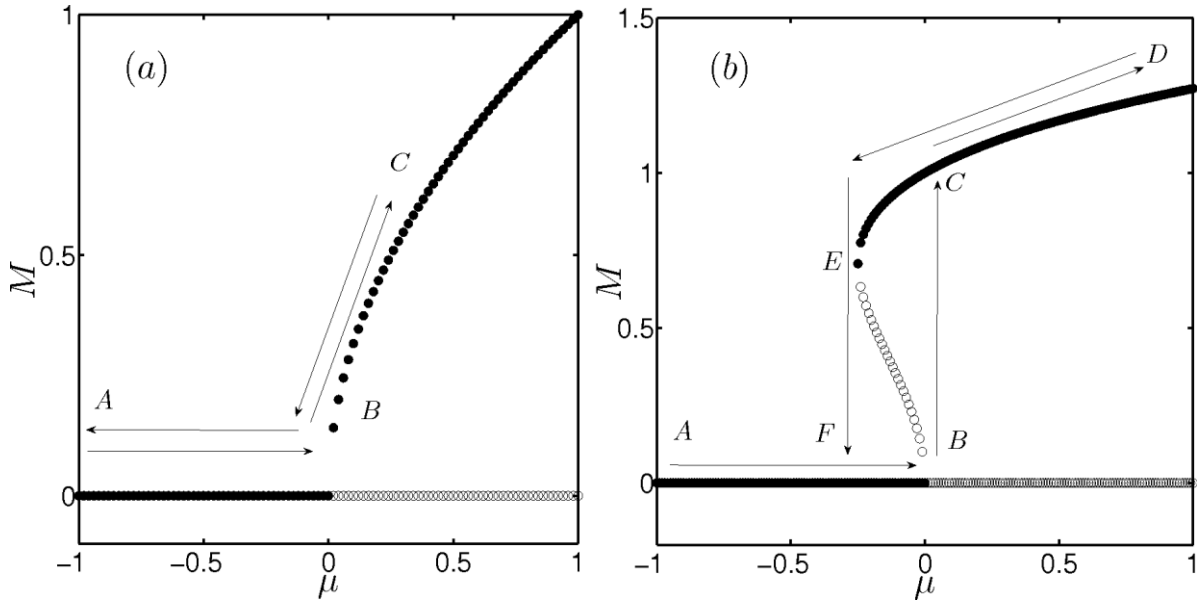


Figure 1.1: Bifurcation characteristics of a measure M when a control parameter μ is varied.
 (a) Supercritical bifurcation. (b) Subcritical bifurcation. In supercritical bifurcation, as the control parameter reaches the value of zero, low amplitude stable limit cycle oscillations are born. Unlike the supercritical bifurcation, large amplitude oscillatory solutions are present right at the onset of instability in the case of a subcritical bifurcation. The system is bistable in the hysteresis region $BCEF$ and the stability of the system is dependent on the initial conditions in this region. ● – Stable oscillatory solutions. ○ – Unstable oscillatory solutions. The figures are obtained from the normal form equations of Hopf bifurcation.

The system is said to be bistable in the hysteresis region as the system can remain in two different asymptotic states depending upon the initial conditions. However, in a supercritical bifurcation,

the stability of the system is independent of the initial conditions. As soon as the control parameter value is brought back to the critical value, the system goes back to the non-oscillatory state in the case of supercritical bifurcation (figure 1(a)). Thus the presence of the bistable region can be used as a good indicator to establish the presence of subcritical Hopf bifurcation (Hilborn, 2000; Strogatz, 2000).

1.4.2 Bifurcations in thermoacoustic systems

Lieuwen (2002) reported the presence of both subcritical and supercritical Hopf bifurcations in an industrial gas turbine simulator. He also reported that the nature of Hopf bifurcation is sensitive to background noise. Ananthakrishnan *et al.* (2005) proposed reduced order models which captured the nonlinear behavior of thermoacoustic systems. The models proposed by Ananthakrishnan *et al.* (2005) were able to exhibit the phenomenon of *triggering* reported in thermoacoustic systems. The process in which a system remains stable for perturbations of low amplitude, but becomes unstable for a perturbation of finite amplitude, is termed *triggering* in thermoacoustic literature (Dickinson, 1962; Brownlee, 1964; Cantrel *et al.*, 1965; Brownlee & Kimbell, 1966; Marxman & Wooldridge, 1971; Levine & Baum, 1982; Wicker *et al.*, 1996).

A model of the horizontal Rijke tube, proposed by Balasubramanian & Sujith (2008), captured many of the features including the subcritical nature of the transition, often observed in experiments. They established the non-normal and nonlinear nature of thermoacoustic oscillations using the model. It was shown that non-normal nature of the system will cause the short term growth of oscillations before their eventual decay even when it is linearly stable. It was also observed that this transient growth can trigger the nonlinear oscillations. The major conclusion

from this study was that the linear stability analysis is insufficient; instead transient growth factor has to be determined in the case of non-normal systems.

Mariappan (2011) performed a set of experiments on a horizontal Rijke tube to provide the experimental evidence for the existence of non-normality in thermoacoustic systems. Threshold amplitude levels for linear behavior of the system were established. The technique of Dynamic Mode Decomposition (DMD) was used to extract the eigenmodes of the duct. The eigenmodes were shown to be non-orthogonal by finding their inner product. An increase in the value of inner product was found to occur with increase in the power supplied to heater. This work provided experimental evidence for the non-normal nature of thermoacoustic oscillations. He also observed subcritical transition to limit cycle oscillations in experiments.

Subramanian *et al.* (2010) employed the numerical continuation method to find out the stability boundaries and to obtain the bifurcation plots. The horizontal Rijke tube model developed by Balasubramanian & Sujith (2008) was used by Subramanian *et al.* (2010). They identified the stability boundaries of the Rijke tube model for different system parameters such as heater power, heater location, damping ratio and time lag. Further, they reported the period doubling route to chaos in the Rijke tube model. They also identified the parameter regimes of quasiperiodic oscillations in the Rijke tube model. In a subsequent study, Subramanian *et al.* (2012) used the method of multiple scale to recast the Rijke tube model developed by Balasubramanian & Sujith (2008) to Stuart-Landau equation near the Hopf point. Further, they identified that the transition to thermoacoustic instability happens via a subcritical Hopf bifurcation. They also found the parameter regimes where triggering is possible.

Kabiraj *et al.* (2012a) performed experiments in a ducted laminar premixed flame and established the presence of secondary bifurcations in thermoacoustic systems. They observed a series of bifurcations with change in the control parameter. The technique of phase space reconstruction from a time series obtained from experiments was clearly explained by Kabiraj *et al.* (2012a). They established the routes to chaos for the first time in thermoacoustics. In a subsequent work, Kabiraj *et al.* (2012b) identified the different routes to chaos in a thermoacoustic system. They observed that the thermoacoustic system transitions to chaos via a Ruelle-Takens scenario. Kabiraj & Sujith (2012) reported intermittent oscillations prior to blow out in a ducted laminar premixed flame. They identified the intermittent oscillations to be of Type-II intermittency and also observed subcritical Hopf bifurcation during the transition to thermoacoustic instability.

1.5 Effect of noise in thermoacoustic systems

A system exhibiting subcritical transition will remain non-oscillating in the bistable region for perturbations within the basin of attraction of the fixed point. On the other hand, the system will oscillate in the bistable region, if the amplitude of perturbations is outside the basin boundary of the fixed point, but well within the basin of attraction of the limit cycle.

Zinn & Lieuwen (2005) reported that perturbations of the order of background noise levels are sufficient to trigger a thermoacoustic system. Lieuwen & Banaszuk (2005) expressed the view that the turbulent fluctuations present in practical thermoacoustic systems can be thought of as additive and parametric sources of noise. Waugh *et al.* (2011) and Waugh & Juniper (2011) performed a detailed numerical study on the effect of various types of noise such as white, pink and blue noise on triggering a thermoacoustic system to instability using the model of horizontal Rijke tube proposed by Balasubramanian & Sujith (2008). White noise is one in which energy is equally

distributed among all the frequencies and the power spectrum is flat, as in the case of white light. In the case of pink noise, the amount of energy content in a particular frequency is inversely proportional to the value of the frequency and the power spectrum varies as $1/f$, where f is the frequency. Blue noise has a power spectrum which varies as f and consequently the higher frequencies contain more energy (Ojalvo & Sancho, 1999).

1.5.1 Noise Induced triggering in thermoacoustic systems

Waugh *et al.* (2011) found that triggering is strongly dependent on the strength and the color of the noise. They suggested that pink noise is the most effective in triggering the system to instability whereas blue noise can even inhibit the phenomenon of triggering. Waugh *et al.* (2011) also observed that a thermoacoustic system can become unstable in the presence of noise even if it is in the linearly stable regime. They reported that the system will reach the state of stable limit cycle oscillations from a non-oscillatory state via a state of unstable limit cycle oscillations. Waugh & Juniper (2011) found that the system will dislodge itself from the oscillatory solution if the noise amplitude is high. They introduced stochastic stability maps to visualize the practical stability regimes of a thermoacoustic system in the presence of noise.

Jegadeesan & Sujith (2013) showed experimentally that for a ducted non-premixed flame, noise-induced triggering to instability is possible. They also obtained the deterministic and stochastic stability maps. Using nonlinear time series analysis, they constructed phase portraits and found that when the system is triggered, the transition to instability happens via an unstable limit cycle oscillation, as predicted by Juniper (2011). Jegadeesan & Sujith (2013) experimentally validated the observation made by Waugh *et al.* (2011) that the transition to instability happens even when the noise level is significantly below the triggering amplitude. However, Waugh *et al.* (2011) and

Waugh & Juniper (2011) reported no change in the amplitude of the limit cycle oscillations in the presence of noise. In contrast, Jegadeesan & Sujith (2013) reported a reduction in the amplitude of the limit cycle oscillations in the presence of noise. They attributed this decrease in amplitude to a decrease in the correlation between the pressure oscillations and the heat release rate fluctuations in the presence of external noise.

Outside the context of thermoacoustics, the effect of noise on the transitions that can happen in nonlinear systems is well studied and it is referred to as noise induced transitions (Horsthemke & Lefever, 2006). Noise induced transition refers to the effect of fluctuations on the dynamics of a system and the appearance of novel dynamical features which are not present in the deterministic system. Horsthemke & Lefever (2006) discussed the various noise induced transitions that can be observed in physical, chemical and biological systems. They also detailed about the noise induced non-equilibrium phase transitions.

Aumaitre *et al.* (2007) studied the noise induced transitions that can be observed in a nonlinear oscillator. They found that noise can suppress a global attractor and also can stabilize an unstable fixed point. They also reported noise induced intermittency and noise induced multi-scaling. They found that both noise induced intermittency and noise induced multi-scaling depend upon the power spectrum of the noise rather than on the amplitude of the noise.

The addition of noise in the normal form equation of Hopf bifurcation changes the dynamics of the system and introduces novel dynamical states (Sastry & Hijab, 1981). The presence of additive or parametric noise can also induce global asymptotic stability in prototypical dynamical systems. The phenomenon of noise induced stability is observed for both supercritical and subcritical Hopf bifurcations (Mackey *et al.*, 1989). In the case of Hopf bifurcation, the presence of additive noise

is found to smear out the sharp transition that is observed in a deterministic system (Juel *et al.*, 1997). Thus the determination of the Hopf point from experimental and numerical observations becomes impossible in the presence of additive noise. This difficulty in determining the bifurcation point is because the measured observable is no longer a deterministic quantity but a stochastic variable. Thus a single realization that we obtain in an experiment or from a mathematical model is incapable of providing the complete information about the state of the system. In the presence of noise, stochastic differential equations (SDEs) are adopted instead of ordinary differential equations to describe the evolution of the system. Hence, we need to calculate the probability density function of the observable rather than its absolute value in the presence of noise. The probability density function of a stochastic variable can be obtained by solving the Fokker-Plank equation associated with the SDE (Stratonovich, 1963, Gardiner, 1997, Risken, 1989). The qualitative changes observed in the probability distribution of the observable are termed as phenomenological bifurcations (P-bifurcation).

Bifurcations observed in the presence of noise in a nonlinear system are termed stochastic bifurcations. There are studies on the effect of additive and multiplicative noise in inducing stochastic bifurcations in nonlinear systems. L'Heureux & Kapral (1989) studied the effect of external white noise on a bistable system which transits between a limit cycle and a fixed point. They found that the stationary probability distribution changes from unimodal to bimodal for moderate noise intensities. Once the noise intensity is high, the bimodal distribution becomes unimodal again. Additive noise does not change the location of the extrema of the stationary probability density function whereas multiplicative noise introduces novel dynamical states (Bashkirtseva *et al.*, 2015).

The phenomenon of stochastic bifurcation is very well studied using models. The stochastic Hopf bifurcation is studied in the context of various nonlinear oscillators (Arnold *et al.*, 1999; Zakharova *et al.*, 2010; Xu *et al.*, 2011; Bashkirtseva *et al.*, 2015) and in biological systems including neuron models, synthetic gene oscillators (Zakharova *et al.*, 2010; Djedundam *et al.*, 2013) and cellular networks (Song *et al.*, 2010). The framework of stochastic bifurcation is also used to study the effect of noise in self-sustained bistable oscillators (Zakharova *et al.*, 2010). However, experimental studies on the concept of stochastic bifurcation are limited to driven laser systems (Billings *et al.*, 2004).

Noiray & Schuermans (2013a, 2013b), in their pioneering work, introduced Fokker-Planck formalism in the thermoacoustic literature. They derived the F-P equation for a thermoacoustic system undergoing supercritical Hopf bifurcation. Their primary focus was to derive growth and decay rates of thermoacoustic oscillations for the unsteady pressure data obtained from a gas turbine engine and compare it with the numerical model.

Yamapi *et al.* (2012) derived an effective F-P equation for a birhythmic Van der Pol oscillator. They derived the probability distributions both analytically and numerically. They found that the bistable region decreases with increase in noise intensity and gets completely suppressed beyond a threshold noise intensity.

1.6 Precursors for transitions in thermoacoustic systems

The presence of bistable region and the presence of large amplitude oscillations right at the onset of instability make the subcritical transitions difficult to deal with. It becomes difficult to bring back the system to the non-oscillatory state once the system is transitioned to oscillatory state in

the case of subcritical transition. The transitions observed in such bistable systems are referred to as *catastrophic transitions* (Scheffer *et al.*, 2009; Kuhen, 2011; Scheffer *et al.*, 2012). The catastrophic nature of these transitions creates the need to develop precursors.

Recently, Sujith & co-workers developed a plethora of precursors by employing the concepts of dynamical system theory and complex system theory. Nair *et al.* (2013) proposed that transition to thermoacoustic instability in turbulent combustion systems can be viewed as a transition from chaos to order. They employed 0-1 test to predict the onset of thermoacoustic instability. Nair & Sujith (2014) reported that the transition to thermoacoustic instability represents loss of multifractality of acoustic pressure time series. They proposed Hurst exponent as a measure to predict the impending instability. Later, Unni & Sujith (2015) showed that the transition to blowout can also be predicted by computing the Hurst exponent of the acoustic pressure time series. Murugesan & Sujith (2015 a & b) applied the concepts from complex system theory and developed a set of precursors based on complex networks derived from the time series of unsteady pressure.

Gotoda *et al.* (2014) proposed an online method to detect combustion instability by utilizing the precursors developed based on dynamical system theory. They used translation error as a precursor and they also determined the nature of dynamical states close to blow out by recurrence analysis. Further, Domen *et al.* (2015) employed methods of multiscale entropy and nonlinear forecasting to detect and predict the occurrence of lean blowout. They also adopted measures such as correlation coefficient and permutation entropy to identify the complex dynamical states near the lean blowout limit.

It should be noted that the precursors discussed above are effective in predicting transitions in turbulent systems. Nair *et al.* (2014) showed that the transition to thermoacoustic instability

happens via a state of intermittency in turbulent systems. Further, Nair (2014) clearly explained the role of intermittency in developing the early warning measures to predict thermoacoustic instability. As pointed out by Nair (2014), the effectiveness of these precursors to predict thermoacoustic instability depends on the presence of intermittency.

Another set of precursors that can be found in literature are developed for noisy systems. Wiesenfeld (1985) in his pioneering work proposed noisy precursors to predict the occurrence of bifurcations in nonlinear systems. He reported that the width of the peak frequency in the amplitude spectrum acts as a measure of proximity to an impending transition. He also showed that the nature of the impending bifurcation can be clearly understood by observing the appearance of peak in the amplitude spectrum. Thus the presence of an optimum amount of noise in a nonlinear system enhances the possibility of detecting the impending transition.

Later, this noise induced enhancement of the output from a nonlinear system was observed in both forced and self-excited systems. In a forced system, the noise induced enhancement of the output was termed stochastic resonance and in a self-excited system, similar phenomenon was termed coherence resonance. Recently Kabiraj *et al.* (2015) observed the phenomenon of coherence in an experiment performed in a thermoacoustic system and suggested the use of noisy precursors to predict the transitions observed in a thermoacoustic system.

Apart from the precursors described above, there exists another important class of precursors based on critical slowing down. Critical slowing down refers to the phenomenon where the real part of the dominant eigenvalue approaches zero as a nonlinear system undergoes a bifurcation. As the real part of the dominant eigenvalue approaches zero, the time taken for the perturbations to die down increases. The critical slowing down also results in an increase in autocorrelation, as the

system memory increases. Since the perturbations do not decay as we approach a bifurcation due to critical slowing down, the variance also increases.

Over the years, many early warning measures based on critical slowing down were developed to detect critical transitions in nonlinear systems. A pioneering study on early warning signals was carried out by Scheffer *et al.* (2009). They proposed a plethora of early warning measures to predict the sudden changes in eco systems, climatic shifts, collapse of financial markets and the onset of asthmatic attacks and epileptic seizures. In a subsequent work Scheffer *et al.* (2012) elaborated the principle behind the working of early warning indicators. They proposed early warning indicators based on critical slowing and also based the phenomenon of *flickering*. Flickering is the phenomenon where a nonlinear system switches between two alternative stable states in the presence of noise. Scheffer *et al.* (2012) proposed autocorrelation and variance as the early warning indicators based on the theory of critical slowing down. They also advocated the use of another set of early warning indicators in the presence of noise.

Dakos *et al.* (2012) compared the different early warning indicators in terms of ease of implementation and their effectiveness in predicting the impending transition. They carried out their investigations on two simulated data sets which depict critical transition. They discussed the metric based and the model based early warning indicators.

We can find an extensive use of these early warning measures to predict critical transitions in almost every field of science starting from ecology and extending up to medicine where these measures are used for prognosis (Dakos *et al.*, 2008; Meisel *et al.*, 2015; Livina *et al.*, 2015; Trefois *et al.*, 2015). Many studies applied these early warning measures to mathematical models of complex systems. The viability of these measures proved also with the help of experiments (Drake

& Griffien, 2010; Kramer & Rose, 1985; Tredicce *et al.*, 2004; Carpenter *et al.* 2011). Recent findings indicate that critical transitions that happen via subcritical Hopf bifurcation in spiking neurons can be predicted using these early warning measures (Meisel *et al.*, 2015). The applicability of early warning measures are not limited to low dimensional reduced order models but also extends to high dimensional complex systems (Kuehn *et al.* 2015).

1.7 Summary of the state of the art

In summary, the experimental and numerical investigations conducted on horizontal Rijke tubes indicate that the transition from non-oscillatory to oscillatory state is subcritical in nature (Balasubramanian & Sujith, 2008; Subramanian *et al.*, 2010; Juniper, 2011; Mariappan, 2011). Nonetheless, experimental studies on horizontal Rijke tube where system parameters other than heater power are varied are not present in the literature to the best knowledge of the author. The subcritical nature of transition observed in the case of Rijke tube model are not yet confirmed by experimental observations for system parameters such as heater location.

Although some experimental studies allude to the reduction in the width of the hysteresis zone with decrease in mass flow rate (Matveev, 2003; Mariappan, 2011), further investigations were not performed. It is essential to analyze the influence of system parameters on the presence of bistable region in the context of a horizontal Rijke tube to get a clear idea on the nature of transition.

The existing literature on effect of noise in thermoacoustics focuses on noise induced triggering (Juniper, 2011; Waugh *et al.*, 2011; Waugh & Juniper, 2011; Jegadeesan & Sujith, 2013). In noise induced triggering, the focus is on the ability of the noise pulses or continuous noise, both of which

can be colored or white, to trigger a system, which is otherwise linearly stable, to instability. Moreover, the effect of high intensity noise on the dynamics of thermoacoustic systems remains to be explored. The concept of stochastic bifurcation to describe the transitions in the presence of noise is not yet employed in thermoacoustics.

Precursors based critical slowing down are not yet employed to predict impending transitions in thermoacoustic systems. Although there exist enough literature on the use of early warning signals based on critical slowing down for predicting the transitions in natural systems, the applicability of the measures based on critical slowing down to an engineering system is not yet explored. Moreover, the robustness of the early warning indicators in the presence of fluctuations is not yet studied in the context of a physical system. As most of the transitions that we observe in thermoacoustic systems are associated with bifurcations and as the phenomenon of critical slowing down precedes bifurcations, it is possible to develop early warning measures based on critical slowing down for thermoacoustic systems. Furthermore, the transitions that we observe in thermoacoustic systems are often catastrophic which demands the development of forewarning measures.

1.8 Objectives of the Thesis

The objective of the present work is to understand the effect of system parameters and noise on the bistable characteristics of a prototypical thermoacoustic system. Further, the study aims to develop early warning measures for critical transitions observed in thermoacoustic systems. The major objectives are:

1. To understand the effect of system parameters such as heater power and heater location on the nature of transition and on the bistable characteristics of a prototypical thermoacoustic system.
2. To investigate the effects of external noise on the bistable characteristics of a prototypical thermoacoustic system and to analyze the effect of high intensity noise by calculating stationary probability distribution from Fokker-Planck equation.
3. To develop early warning measures based on critical slowing down for the catastrophic subcritical transitions observed in a prototypical thermoacoustic system.

1.9 Overview of the thesis

The objectives of this study were achieved with the help of experiments conducted in a horizontal Rijke tube and numerical simulations performed in a mathematical model of the Rijke tube. The time series obtained from the experiments and the mathematical model are analyzed using the tools from dynamical system theory. In order to understand the effect of noise on the bistable characteristics of the system, external noise was applied with the help of loud speakers in the experiment. The numerical model is perturbed with additive Gaussian white noise to understand the influence of noise on the nature of transition. The early warning measures were developed by exploiting the concepts of critical slowing down.

The rest of the thesis is arranged as follows. Chapter 2 describes the tools from dynamical system theory used for phase space reconstruction. The technique of phase reconstruction along with the methods to find the minimum embedding dimension and the optimum time delay is described in

this chapter. This chapter also discusses about the bifurcations that we observe in a bistable thermoacoustic system and the associated normal form equations.

The experimental set-up used in the current study is described in Chapter 3. A horizontal Rijke tube with an electric heater as the heat source is used in the present study. Chapter 4 details the numerical model used in the present study. The Rijke tube model proposed by Balasubramanian & Sujith (2008) is recast into a set of stochastic delay differential equations to understand the influence of noise and system parameters on the nature of transition observed in the Rijke system.

Chapter 5 describes the effect of systems parameters, heater power and heater location, on the nature of transition to thermoacoustic instability. In this chapter, the dependence of width of the bistable zone on Strouhal number is brought out. The decrease in the width of the bistable zone with the increase in Strouhal number is shown both in experiments and in the numerical model. Moreover, the power law dependence between the width of the bistable zone and the Strouhal number is also described in this chapter.

The effect of noise on the nature of transition and the reduction in the width of the bistable zone with increase in noise intensity are discussed in Chapter 6. The influence of noise on Rijke oscillations is described with the help of results from experiments and from the mathematical model. The decrease in the non-dimensional hysteresis width with non-dimensional noise intensity is shown to be linear and independent of Strouhal number in this chapter. The complete suppression of bistable zone in the presence of high intensity noise is also described in Chapter 6.

The phenomenon of stochastic bifurcation observed in the horizontal Rijke tube is discussed in Chapter 7. A simplified theoretical model depicting a bistable oscillator is considered to determine the probability distribution of acoustic pressure amplitude. The changes in the stationary

probability distribution of acoustic pressure are obtained by solving the Fokker-Planck equation associated with the governing equations. The regions of bimodality, where the thermoacoustic system is bistable are identified.

Chapter 8 describes the techniques to develop early warning measures for predicting the impending transitions observed in a thermoacoustic system. The early warning measures are developed by exploiting the concept of critical slowing down near a bifurcation. Lag-1 autocorrelation and variance are mainly used as the early warning indicators. The robustness of the early warning measures based on critical slowing down in the presence of noise is also established in this chapter.

The conclusions that can be drawn from the present study are detailed in Chapter 9. This chapter also describes the possible extension of the present work to thermoacoustic systems other than the one considered here.

CHAPTER 2

TOOLS FROM DYNAMICAL SYSTEM THEORY

This chapter describes the tools and techniques adopted from dynamical system theory which are employed in the current thesis. A detailed description of various types of bifurcations that can be observed is provided in this chapter. A discussion on the reconstruction of phase space from a scalar time series is also included in this chapter. In many practical situations, the governing equations of a dynamical system generating a time series is not known. However, it is still possible to understand the dynamics of the system by reconstructing the phase space from the measured time series. The two important parameters necessary for the reconstruction of phase space are the minimum embedding dimension and the optimal delay. The methods to calculate the embedding dimension and time delay for time series obtained from experiments are described in this chapter.

2.1 Bifurcations in a dynamical system

A system whose state evolves in time according to a dynamical law can be defined as a dynamical system. The most general description of a dynamical system is

$$\frac{dX}{dt} = F(X, Z) \quad (2.1)$$

where, X represents the state space vector and Z represents the vector of system parameters. As explained in Chapter 1, a dynamical system will undergo sudden change in its qualitative behavior for an infinitesimal change in any of the system parameters. This sudden change in qualitative

behavior is termed as bifurcations in the dynamical system literature (Strogatz, 2000; Anishchenko, 2006).

A complete information about the dynamical system can be obtained by tracking the evolution of the trajectories in the phase space. Phase space of a dynamical system is constructed by considering the independent variables that describe the state of the system as the coordinates. The asymptotic state of the system can be identified by *attractors* present in the phase space of the system. An attractor refers to the subset of the phase space towards which the system will eventually evolve. An attractor can be a fixed point, a limit cycle or a chaotic one. Bifurcations can result in the emergence of new attractors in the phase space or the annihilation of existing attractors.

The bifurcations that can happen in a dynamical system can be studied with the help of prototypical examples which are otherwise known as the normal form equations. The normal form equations provide a framework for identifying the bifurcations associated with a dynamical system.

A detailed description of bifurcations observed in a bistable thermoacoustic system along with their normal forms is provided in the following section.

2.1.1 Saddle node bifurcation

The saddle node bifurcation or fold bifurcation refers to the situation where two fixed points are created or annihilated. As we vary the system parameter, the two fixed points move towards each other, collides and eventually gets annihilated. The normal form associated with saddle node bifurcation is

$$\frac{dx}{dt} = \mu + x^2 \quad (2.2)$$

where, x is the state variable and μ is the control parameter. It can be seen from equation (2.2) that for $\mu < 0$, there exist no solution and for $\mu > 0$, we will have two solutions $+\sqrt{\mu}$ and $-\sqrt{\mu}$. Out of the two solutions, one will be stable ($-\sqrt{\mu}$) and the other one will be unstable ($+\sqrt{\mu}$). Since the two solutions appear to arise out of nowhere in the phase space, often this bifurcation is termed *blue sky* bifurcation.

2.1.2 Hopf bifurcation

If a bifurcation results in the birth of an oscillatory state or rather in the introduction of new frequency, the bifurcation is termed as Hopf bifurcation. Since Hopf bifurcation is associated with oscillatory states, the minimum phase space dimension to observe Hopf bifurcation is two. In a two dimensional system, we will have two eigenvalues which will determine the stability of the system. If two of these eigenvalues are in the left half of the complex plane, the resulting dynamical state of the system will be a stable fixed point. The two eigenvalues can also be complex conjugates. Hopf bifurcation results when a pair of eigenvalues with non-zero real parts (which are complex conjugates), cross the imaginary axis. As stated earlier, Hopf bifurcation results in the birth of a new oscillatory state.

As described in Chapter 1, Hopf bifurcation can be supercritical or subcritical in nature. The normal form associated with the supercritical Hopf bifurcation is as follows

$$\dot{r} = \mu r - r^3 \quad (2.3)$$

$$\dot{\theta} = \omega + br^3 \quad (2.4)$$

The state space variables are represented by r and θ and the frequency of the oscillatory state is represented by ω . For $\mu < 0$, we will have a stable fixed point and as we increase the control

parameter, the fixed point at the origin becomes a very weak stable spiral at $\mu = 0$. When $\mu > 0$, we will have an unstable spiral at the origin and a stable limit cycle at $r = \sqrt{\mu}$. We can see that the cubic nonlinearity in equation (2.3) is stabilizing and the supercritical Hopf bifurcation results in the birth of low amplitude stable limit cycle.

If the cubic nonlinearity is destabilizing, then we will have subcritical Hopf bifurcation. The normal form equations associated with subcritical Hopf bifurcation are

$$\dot{r} = \mu r + r^3 - r^5 \quad (2.5)$$

$$\dot{\theta} = \omega + br^3 \quad (2.6)$$

In the case of subcritical Hopf bifurcation, the origin remains a stable spiral for $\mu < 0$ and there also exists a stable limit cycle away from the origin. The stable limit cycle and the stable fixed point are separated by an unstable limit cycle. As the control parameter is increased, the unstable limit cycle shrinks in size and finally engulfs the stable fixed point at the origin at $\mu = 0$. The origin becomes unstable and the only attractor present to the system is the large amplitude limit cycle. Thus, when the system undergoes subcritical Hopf bifurcation, there will be sudden onset of large amplitude limit cycle oscillations.

The normal form equations (2.5) and (2.6) also correspond to saddle-node bifurcation of cycles. The saddle-node bifurcation of cycles refers to the phenomenon where two limit cycles coalesce and annihilate. It should be noted that the fixed points that we will get by finding the roots of Eqn. (2.5) corresponds to limit cycle oscillations. A saddle-node bifurcation of fixed points of Eqn. (2.5) can be observed for a control parameter value of $\mu = -\frac{1}{4}$. For $\mu < -\frac{1}{4}$, there will be a stable spiral situated at the origin and for $\mu = -\frac{1}{4}$, a half-stable limit cycle is born. A stable fixed point

and a stable limit cycle, separated by an unstable limit cycle, coexist for $-\frac{1}{4} < \mu < 0$ (Strogatz, 2000). In a bitstable thermoacoustic system, we observe this fold bifurcation which results in the birth or death of a stable and an unstable limit cycle solution (Subramanian *et al.*, 2010). The Hopf bifurcation and the fold bifurcation of limit cycles observed in experiments are described in Chapter 5.

The bifurcations that happen in a dynamical system can be understood with help of phase portraits. The next section describes the technique to reconstruct the phase space from scalar time series obtained from experiments.

2.2 Phase space reconstruction

In order to construct the phase space and to identify the topological structures present in the phase space, we need a complete information about the independent state variables required to describe the state of the dynamical system. The information of independent state variables can be obtained from the governing equations of the dynamical system. However, for many physical systems such as a thermoacoustic system or an aero-elastic system, we will not have access to all the relevant dynamical variables. The time series of only one of the state variables may be available from experiments. Nevertheless, we can reconstruct the phase space from the time series measurements of a single dynamical variable using Taken's theorem (Takens, 1981).

The central idea behind the phase space reconstruction is to obtain sufficient number of delayed variables from the scalar time series data. The number of delayed variables to be obtained depends on the minimal embedding dimension. The single time series data is converted into d time delayed independent vectors. The number of independent vectors depend upon the minimal embedding

dimension. The time delay $\hat{\tau}$ between the vectors and the minimal embedding dimension can be found by various algorithms as described in Abarbanel (1996).

2.2.1 Optimum time delay

There exist different techniques to calculate the optimum time delay that needed for reconstructing the phase space. One of the common methods employed is to calculate the first zero-crossing of the autocorrelation function of the obtained time series. The method employed in the current study to calculate the optimal time delay employs the concept of Average Mutual Information (AMI) between the delayed vectors rather than the autocorrelation of the time series.

The AMI between the delayed vectors of a signal $x(t)$ is defined by the following equation

$$I(\hat{\tau}) = \sum_{t=1}^{N'} P(x(t), x(t + \hat{\tau})) \log_2 \left[\frac{P(x(t), x(t + \hat{\tau}))}{P(x(t))P(x(t + \hat{\tau}))} \right] \quad (2.7)$$

where, $P(X)$ refers to the probability of the event X .

The time series $x(t)$ is normalized to lie between 0 and 1 to begin with and the time series data is sorted into different bins. The histograms on these bins are normalized and the probability distributions $P(x(t))$ and $P(x(t + \hat{\tau}))$ are obtained. A two dimensional bin in $x(t)$ and $x(t + \hat{\tau})$ is normalized to obtain the joint probability distribution $P(x(t), x(t + \hat{\tau}))$. AMI is the measure of amount of information shared by two different time delayed vectors. As it can be seen from Eqn. (2.7), AMI is a function of the time delay $\hat{\tau}$. Hence, to construct independent time delayed vectors, the value of the time delay corresponding to the first local minimum of AMI is chosen. In other words, the first local minimum of AMI corresponds to the optimal time delay.

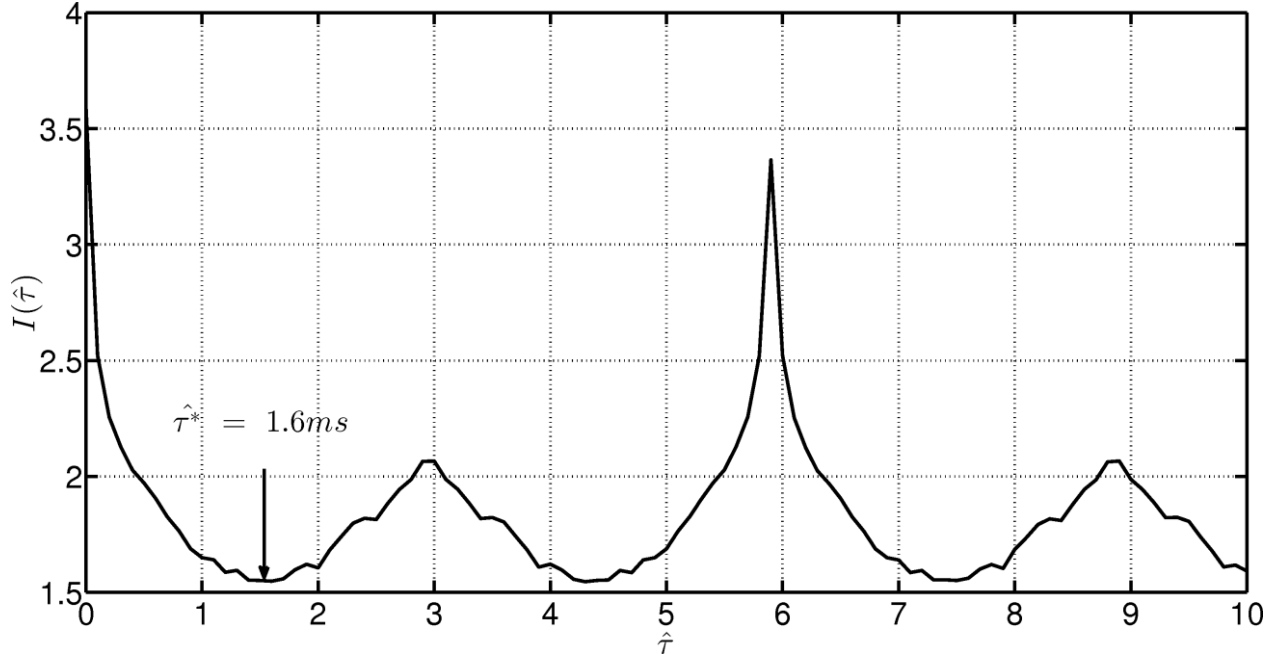


Figure 2.1: The variation of $I(\hat{\tau})$ with $\hat{\tau}$ for acoustic pressure time series corresponding to limit cycle oscillations observed in horizontal Rijke tube. The time delay corresponding to the first minima of AMI is considered as the optimal time delay.

We can see from Fig 2.1 that the AMI changes with time delay and the optimal time delay $\hat{\tau}^*$ corresponds to the value of time delay at the first minima of AMI. It is interesting to note that this value of optimal time delay is close to one fourth of the time period of acoustic pressure oscillations which corresponds to the phase difference between acoustic velocity and acoustic pressure for a standing wave with perfect reflecting boundary conditions.

2.2.2 Minimal embedding dimension

In order to reconstruct the phase space from the scalar measurements, we need to find the minimal dimensions of the phase space. The criterion for choosing the minimal embedding dimension is that the topological features observed in the reconstructed phase space are due to the dynamics of the system and not an artifact of the specific embedding dimension. The most popular algorithm

to calculate the minimal embedding dimension is the method of False Nearest Neighbors (FNN).

In FNN, the number of false neighbors are calculated for each point in the phase space as a function of the embedding dimension. A false neighbor is defined as the one which will move away from a point in a phase space, once we increase the embedding dimension. So if we choose an embedding dimension less than the minimal embedding dimension required, then we will be observing false crossing of trajectories in the phase space.

After obtaining the optimum time delay, a measure $a(i, d)$ of the following form is constructed in FNN.

$$a(i, d) = \frac{\|X_i(d+1) - X_{n(i,d)}(d+1)\|}{\|X_i(d) - X_{n(i,d)}(d)\|} \quad (2.8)$$

where, $i = 1, 2, \dots, (N' - d\hat{\tau})$ and $n(i, d)$ represents the index of the nearest neighboring point to X_i in phase space. The Euclidian norm is represented by $\| \dots \|$.

Any two points in the d – dimensional reconstructed phase space which are close to each other will remain close to each other in the $(d + 1)$ – dimensional reconstructed space, if they are true neighbors. Essentially the minimal embedding dimension is calculated by comparing the value of the measure $a(i, d)$ with a threshold value which will be dependent on i . Cao (1997) proposed a new measure which is independent of I to calculate the minimal embedding dimension. The measure $E(d)$ proposed by Cao (1997) is defined as:

$$E(d) = \frac{1}{N' - d\hat{\tau}^*} \sum_{i=1}^{N' - d\hat{\tau}^*} a(i, d) \quad (2.9)$$

The variation of $E(d)$ with d is calculated by introducing another quantity $E_1(d)$ such that

$$E_1(d) = \frac{E(d+1)}{E(d)} \quad (2.10)$$

The variation of $E_1(d)$ with d is calculated and the minimal embedding dimension ($d_0 + 1$) is chosen when $E_1(d_0 - 1) = E_1(d_0)$. $E_1(d)$ always saturates for a deterministic signal whereas for uncorrelated noise it never saturates. Nair *et al.* (2014) proposed a new measure $E_2(d)$ to distinguish deterministic signals from uncorrelated noise, where $E_2(d)$ is given by

$$E_2(d) = \frac{E^*(d+1)}{E^*(d)} \quad (2.11)$$

$$E^*(d) = \frac{1}{N' - d\hat{\tau}^*} \sum_{i=1}^{N' - d\hat{\tau}^*} |X(i + d\hat{\tau}^*) - X(n(i, d) + d\hat{\tau}^*)| \quad (2.12)$$

$E_2(d)$ will always be one for an uncorrelated signal as the future values are independent of the past values, whereas for a deterministic signal, there must be some values of d for which the value of $E_2(d)$ will not be one. In the present study, the minimal embedding dimension is calculated by employing the modified FNN method as suggested by Cao (1997).

Figure 2.2 depicts the variation of $E_1(d)$ and $E_2(d)$ with d for acoustic pressure time series corresponding to limit cycle oscillations observed in horizontal Rijke tube. As the measure $E_1(d)$ saturates at an embedding dimension of 11, the minimal embedding dimension should be chosen as 12.

The reconstructed phase space of the pressure time series is shown in Fig. 2.3. The optimum time delay corresponding to the first minima of AMI and the minimal embedding dimension obtained from Cao's method are used to reconstruct the phase space.

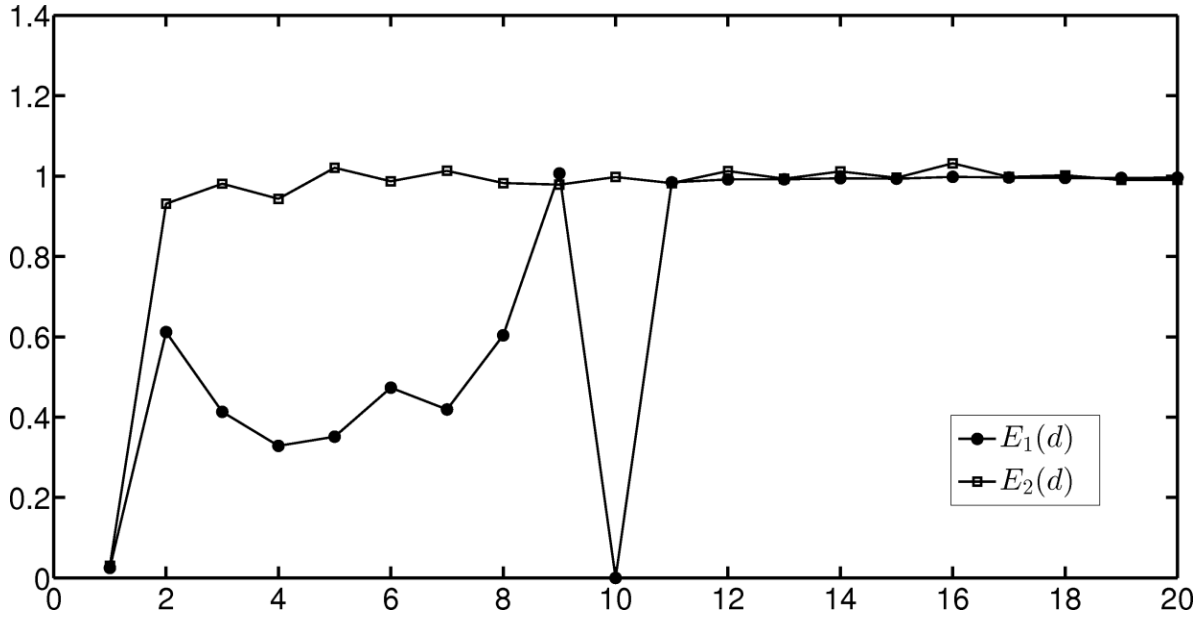


Figure 2.2: The variation of $E_1(d)$ and $E_2(d)$ with d for acoustic pressure time series corresponding to limit cycle oscillations observed in horizontal Rijke tube. It can be seen that $E_1(d)$ saturates around $d = 11$. Hence, the minimal embedding dimension is taken as 12.

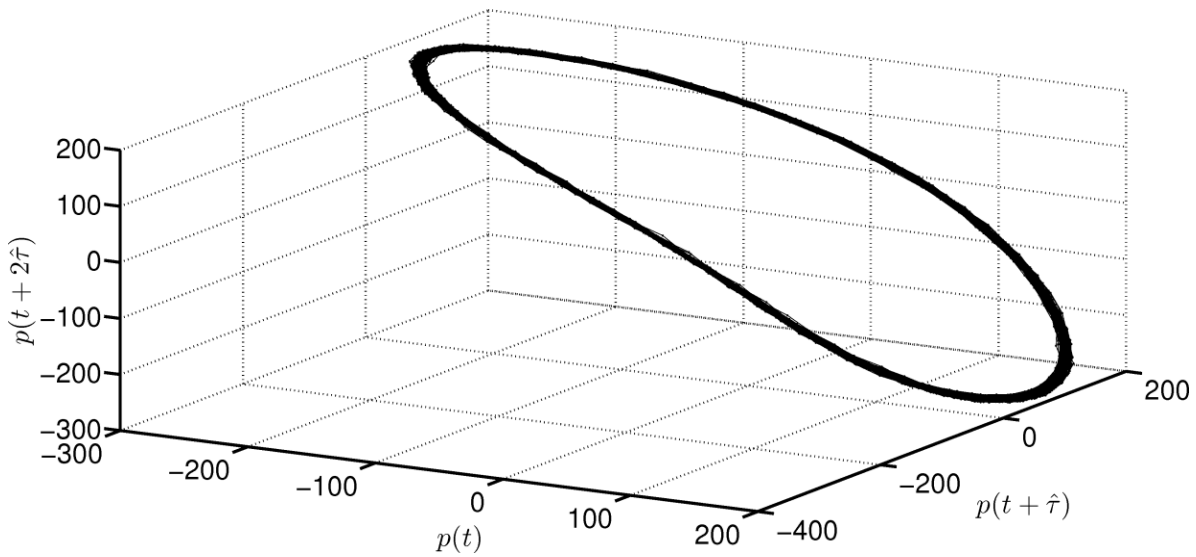


Figure 2.3: The reconstructed phase portrait of the time series of acoustic pressure corresponding to limit cycle oscillations observed in horizontal Rijke tube. It can be seen that the topological structure in the phase space is an isolated closed trajectory which represents a limit cycle.

We observe from Fig. 2.3 that the attractor in the phase space is a limit cycle. So, it can be seen that using the technique of phase space reconstruction, the asymptotic dynamics of the thermoacoustic system is completely understood although we only had the time series of the acoustic pressure. Thus, even when we have access to only one of the dynamical variables of the system, the reconstructed phase space will provide the information about the asymptotic state of the system.

2.3 Concluding remarks

In this chapter, the different types of bifurcations that can be observed in prototypical thermoacoustic systems are discussed in detail. The associated normal form equations are also presented. The technique of phase space reconstruction from the time series of a single state space variable is described. The methods to find optimum time delay and the minimal embedding dimension are also presented.

CHAPTER 3

EXPERIMENTAL SET-UP

This chapter focuses on the experimental set-up employed in the current study. The instrumentation used to acquire data is also described in this chapter. The procedure adopted to perform experiments is also detailed.

3.1 Experimental set-up

The experimental setup used for the present study is shown in figure 2. A horizontal Rijke tube with an electrically heated wire mesh is used to perform the experiments. The tube is of square cross-section and 1 m long. The cross-sectional area of the duct is $93 \times 93 \text{ mm}^2$. A blower (1 HP, Continental Airflow Systems, Type-CLP-2-1-650) operated in the suction mode, is used to provide the mean flow. The flow rate is measured using a compact orifice mass flow meter (Rosemount 3051 SFC). The measurement range of the flow meter is 0-5 g/s with an accuracy of $\pm 2.1\%$. A decoupler of dimensions $120 \times 45 \times 45 \text{ cm}^3$ is located at the outlet end of the Rijke tube to reduce the acoustic interactions between the blower and the duct, at the same time enforcing the “open” end condition. A DC power supply unit (TDK-Lambda, GEN 8-400, 0-8 V, 0-400 A) provides the necessary electrical power to the wire mesh. The uncertainty in the heater power is 0.4 W. The mesh and the power supply unit are connected using copper rods and copper wires. A mesh type electric heater is used because it can supply high amount of electric power for a fairly long duration without any significant structural deformation (Matveev, 2003). The electric heater is housed in a ceramic material to ensure thermal and electrical insulation. A traversing mechanism with a least count of 1 mm is used to change the heater location.

The measurement system consists of a pressure transducer (PCB103B02) connected to a PCI 6221 data acquisition card to record the acoustic pressure and a K-type thermocouple to measure the steady state temperature. The sensitivity of the pressure transducer is 217.5 mv/kPa and the resolution is 0.2 Pa. The transducer is mounted 30 cm from the inlet of the Rijke tube and the thermocouple is located 35 cm from the inlet. The pressure data was acquired at a sampling frequency of 10 kHz for 3 seconds. The bin size for computing the FFT of the pressure time series signal was 0.3 Hz. Loudspeakers (Ahuja AU 60) are used to apply external noise and are located 62.5 cm from the inlet. Gaussian white noise is generated using LabVIEW Signal Express and is input to a loudspeaker through an amplifier.

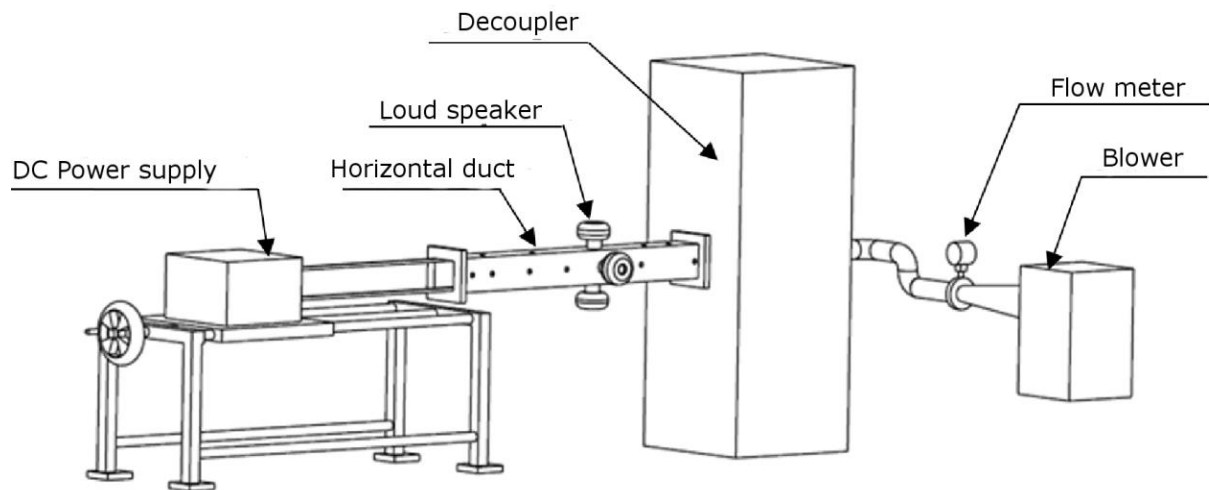


Figure: 3.1 Schematic of the experimental setup. A blower is used to provide the mean flow and a flow meter is used to measure the flow rate. A DC power supply unit is used to heat the wire mesh. The acoustic pressure is measured using piezoelectric transducers and the temperature is measured with the help of K- type thermocouple. A traverse mechanism is used to change the location of the electrical heater.

To ensure repeatability in ambient conditions between different experiments, a relative humidity level of $50 \pm 10\%$ and an ambient temperature of $19 \pm 3^\circ\text{C}$ were maintained at the laboratory

during all the experiments. To maintain the repeatability of the experiments, we maintained the cold decay rate value α at $15.0 \pm 1 \text{ s}^{-1}$ for all the experiments, thereby ensuring that the acoustic damping in the system remains nearly the same.

In order to measure the cold decay rate, the system is excited at the first eigenmode frequency of 155 Hz for a short duration in the absence of flow and with the heater switched off. Then the forcing is switched off and the logarithmic decay of the instantaneous acoustic pressure amplitude is calculated using the Hilbert transform of the pressure signal. The detailed procedure to determine the cold decay rate for a thermoacoustic system can be found in Mariappan (2011).

The influence of system parameters on the width of the bistable region is studied, by performing experiments where a bifurcation parameter is varied in fine steps. The bifurcation parameter is varied till the system attains its oscillatory state from steady state and then the bifurcation parameter is decreased in steps to bring the system back to steady state. When a particular parameter, say heater power, is chosen as the bifurcation parameter, the other parameters, say heater location, mass flow rate and cold decay rate are maintained constant during a single experiment. In the current study, the influence of heater power (K) and heater location (x_f) on the bistable characteristics of the system are investigated (reported in Chapter 3).

A bifurcation parameter is varied in a quasi-steady manner in each experiment and the variation of the acoustic pressure for each value of the system parameter is recorded. The median of the peak acoustic pressure P from the recorded pressure time series is calculated. A bifurcation plot depicting the variation of the median of peak acoustic pressure with heater power is obtained for each experiment. The width of the bistable zone is obtained from this bifurcation plot. Then the

non-dimensional width of the bistable zone χ which is defined as $(\mu_H - \mu_f)/\mu_H$, where μ_H & μ_f represent the system parameter values at Hopf point and fold point respectively.

In the set of experiments intended to study the effect of noise on the bistable characteristics of a horizontal Rijke tube, the heater power K is chosen as the bifurcation parameter (reported in Chapter 4). The non-dimensional noise intensity β was maintained constant during a specific experiment. The non-dimensional noise intensity β is defined as the ratio between the amplitudes of the applied noise and the limit cycle oscillations in the absence of noise. The procedure suggested by Jegadeesan (2012) is followed to determine the amplitude of the applied noise of a given intensity. In the experiments to determine the amplitude of the applied noise, the heater is located at the middle of the duct so that the system will not reach a state of limit cycle oscillations. The amplitude of the applied noise corresponding to a particular value of noise intensity is calculated by finding the median of the peak acoustic pressure measured in the presence of the noise of same intensity. Experiments are performed for different values of non-dimensional noise intensity, while keeping the mass flow rate constant. From these experiments, the variation of non-dimensional width of the bistable zone with non-dimensional noise intensity is obtained.

The experiments where we studied the effect of heater power and heater location on bistable characteristics are performed for eight different mass flow rates (\dot{m}) namely 1.25 g/s, 1.41 g/s, 1.56 g/s, 1.72 g/s, 1.88 g/s, 2.03 g/s, 2.19 g/s and 2.34 g/s. The set of experiments, where we studied the effect of noise intensity, is performed for four different mass flow rates 2.19 g/s, 2.34 g/s, 2.50 g/s and 2.97 g/s.

CHAPTER 4

THEORETICAL MODEL

This chapter focuses on the theoretical model used to investigate the effect of noise and system parameters on the bistable characteristics of a thermoacoustic system. The derivation of the theoretical model from the conservation equations are also described in this chapter along with the techniques employed for numerical integration.

In the current study, we modified the theoretical model proposed by Balasubramanian & Sujith (2008) to study the effect of external noise and system parameters on the bistable characteristics of a horizontal Rijke tube. The Balasubramanian- Sujith oscillator models the thermoacoustic oscillations in a horizontal duct open at both ends with a heated wire inside. The variation of temperature along the duct is neglected. The Mach number of the flow is assumed to be negligible which is relevant even for industrial combustors where the speed of sound will be much higher than the mean velocity of the flow.

Based on the low Mach number approximation, the governing equations are linearized and the linearized Partial Differential Equations (PDEs) are further converted to Ordinary Differential Equations (ODEs). The resulting ODEs are perturbed with Gaussian white noise to include the effect of fluctuations. The Stochastic Differential Equations (SDEs) are then numerically integrated.

4.1 Conservation equations of momentum and energy

The conservation equations of momentum and energy are written for a horizontal duct with a concentrated heat source. The variation of temperature along the length of the duct is considered to be negligible. The heat source is considered as a point source as the thickness of the heater is negligible compared to the characteristic length scales associated with acoustics.

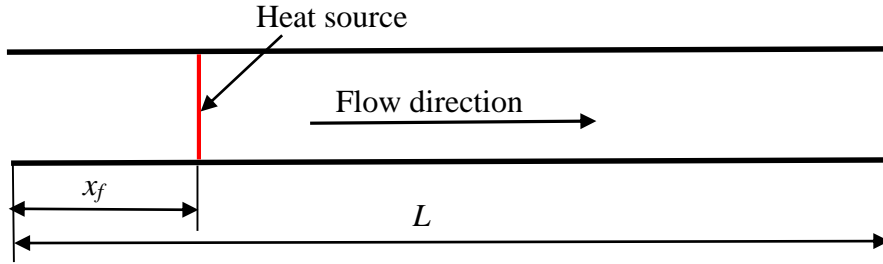


Figure 4.1: Schematic of the Rijke tube setup considered for numerical modelling. The thickness of the heater wire is negligible compared to the acoustic length scale L .

The conservation equations for the momentum and energy in one-dimension for the horizontal duct (Kundu & Cohen, 2004) shown in Fig. 4.1 will be

$$\tilde{\rho} \frac{\partial \tilde{u}}{\partial t} + \tilde{\rho} \tilde{u} \frac{\partial \tilde{u}}{\partial \tilde{x}} + \frac{\partial \tilde{p}}{\partial \tilde{x}} = 0 \quad (4.1)$$

$$\frac{\partial \tilde{p}}{\partial t} + \tilde{u} \frac{\partial \tilde{p}}{\partial \tilde{x}} + \gamma \tilde{\rho} \frac{\partial \tilde{u}}{\partial \tilde{x}} = (\gamma - 1) \tilde{\dot{Q}} \quad (4.2)$$

The ratio of specific heats is represented by γ . The quantities with tilde are dimensional. We decompose the pressure (\tilde{p}), density ($\tilde{\rho}$), velocity (\tilde{u}) and the heat release rate ($\tilde{\dot{Q}}$) into mean and fluctuating quantities. For example, the pressure is decomposed as $\tilde{p} = \bar{p} + \tilde{p}'$.

By neglecting the effect of mean flow (i.e; by employing zero Mach number approximation) (Nicoud & Wiecekorek, 2009), we get the following linearized equations

$$\bar{\rho} \frac{\partial \tilde{u}'}{\partial \tilde{t}} + \frac{\partial \tilde{p}'}{\partial \tilde{x}} = 0 \quad (4.3)$$

$$\frac{\partial \tilde{p}'}{\partial \tilde{t}} + \gamma \bar{p} \frac{\partial \tilde{u}'}{\partial \tilde{x}} = (\gamma - 1) \dot{\tilde{Q}}' \quad (4.4)$$

Mean density and mean pressure are represented by $\bar{\rho}$ and \bar{p} respectively. The acoustic velocity and the acoustic pressure are represented by u' and p' respectively. The length along the axial direction is represented by \tilde{x} and the time is represented by \tilde{t} . and $\dot{\tilde{Q}}'$ represents the unsteady heat release rate from the heat source.

In this theoretical model, modified King's law suggested by Heckl (1990) is used to model the unsteady heat release rate from the heater wire. The heat release rate $\dot{\tilde{Q}}'$ is represented by the following empirical model

$$\dot{\tilde{Q}}' = k \left[\sqrt{\left| \frac{u_0}{3} + u'_f(t - \tau) \right|} - \sqrt{\frac{u_0}{3}} \right] \delta(\tilde{x} - \tilde{x}_f) \quad (4.5)$$

where

$$k = \frac{2L_w(T_w - \bar{T})}{S\sqrt{3}} \sqrt{\pi \lambda C_v \bar{\rho} \frac{d_w}{2}} \quad (4.6)$$

L_w , d_w and T_w represent the length, diameter and the temperature of the heater wire. The mean temperature and the mean velocity are represented by \bar{T} and u_0 respectively. S represents the cross sectional area of the duct. The heat conductivity and specific heat at constant volume of the medium in the duct are represented by λ and C_V . The time delay between heat release rate fluctuations and acoustic velocity fluctuations is represented by τ . The term $u'_f(t-\tau)$ which represents the acoustic velocity at the heater location at a time $(t-\tau)$, is inside the square root in the heat release rate term. Thus, we have a square root nonlinearity present in the heat release rate term.

4.2 Non-dimensional equations

The following scales are used for converting the dimensional Eqns (4.3) and (4.4) to non-dimensional equations

$$x = \frac{\tilde{x}}{L}, \quad t = \frac{\tilde{t}}{L/c_0}, \quad u' = \frac{\tilde{u}'}{u_0}, \quad p' = \frac{\tilde{p}'}{\bar{p}}, \quad M = \frac{u_0}{c_0} \quad (4.7)$$

The speed of sound at mean temperature \bar{T} is represented by c_0 . The non-dimensional length and time scales are represented by x and t . The non-dimensional acoustic pressure and the non-dimensional acoustic velocity are represented by p' and u' respectively. Mach number is represented by M . By applying the scaling described in Eqn. (4.7) in Eqn. (4.5), the following non-dimensional partial differential equations are obtained (Balasubramanian & Sujith, 2008).

$$\gamma M \frac{\partial u'}{\partial t} + \frac{\partial p'}{\partial x} = 0 \quad (4.8)$$

$$\frac{\partial p'}{\partial t} + \gamma M \frac{\partial u'}{\partial x} = k \left[\sqrt{\left| \frac{1}{3} + u'_f(t - \tau) \right|} - \sqrt{\frac{1}{3}} \right] \delta(x - x_f) \quad (4.9)$$

The above set of PDEs (Eqns (4.8) and (4.9)) are reduced to ODEs by expanding the acoustic velocity and acoustic pressure in terms of basis functions using Galerkin technique (Lores & Zinn, 1973). The natural acoustic modes of the duct in the absence of heater are chosen as basis functions. The acoustic velocity and acoustic pressure can be expressed in terms of duct modes as (Balasubramanian & Sujith, 2008)

$$u' = \sum_{j=1}^{\infty} \eta_j \cos j\pi x \quad (4.10)$$

$$p' = \sum_{j=1}^{\infty} \frac{\gamma M}{j\pi} \dot{\eta}_j \sin j\pi x \quad (4.11)$$

Substituting Eqns. (4.8) and (4.9) into Eqns. (4.6) and (4.7) and projecting along the basis functions, the following ODE's are obtained.

$$\frac{d\eta_j}{dt} = \dot{\eta}_j \quad (4.12)$$

$$\frac{d\dot{\eta}_j}{dt} + 2\zeta\omega_j \dot{\eta}_j + \omega_j^2 \eta_j = \frac{-2k}{\gamma M} j\pi \left[\sqrt{\left| \frac{1}{3} + u'_f(t - \tau) \right|} - \sqrt{\frac{1}{3}} \right] \sin j\pi x_f \quad (4.13)$$

Here, η and $\dot{\eta}$ correspond to the time-varying coefficients of the acoustic velocity and the acoustic pressure in the Galerkin expansion. ω_j refers to the non-dimensional angular frequency of the j^{th} acoustic mode of a duct with open-open boundary condition. The details of non-dimensional

equations and the details of the Galerkin technique can be found in Balasubramanian & Sujith (2008).

To highlight the nonlinearity in the heat release rate, we expand the term $\sqrt{\left|\frac{1}{3} + u'_f(t - \tau)\right|}$ in Eqn.

(4.13) for small u_f ($|u_f| \leq 1/3$) as

$$\sqrt{\left|\frac{1}{3} + u'_f(t - \tau)\right|} = \frac{1}{3^{\frac{1}{2}}} (1 + 3u'_f(t - \tau))^{\frac{1}{2}} \quad (4.14)$$

The second term on the right hand side of Eqn. (4.14) when expanded using binomial expansion gives

$$(1 + 3u'_f(t - \tau))^{\frac{1}{2}} = \left[1 + \frac{3}{2}u'_f(t - \tau) - \frac{3}{8}(u'_f(t - \tau))^2 + \frac{3}{16}(u'_f(t - \tau))^3 - \dots \right] \quad (4.15)$$

Now the non-dimensional heat release rate can be written in terms of acoustic velocity at the heater location as

$$\dot{Q}' = \frac{k}{\sqrt{3}} \left[\frac{3}{2}u'_f(t - \tau) - \frac{3}{8}(u'_f(t - \tau))^2 + \frac{3}{16}(u'_f(t - \tau))^3 - \dots \right] \quad (4.16)$$

From Eqn. (4.16) it is clear that the non-dimensional heat release rate \dot{Q}' is nonlinear in acoustic velocity at the heater location $u'_f(t - \tau)$. When we substitute Eqn. (4.16) in Eqn. (4.13), we get

$$\begin{aligned} \frac{d\dot{\eta}_j}{dt} + 2\zeta\omega_j\dot{\eta}_j + \omega_j^2\eta_j \\ = \frac{-2k}{\sqrt{3}\gamma M} j\pi \left[\frac{3}{2}u'_f(t - \tau) - \frac{3}{8}(u'_f(t - \tau))^2 + \frac{3}{16}(u'_f(t - \tau))^3 - \dots \right] \sin j\pi x_f \end{aligned} \quad (4.17)$$

where,

$$u'_f(t-\tau) = \sum_{i=1}^N \eta_i(t-\tau) \cos i\pi x_f \quad (4.18)$$

Here, N represents the number of Galerkin modes considered. Thus, the evolution of the acoustic pressure is nonlinearly coupled with the evolution of the acoustic velocity at the heater. This nonlinear coupling makes the system exhibit rich dynamical behavior such as limit cycle oscillations, quasi-periodic oscillations and chaotic fluctuations (Subramanian *et al.*, 2010; Juniper, 2011; Waugh *et al.*, 2011). We have performed the binomial expansion to explicitly highlight the nonlinear terms. However, in the calculations, we have used the square root term as it is, without any simplifications.

The damping model used here is the same as that used by Matveev (2003), where

$$\zeta_j = \frac{1}{2\pi} \left[c_1 \frac{\omega_j}{\omega_l} + c_2 \sqrt{\frac{\omega_l}{\omega_j}} \right] \quad (4.19) \quad \omega_j = j\pi$$

Here, c_1 and c_2 are constants that determine the amount of damping. For all the simulations performed in the present study, the value of x_f is chosen as 0.25 and the values of damping coefficients c_1 and c_2 are 0.1 and 0.06 respectively. The value of the damping coefficient is selected such that it matches with the cold decay rate calculated from experiments.

The Balasubramanian-Sujith oscillator described by Eqns. (4.12) and (4.13) will show limit cycle oscillations when the phase difference between acoustic fluctuations and heat release rate fluctuations evolves to a value where the acoustic driving balances the damping (Balasubramanian & Sujith 2008). This will cause the saturation of acoustic velocity and acoustic pressure. Past studies have shown that this model has captured many of the dynamical features observed in experiments such as limit cycle oscillations, triggering and subcritical Hopf bifurcation

(Balasubramanian & Sujith, 2008; Subramanian *et al.*, 2010; Juniper, 2011). A good qualitative agreement exists between the results of the model and that obtained from experiments.

Waugh *et al.* (2011) and Waugh & Juniper (2011) extended the model proposed by Balasubramanian & Sujith (2008) to include the effect of noise. The numerical model that we use in the current study is similar to the one used by Waugh, Geuß & Juniper (2011) and Waugh & Juniper (2011). However, our model differs from the numerical model used by them in the numerical method used and also the manner in which noise is generated. Waugh & Juniper (2011) and Waugh *et al.* (2011) used colored noise and white noise to perturb the system and they considered the effect of both additive and multiplicative noise. They used a deterministic Runge-Kutta solver to integrate the deterministic system in time and at the end of each iteration, they added the noise increments generated by a general noise generating process. The type of white noise used by them had an amplitude spectrum of constant value of amplitude up to the frequency of the highest Galerkin mode, and after that the spectral content is zero (Waugh, 2012).

4.3 Stochastic delay differential equations

In the current analysis, the system of equations are treated as a system of stochastic delay differential equations (SDDE). The stochastic Runge-Kutta method is employed to integrate the SDDEs in time. Stochastic Runge-Kutta method uses the stochastic Taylor expansion of a function (Burrage, 1999; Kurtz, 2007; Picchini, 2007; Richardson, 2009). A step-by-step procedure of stochastic Runge-Kutta method as applied to a general stochastic differential equation is presented in the appendix. Additive Gaussian white noise is used to perturb the system. The increments in the white noise are generated from a Wiener process (Richardson, 2009). The white noise generated in our study has an amplitude spectrum of constant value of amplitude up to a non-

dimensional frequency of 50 which is higher than the dominant frequency by an order of magnitude. When we include additive Gaussian white noise in Eqn. (4.13), we have

$$\frac{d\eta_j}{dt} = \dot{\eta}_j \quad (4.19)$$

$$\frac{d\dot{\eta}_j}{dt} + 2\zeta\omega_j\dot{\eta}_j + \omega_j^2\eta_j = \frac{-2k}{\gamma M} j\pi \left[\sqrt{\frac{1}{3} + u'_f(t-\tau)} - \sqrt{\frac{1}{3}} \right] \sin j\pi x_f + \sigma\xi(t) \quad (4.20)$$

where σ represents the strength of the additive noise and $\xi(t)$ is the Gaussian white noise with zero mean and a variance proportional to square root of Δt , where Δt is the time step used in numerical integration. Eqns. (4.19) and (4.20) are integrated using stochastic Runge-Kutta method of 4th order to obtain the acoustic pressure and the acoustic velocity for a set of system parameters.

We find from the earlier numerical studies that including 20 modes (10 modes of η and 10 modes of $\dot{\eta}$) is adequate to capture the evolution of acoustic pressure and any further addition of modes will result only in marginal improvements (Subramanian *et al.*, 2010). We obtain the bifurcation plot for different values of the non-dimensional heater power while keeping the non-dimensional noise intensity β , a constant. Following this procedure, the bifurcation plots are obtained for different values of β .

We calculate the non-dimensional width of the bistable zone χ from each of the bifurcation plots and estimate the variation of the width of the non-dimensional bistable zone with non-dimensional noise intensity. Earlier study on the deterministic system shows that the time lag τ influences the width of the bistable zone in a significant manner (Subramanian *et al.*, 2010). Hence the variation of non-dimensional width of the bistable zone with the non-dimensional intensity of the additive noise is calculated for different values of time lag.

In spite of its simplicity, the numerical model employed here retains the essential features of a thermoacoustic system such as the nonlinearity of the heat release rate and the delay between the acoustic perturbations and the heat release rate fluctuations. Nevertheless, there are differences between the model and the experiments in features such as geometry of the heating element and the amount of mean flow. A mesh type heater is used in the experiments whereas heat transfer from a single cylindrical wire is considered in the numerical model. Further, the model does not account for radiative heat transfer. Due to the differences that exist between the model and experiments, a quantitative match in results is not expected.

CHAPTER 5

INFLUENCE OF SYSTEM PARAMETERS ON THE BISTABLE CHARACTERISTICS OF A HORIZONTAL RIJKE TUBE

The influence of system parameters such as heater power, heater location and mass flow rate on the bistable characteristics of a horizontal Rijke tube is presented in this chapter. We performed experiments by varying the bifurcation parameter while keeping the mass flow rate constant. Heater power and heater location are chosen as bifurcation parameters. From the time series of acoustic pressure acquired from experiments, bifurcation plots are obtained. Using the bifurcation plots, the influence of system parameters on the width of the bistable zone is investigated.

5.1 Effect of heater power on bistable characteristics

Here the effect of changing the heater power on the system dynamics is presented. Experiments were performed by slowly varying the power supplied to the electrical heater. The system was preheated for 20 minutes and the value of acoustic pressure amplitude (P) and the value of heater power (K) were noted down after preheating. The preheating was done in order to lessen the variations in temperature as the heater power is increased (Matveev, 2003). Thereafter, the heater power was increased in a quasi-steady manner. Input voltage to the electrical heater was increased in steps of 0.01 V which corresponds to an increase in electrical power of 2-3 W. If the heater power is increased rapidly, it can cause nonlinear triggering of instability (Matveev, 2003). To avoid this nonlinear triggering of instabilities, a settling time of 2 minutes is imposed between the power increments (Matveev, 2003; Mariappan, 2011).

During this time, the system achieves a stationary state which is confirmed by the steady temperature noted by the thermocouple. Power increment used in the current investigation is 2-3 W, which is comparable to the power increment used by Matveev (2003). However when the heater power was varied in a fine manner, we increment the power in steps of 0.5 W. Figure 3.1 shows the bifurcation diagram obtained by varying the heater power (K). The median value of the peak acoustic pressure (P) is plotted against the heater power (K). During the *forward path*; i.e., while K is increased, the system is stable till the point C which corresponds to a heater power of 337 W.

Further increase in heater power takes the system to a stable limit cycle (point D). From D to E , the amplitude of the limit cycle oscillations increases with increase in heater power. Once the system has reached point E , the heater power is decreased in steps of 2-3 W. The asymptotic state achieved by the system during the decrease of heater power is termed as the *return path*. The system continues in the state of stable limit cycle oscillations up to point F during the return path. When the heater power is reduced below 308 W, the system reverts back to the non-oscillatory state. In the forward path, the system is globally stable for low values of K (line AB). Region BC is termed as bistable where the system can be triggered to instability. Beyond the point C , the system is globally unstable. The difference observed between the forward path ($ABCDE$) and the return path ($EDFBA$) establishes the hysteresis zone. We can observe from Fig 5.1 that the system has two stable states in the region BC . One of the stable state happens to be the non-oscillatory state and the other one pertains to the state of stable limit cycle oscillations. It is to be noted that the system can be triggered to the state of stable limit cycle oscillations even when the system is linearly stable; i.e. even when we are in the forward path (Mariappan, 2011). Hence the system is said to be bistable in the regime BC . In general, the presence of bistability need not necessarily

ensure the presence of hysteresis and vice versa (Guidi & Goldbeter, 1997). However, in the Rijke tube system analysed in this thesis, we observe both bistability and hysteresis.

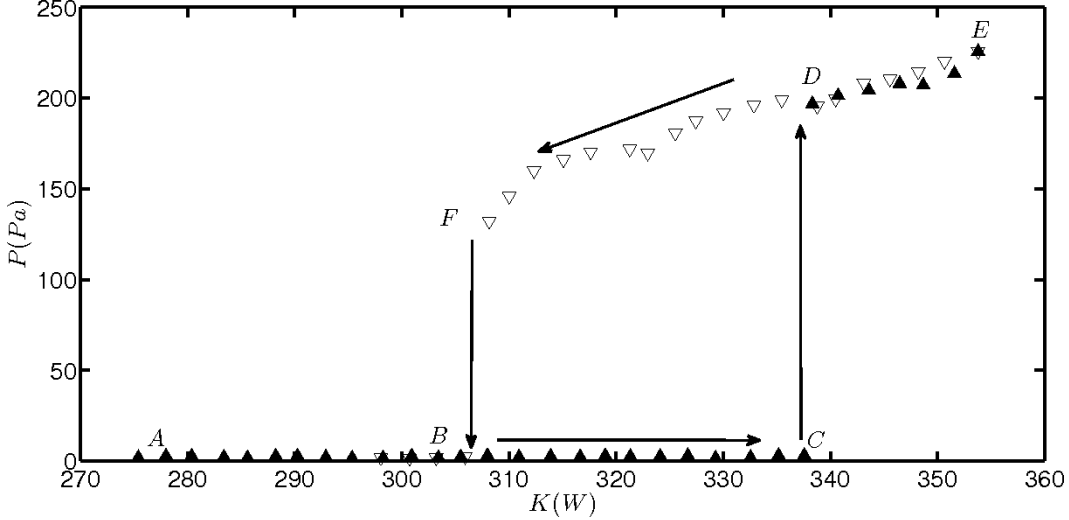


Figure 5.1: Experimental bifurcation diagram displaying the values of acoustic pressure P measured at $x = 30$ cm for a quasi-steady variation in the power supplied to heater K . The system undergoes a subcritical Hopf bifurcation at $K = 337$ W and a fold bifurcation at $K = 307$ W. $BCDF$ represents the bistable region where the system is in a bistable state. The heater is located at $x_f = L/4$. Mass flow rate $\dot{m} = 2.34$ g/s.
▲ - Increasing K , ▽ - Decreasing K .

The asymptotic state of the system can be understood by reconstructing the phase space from the acquired time series. The phase space of a dynamical system is the one which represents all possible states of the system. In general, the phase space will be an ' n ' dimensional vector space constructed using ' n ' state variables. The state variables can be identified from the governing equations of the system. If the governing equations are not known, the phase space can be constructed using indirect methods (Abarbanel & Gollub, 1996). One of them happens to be the method of using time-delayed vectors. These time-delayed vectors are constructed using Takens' embedding theorem, from the time series data of one of the physical variables (Takens, 1980). Time delayed vectors are constructed by calculating the optimum time delay. The dimension of

the reconstructed phase space will be determined by knowing the embedding dimension. The embedding dimension in the present case is determined by the method of False Nearest Neighbours (FNN). The technique of reconstruction of phase space from experimentally obtained time series data is explained by Kabiraj *et al.* (2012) and Nair *et al.* (2013) in the context of thermoacoustic instabilities.

The amplitude spectra of the pressure time series signal along with corresponding phase portrait is shown in Fig. 5.2 for a heater power value of 339 W. A prominent frequency of 168.8 Hz can be seen in the amplitude spectra and phase portrait shows a closed orbit which happens to be a limit cycle (Fig. 5.2b). It is worth mentioning that the prominent frequency 168.8 Hz in the amplitude spectra is nearly equal to the first acoustic mode of a half wave length resonator.

Presence of the bistable zone (Fig. 5.1) and the limit cycle in the reconstructed phase portrait (Fig. 5.2b) confirm that the bifurcation is subcritical Hopf bifurcation. In order to understand the effect of mass flow rate on the dynamics of the system, the experiment is performed for different mass flow rates. When the bifurcation plots for low and high mass flow rates are compared, the bistable zone is clearly visible in the case of high mass flow rates (Fig. 5.3c) whereas it becomes unobservable for low mass flow rates (Fig. 5.3b).

For low mass flow rates, the forward and reverse paths appear to merge together (Fig. 5.3a) and the bistable zone is not observable as in the case of high mass flow rates (Fig. 5.3c). Even though the bistable zone is not observable, a discrete jump in acoustic pressure can be seen during the transition for low mass flow rate (Fig. 5.3a). The sudden jump observed in the acoustic pressure confirms that the transition is subcritical even for low mass flow rates (Strogatz 2000). Since subcritical transitions are characterized by the presence of a bistable zone, experiments were

performed with fine variation in control parameter, to detect the bistable zone present near the transition point. The heater power is varied in a quasi-steady manner with a step size of 0.5 W. The bifurcation diagram with fine variation in heater power is depicted in Fig. 5.3b. We can observe from Fig. 5.3b that the bistable zone is clearly observable in the case of finer variation in control parameter.

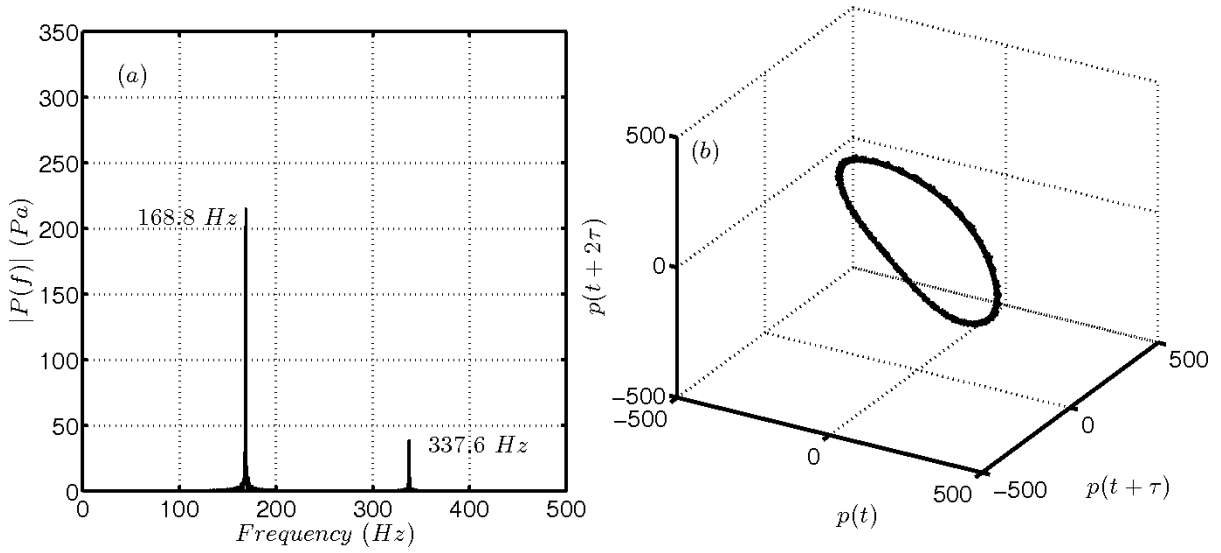


Figure 5.2: (a) The amplitude spectrum of the pressure time series showing distinct peaks indicating limit cycle oscillations. The bin size used is 0.3 Hz (b) Phase portrait reconstructed from pressure time series depicting an isolated closed orbit in the phase space. Heater power $K = 339$ W. The heater is located at $x_f = L/4$. Mass flow rate $\dot{m} = 2.34$ g/s.

Similar set of experiments were performed for mass flow rates 1.41 g/s, 1.56 g/s and 1.72 g/s. For all these four mass flow rates, i.e., for 1.25 g/s, 1.41 g/s, 1.56 g/s and 1.72 g/s the bistable zone is not detectable when the heater power is varied in a coarse manner with a step size of 2 W. However there exists a definite jump in the value of acoustic pressure near the transition. When the step size is reduced to 0.5W the bistable zone became clearly observable for all the four mass flow rates.

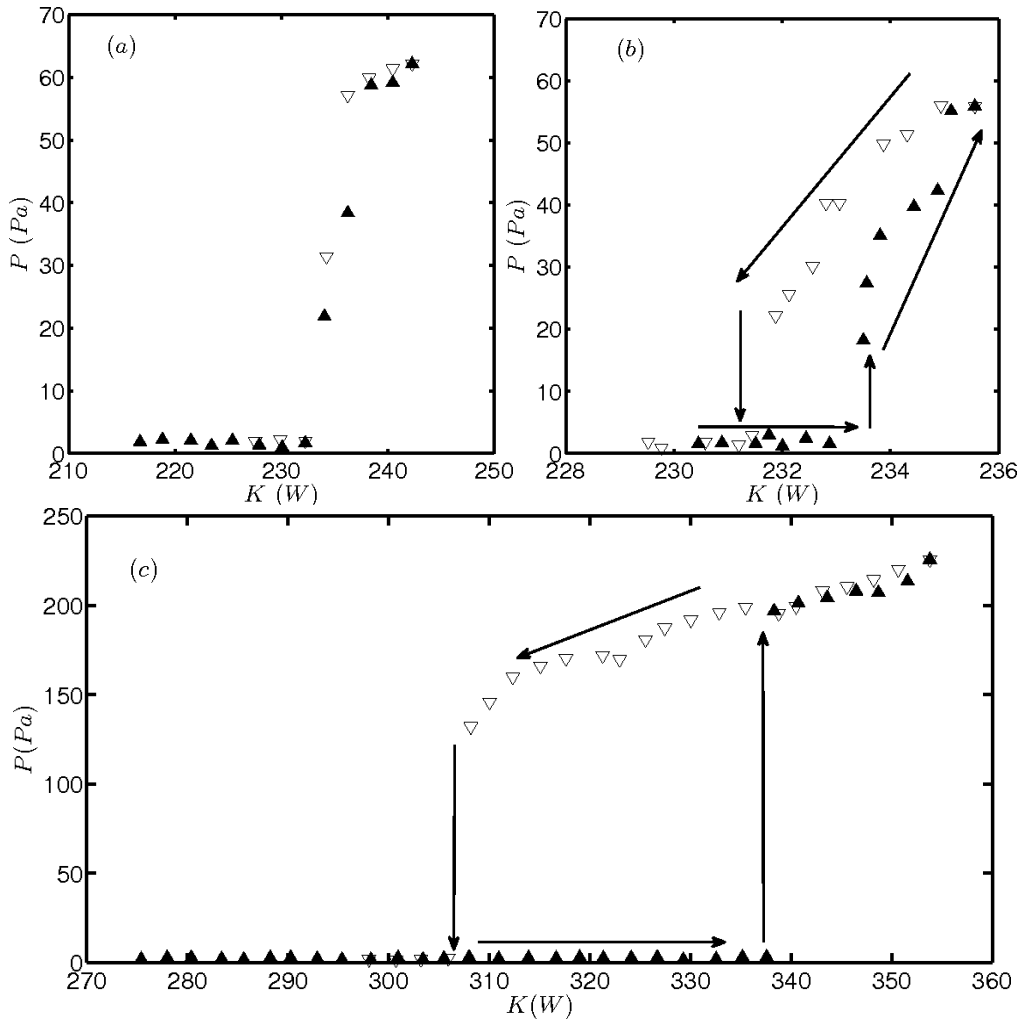


Figure 5.3: (a) Experimental bifurcation plot for mass flow rate $\dot{m} = 1.25$ g/s. The heater power is varied with a step size of 2 W. The bistable zone is not observable in this case, however there is a sudden jump in the value of acoustic pressure during the transition (b) Experimental bifurcation plot for mass flow rate $\dot{m} = 1.25$ g/s. The heater power is varied with step size of 0.5 W. The bistable zone is observable with this fine variation in the control parameter. (c) Experimental bifurcation plot for mass flow rate $\dot{m} = 2.34$ g/s. The heater power is varied with a step size of 2 W. The bistable region is clearly observable. The heater is located at $x_f = L/4$. \blacktriangle -Increasing K , ∇ -Decreasing K

5.2 Effect of heater location on bistable characteristics

The effect of heater location on the bistable characteristics of a horizontal Rijke tube is detailed here. Experiments were conducted by varying the heater location in a quasi-steady manner. The system was preheated for 20 minutes to reduce the variation in temperature along the duct. The heater was located at the inlet end before the start of the experiment. The value of the acoustic pressure amplitude (P) and the value of heater location (x_f) were recorded after preheating. The heater location was changed in steps of 1 cm and a settling time of one minute is chosen. The heater location is measured from the inlet. When the heater is located at the inlet end, x_f is considered as zero. The variation in the median value of the peak acoustic pressure with variation in heater location is shown in Fig. 5.4.

During the forward path, when x_f is increased, the system is stable until x_f becomes 19 cm. The system undergoes a Hopf bifurcation at $x_f = 19$ cm. Thereafter, the amplitude of pressure oscillations increases and reaches a maximum at $x_f = 33$ cm.

Further increase in x_f causes a decrease in the pressure amplitude and the system goes back abruptly to the steady state when $x_f = 36$ cm. While in the reverse path, when x_f is decreased, the system remains stable till $x_f = 29$ cm. When the heater is located at 29 cm away from the inlet, the system undergoes a Hopf bifurcation and reaches a state of stable limit cycle oscillations. As the heater is moved towards the inlet, x_f is decreased; the amplitude of oscillations decreases and the system reverts to the steady state when the heater is located at 18 cm away from the inlet. A clear bistable zone is present near the second Hopf point (29 cm). Although the bistable zone is not observable near the first Hopf point (19 cm) for coarse variation in heater location, a definite jump in the value of acoustic pressure near the transition point can be observed. However with fine variation in heater

location, the bistable zone near the first Hopf point also becomes detectable as shown in the inset of Fig. 5.4.

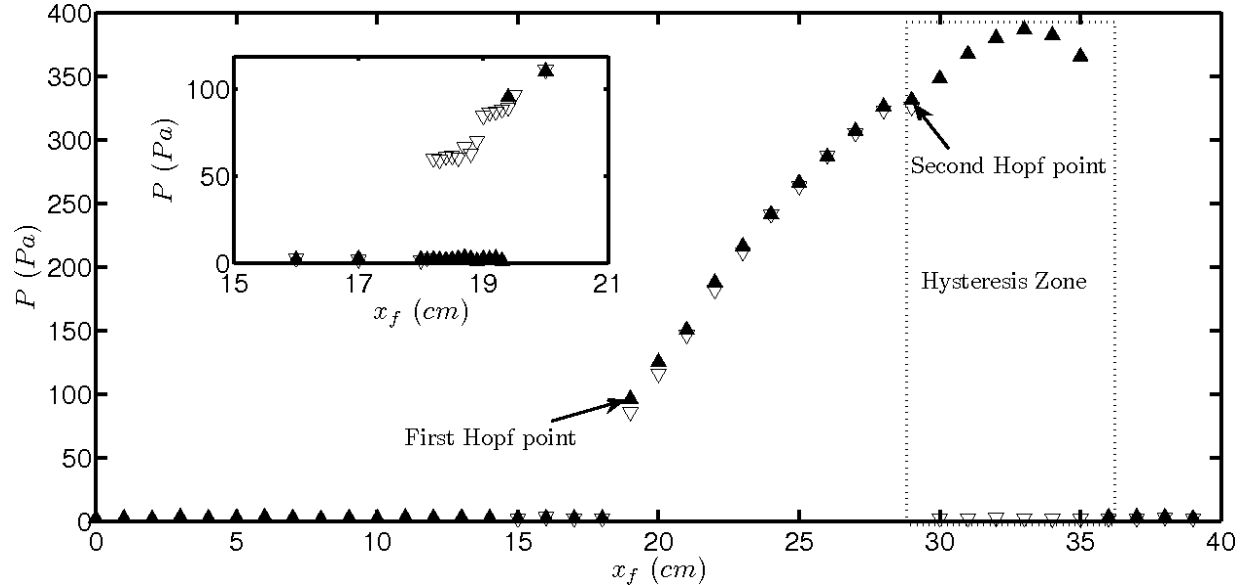


Figure 5.4: Experimental bifurcation diagram displaying the values of acoustic pressure at $x = 30$ cm for a quasi-steady variation in the heater location x_f . Subcritical Hopf bifurcation happens at $x_f = 19$ cm during the forward path and at $x_f = 29$ cm during the reverse path. Bistable zone near the second Hopf point is observable with coarse variation in heater location and the bistable zone near the first Hopf point is shown only with fine variation in heater location (see inset). The heater power $K = 423$ W. Mass flow rate $\dot{m} = 2.34$ g/s. \blacktriangle - Increasing x_f , ∇ - Decreasing x_f

Figure 5.5 shows the Fourier transform of the pressure signal and phase portrait of the system when the heater is located at 19 cm; i.e., at the first Hopf point. The FFT shows a prominent frequency of 169 Hz and the phase portrait is a limit cycle. Just as in the case of heater power, here also the prominent frequency corresponds to the first acoustic mode of a duct with open-open boundary condition. From the presence of a prominent frequency in FFT and the appearance of limit cycle in the phase portrait, we can conclude that the bifurcation occurring at $x_f = 19$ cm is Hopf bifurcation.

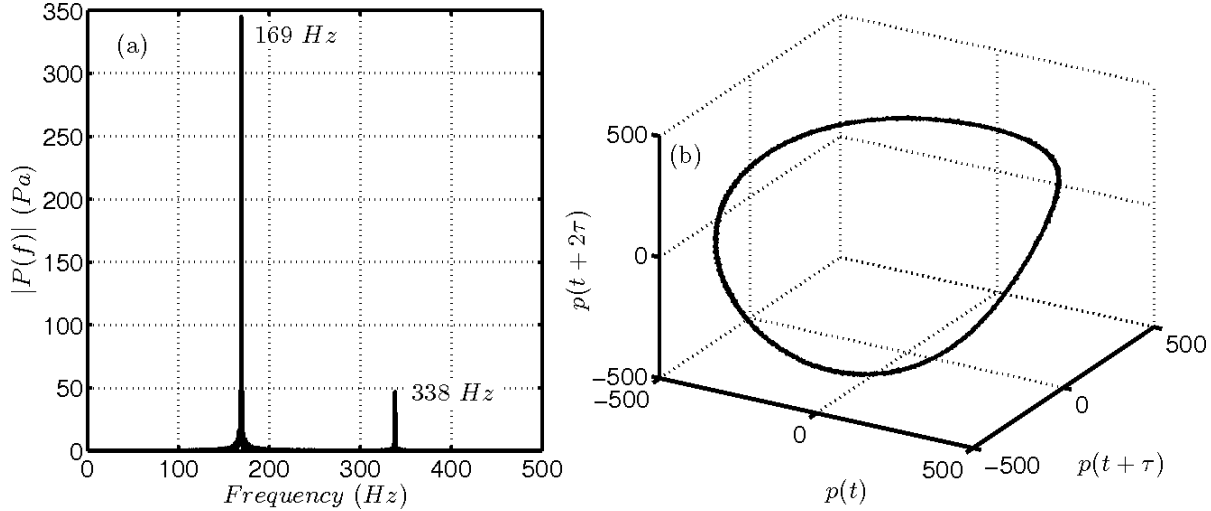


Figure 5.5: (a) The amplitude spectrum of the pressure time series showing distinct peaks indicating limit cycle oscillations. The bin size used is 0.3 Hz (b) Phase portrait reconstructed from pressure time series depicting an isolated closed orbit in the phase space. Heater is located at $x_f = 19 \text{ cm}$. Heater power $K = 423 \text{ W}$. Mass flow rate $\dot{m} = 2.34 \text{ g/s}$.

During the return path, the FFT shows a prominent frequency and the phase portrait is a limit cycle when the heater is located at 29 cm (Fig. 5.6). The presence of a prominent frequency along with the presence of a limit cycle indicates that the system undergoes Hopf bifurcation during the return path. The presence of the bistable zone along with the presence of discrete jump in the value of acoustic pressure near the transition point indicates that the transition is subcritical for both first and second Hopf points (19 cm and 29 cm). The presence of two Hopf points and the subcritical nature of transition observed at both of them is consistent with the results reported by Subramanian *et al.* (2010).

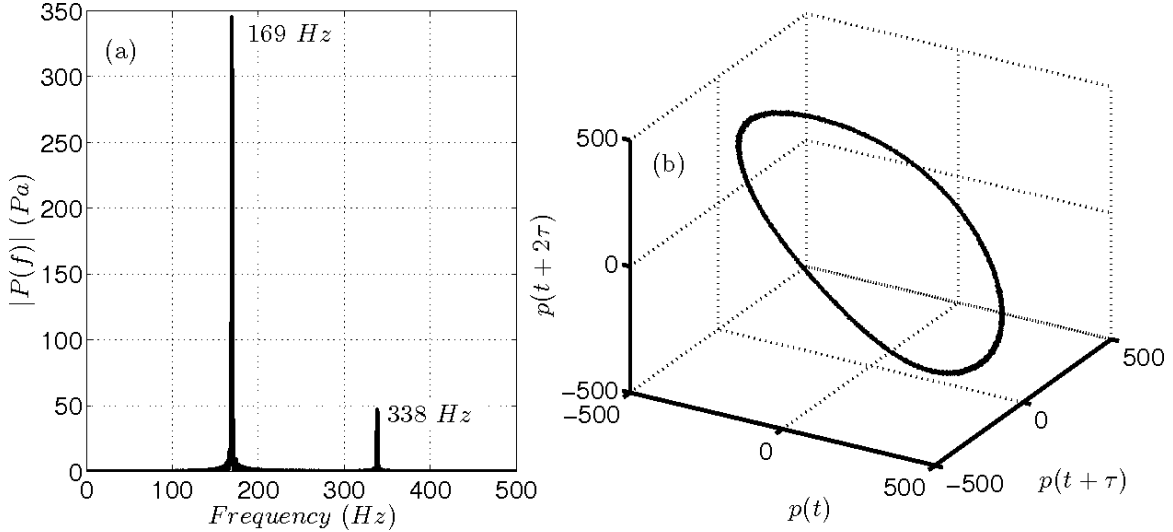


Figure 5.6: (a) The amplitude spectrum of the pressure time series showing distinct peaks indicating limit cycle oscillations. The bin size used is 0.3 Hz (b) Phase portrait reconstructed from pressure time series depicting an isolated closed orbit in the phase space. Heater is located at $x_f = 29 \text{ cm}$. Heater power $K = 423 \text{ W}$. Mass flow rate $\dot{m} = 2.34 \text{ g/s}$.

The experiments where we study the effect of heater location were performed for different values of mass flow rate. A comparison between the bifurcation diagrams obtained for 1.25 g/s (Fig. 5.7a) and for 2.34 g/s (Fig. 5.7b) is shown in Fig. 5.7.

When the mass flow rate is decreased, the bistable zone near the second Hopf point becomes undetectable and the forward and reverse paths appear to merge together. Even when the bistable zone becomes undetectable, a definite jump in the amplitude of acoustic pressure is seen during transition and the observed jump is sufficiently above the noise floor. This jump observed in the amplitude of acoustic pressure confirms that the transition is subcritical (Strogatz, 2000). The variation in the control parameter, heater location, is made finer to detect the bistable zone as in the case of heater power. As the heater location is varied in a finer manner, with a step size of 1 mm, near the Hopf point, the bistable zone becomes observable for the case of 1.25 g/s .

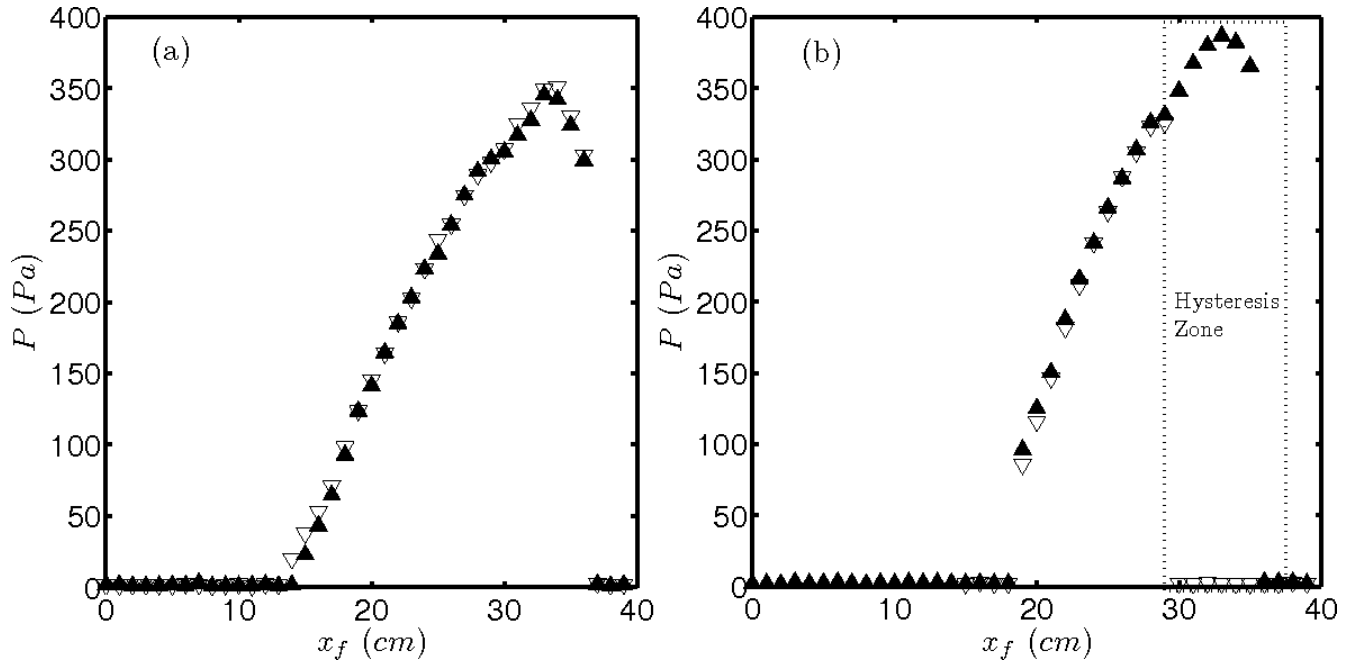


Figure 5.7: Experimental bifurcation diagrams displaying the variation of acoustic pressure P at $x = 30$ cm with a quasi-steady variation of heater location x_f (a) for mass flow rate $\dot{m} = 1.25$ g/s and (b) for mass flow rate $\dot{m} = 2.34$ g/s. The bistable zone is not observable for $\dot{m} = 1.25$ g/s whereas the bistable zone is observable for $\dot{m} = 2.34$ g/s. The heater power $K = 423$ W. \blacktriangle - Increasing x_f ; ∇ - Decreasing x_f .

The bifurcation diagrams with fine variation in control parameter are shown in Fig. 5.8. It is observed that the bistable zone is detectable for a fine variation of the control parameter. Since the width of the bistable zone is much smaller than the overall range in which the control parameter is varied, only the portion of the bistable zone near the Hopf point is shown in Fig. 5.8. Even for a low mass flow rate of 1.25 g/s, we can conclude that the transition to instability is clearly subcritical when the heater location is chosen as the control parameter. The subcritical nature of the transition to instability is confirmed by the presence of bistable zone and a discrete jump in the values of acoustic pressure during transition (Fig. 5.8 a & b) (Strogatz, 2000).

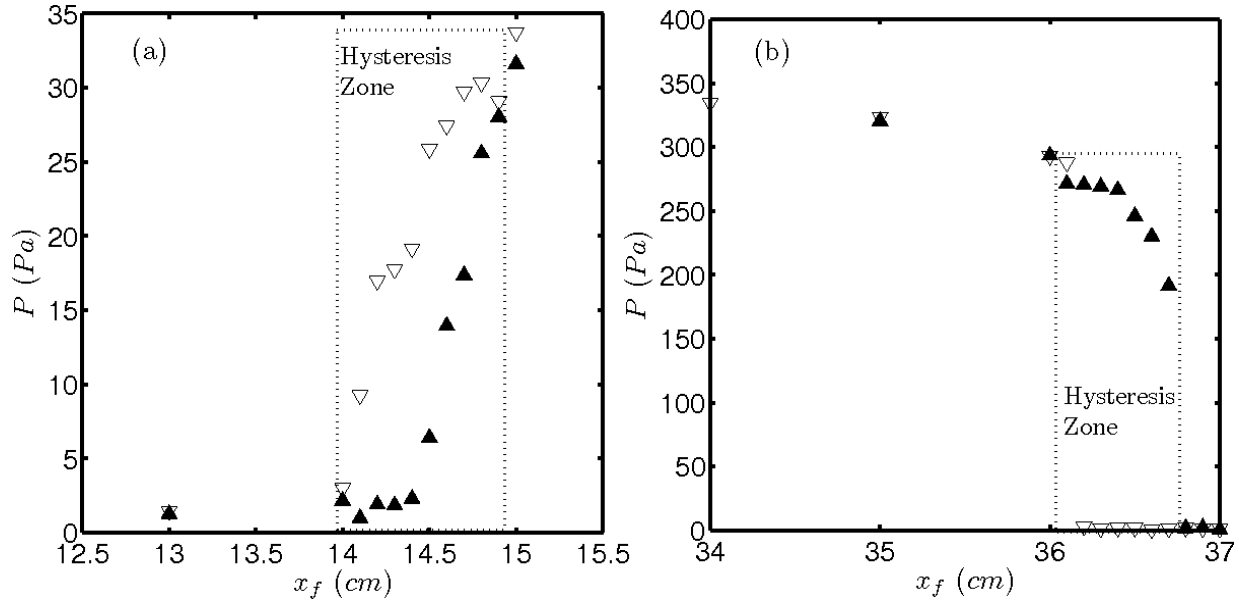


Figure 5.8: Experimental bifurcation diagram displaying the values of acoustic pressure at $x = 30$ cm versus the location of the heater (a) near the first Hopf point and (b) near the second Hopf point. Heater location is varied in fine steps of 1 mm. With this fine variation in heater location, the bistable zones at first and second Hopf points become observable. The heater power $K = 423$ W. Mass flow rate $\dot{m} = 1.25$ g/s. ▲ - Increasing x_f ; ▽ - Decreasing x_f

The experiment is performed for different mass flow rates by varying the heater location in a fine manner. We find that a bistable zone of definite width exists even for very low mass flow rates. However, for the case of low mass flow rates, the bistable zone is often perceptible only when the parameter variation is made finer.

The experiment was performed for a mass flow rate of 2.97 g/s to understand the system dynamics at a higher mass flow rate. The power supplied to the heater in the earlier experiments was found to be insufficient to make the system unstable at a mass flow rate of 2.97 g/s. So the heater power is increased from its previous value of 423 W to 482 W. Since the heater power was changed, the results for the mass flow rate of 2.97 g/s are presented separately. It can be observed that there are

two distinct regimes of heater location for which oscillations are present (Regions 1&2 in Fig. 5.9).

The absence of oscillations near the open end is due to the fact that the acoustic pressure becomes zero at the open end. Since the acoustic velocity becomes zero at $L/2$, thermoacoustic instability does not occur as the heater is moved near this point. For the heater power value (482 W) used in the present study, instability did not occur when the heater was located beyond $L/2$. When the heater is located at 8 cm from the inlet, the system undergoes a subcritical Hopf bifurcation. The subcritical nature of transition can be confirmed by the discrete jump in the value of acoustic pressure when x_f is 8 cm (Region 1 in Fig. 5.9).

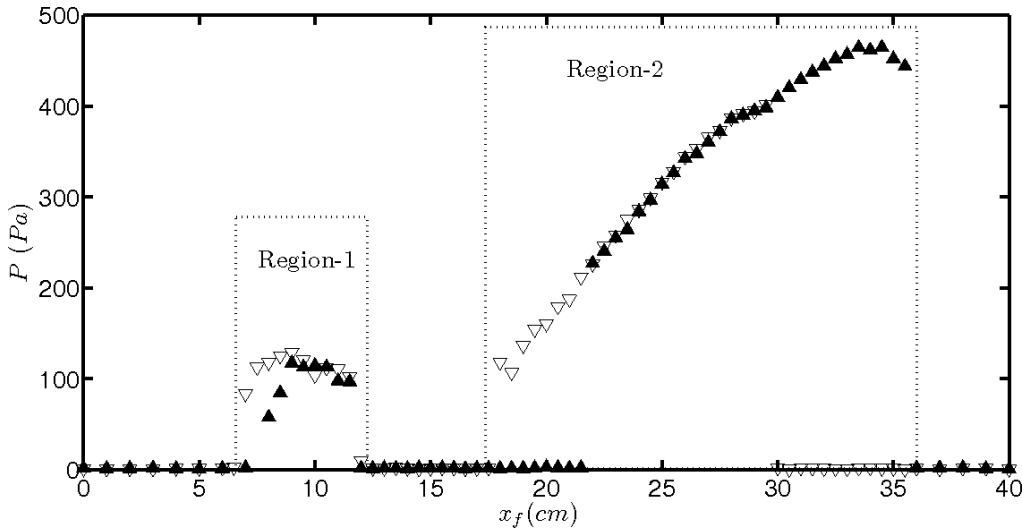


Figure 5.9: Experimental bifurcation diagram displaying the variation of acoustic pressure P at $x = 30$ cm for a quasi steady variation in the heater location x_f for a mass flow rate of $\dot{m} = 2.97$ g/s. Two distinct regions of instability can be seen. The bifurcations that happen in both region-1 and region-2 are subcritical Hopf bifurcations confirmed by the presence of bistable zones. The heater power $K = 482$ W. \blacktriangle -Increasing x_f ; ∇ - Decreasing x_f

Figure 5.10 shows the Fourier transform of pressure time series and the corresponding reconstructed phase portrait when the heater is located at 8 cm away from the inlet. The presence of a distinct frequency of 352.8 Hz which is approximately equal to the frequency of the second

acoustic mode of a half wavelength resonator (Fig. 5.10a) and the presence of a limit cycle in the reconstructed phase portrait (Fig. 5.10b) confirm that the system undergoes a subcritical Hopf bifurcation.

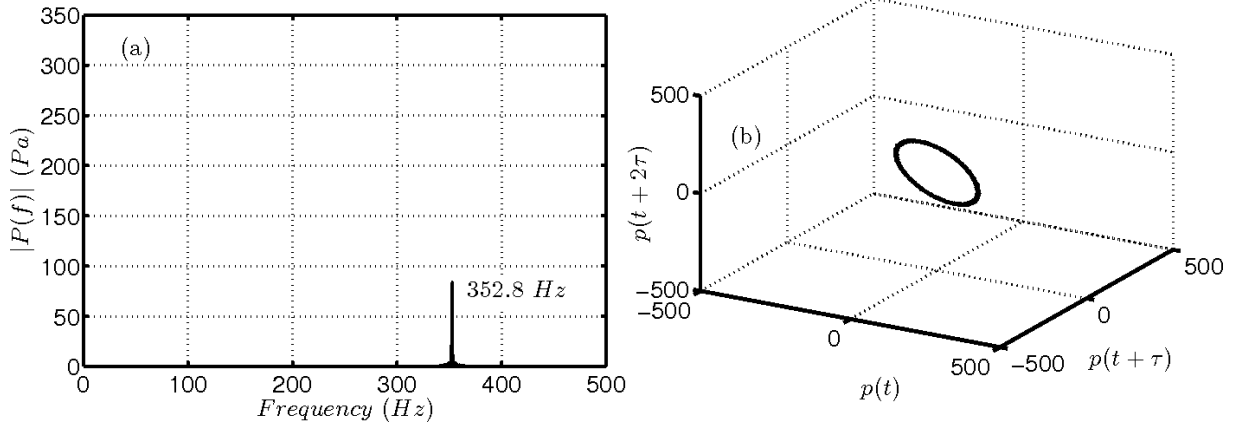


Figure 5.10: (a) The amplitude spectrum of the pressure time series showing distinct peak indicating limit cycle oscillations. The bin size used is 0.3 Hz (b) Phase portrait reconstructed from pressure time series depicting an isolated closed orbit in the phase space. Heater is located at $x_f = 8 \text{ cm}$. Heater power $K = 482 \text{ W}$. Mass flow rate $\dot{m} = 2.97 \text{ g/s}$.

Figure 5.11 depicts the local maxima of the pressure time series with heater location, for forward path (Fig. 5.11a) and for reverse path (Fig. 5.11b). It can be observed that the local maxima has a single value till $x_f = 9 \text{ cm}$ during the forward path and till $x_f = 8.5 \text{ cm}$ during the reverse path. After that two branches are born. The presence of two distinct branches is a characteristic feature of period-2 oscillations (Strogatz, 2000). These two branches represent the two distinct values of local maxima of pressure time series. Before the onset of period-2 oscillations, the acoustic pressure has single local maxima. Once the period-2 oscillations set in, the local maxima of pressure time series has 2 distinct values. It should be observed that till $x_f = 9 \text{ cm}$ in the forward path and till $x_f = 8.5 \text{ cm}$ during the reverse path, the second mode alone is linearly unstable in Region-1. Whereas after the heater locations 9 cm and 8.5 cm in the forward and reverse paths

respectively, first mode also becomes linearly unstable which gives rise to the occurrence of period-2 oscillations. Thus Region-1 in Fig.5.9 has two sub-regions in it, in one of which the second mode is unstable. This sub-region where the second mode is unstable extends up to $x_f = 9$ cm in the forward path and till $x_f = 8.5$ cm during the reverse path. In the second sub-region (for x_f values from 9.5 cm to 11.5 cm in the forward path and for x_f values from 8.5 cm to 11.5 cm in the reverse path), the system remains in a state of period-2 oscillations.

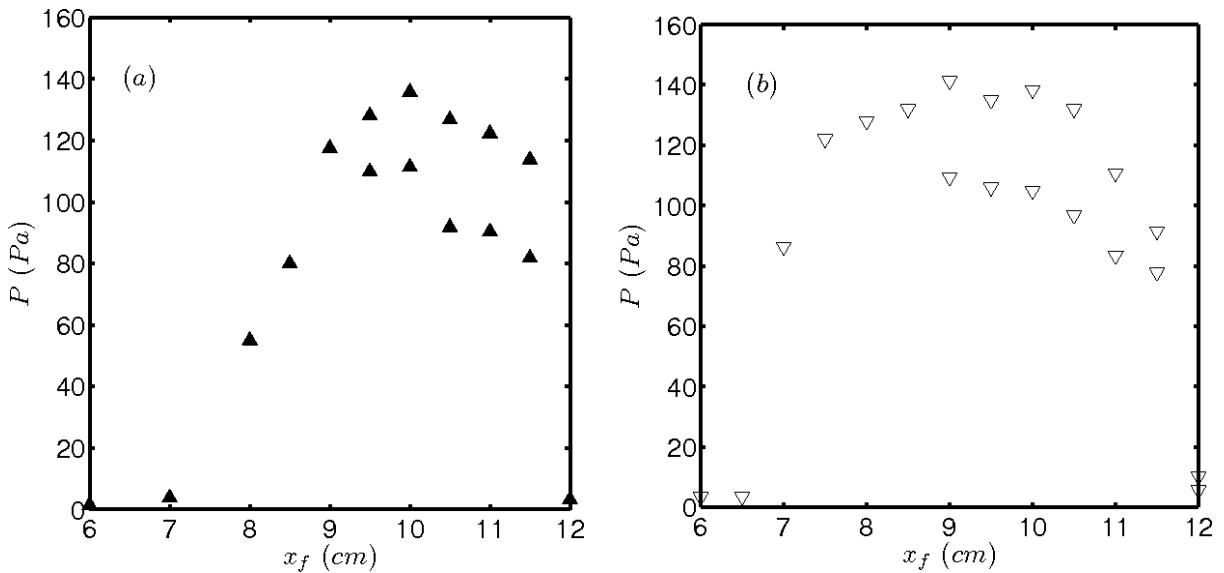


Figure 5.11: Variation of peak pressure P at $x = 30$ cm for a quasi steady variation of the heater location x_f (a) during the forward path (b) during the return path showing the presence of period-2 oscillations for a mass flow rate $\dot{m} = 2.97$ g/s. $K = 482$ W. ▲-Increasing x_f . ▽-Decreasing x_f

The presence of period-2 orbit can be clearly seen in Figure 5.12. A new frequency of the oscillations of value 176.4 Hz which is quite close to the frequency of first acoustic mode gets introduced as the heater is moved from 9.5 cm to 10 cm (Fig. 5.12a). The value of the new frequency happens to be exactly half of the existing one. This marks the onset of period-2

oscillations. The phase portrait pertinent to the aforementioned heater location represents a double loop (Fig. 5.12b).

The presence of a period-2 orbit is in agreement with the observations made by Subramanian *et al.* (2010); they reported the presence of a period-2 orbit for a non-dimensional heater location of 0.1. The length of the Rijke tube used in the present study is 1 m, thus the non-dimensional heater location at which period-2 orbit is found happens to be 0.095. This is quite close with the value reported by Subramanian *et al.* (2010).

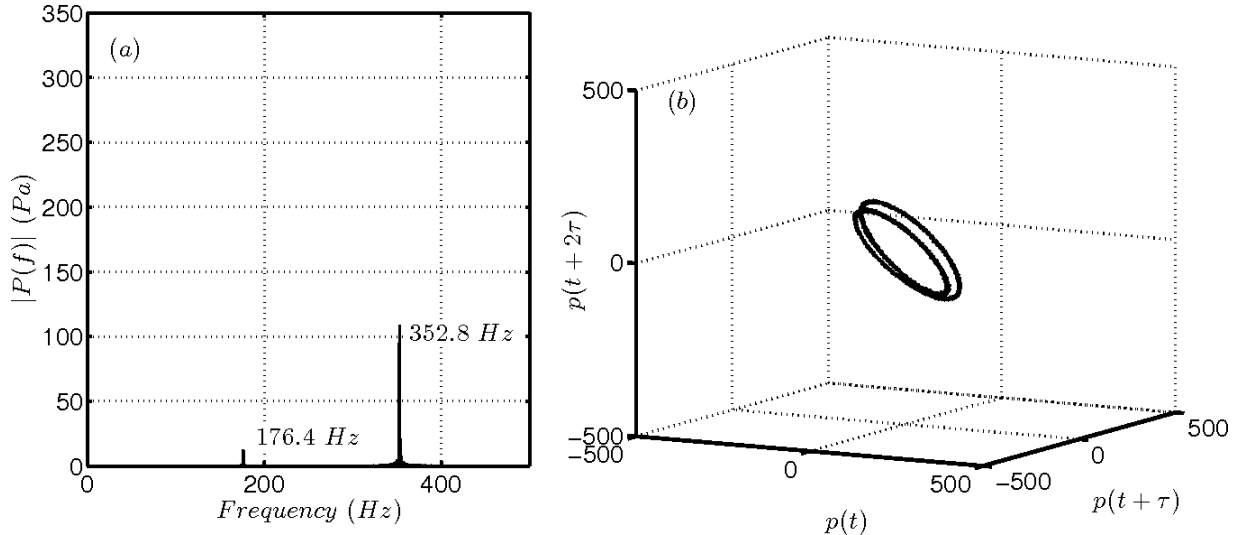


Figure 5.12: (a) The amplitude spectrum of the pressure time series showing distinct peaks at f and $f/2$, where f is 352.8 Hz, indicating period-2 oscillations. The bin size used is 0.3 Hz (b) Phase portrait reconstructed from pressure time series depicting a double loop in the phase space. Heater is located at $x_f = 10$ cm. Heater power $K = 482$ W. Mass flow rate $\dot{m} = 2.97$ g/s.

5.3 Variation of the width of the bistable zone with Strouhal number

In this section, the variation in the width of the bistable zone with Strouhal number is discussed, when any of the control parameter, say heater power or heater location, is changed continuously

while the other parameter is maintained constant. The variation of non-dimensional width of the bistable zone with Strouhal number is shown in Fig. 5.13. Non-dimensional width of the bistable zone and Strouhal number are calculated as follows

$$\text{Non-dimensional width of the bistable zone} = \chi = |\mu_H - \mu_f| / \mu_H \quad (5.1)$$

$$\text{Strouhal number} = \{\text{Flow time scale/ Acoustic time scale}\} = S_t \quad (5.2)$$

$$\text{Flow time scale} = d_w \rho A / \dot{m} \quad (5.3)$$

$$\text{Acoustic time scale} = 2L / c_0 \quad (5.4)$$

μ_H is the parameter value at the Hopf point and μ_f is the parameter value at the fold point. Speed of sound at ambient temperature is represented by c_0 and d_w represents the diameter of the heater wire. Mean density is represented by ρ , A represents the area of the duct and the length of the duct is L .

Flow time scale is the time scale dictated by the mean flow velocity and the diameter of the heater wire. The significance of this flow time scale can be understood by the fact that the dynamics of the Rijke tube is influenced by both the mean flow velocity and the diameter of the heater wire.

It is interesting to note that the variation of the non-dimensional width of the bistable zone as a function of Strouhal number is nearly identical for both heater power and heater location. The width of the bistable zone decreases with increase in Strouhal number for both heater power and for heater location. Nevertheless, even for high values of Strouhal number, there exists a definite bistable zone which indicates that the transition to instability is subcritical in nature (Fig.5.13a) for the range of parameters covered in this study. The uncertainty in non-dimensional width of the bistable zone for heater power and heater location happens to be 0.003 and 0.004 respectively. The minimum non-dimensional width of the bistable zone reported is 0.006 in the case of heater power

and 0.016 in the case of heater location; these minimum values are well above the uncertainties involved in the measurements.

Figure 5.13b shows the variation of non-dimensional width of the bistable zone with Strouhal number in a log-log scale. It can be seen that there is a linear relation between non-dimensional width of the bistable zone and Strouhal number up to a Strouhal number value of 0.33. This is suggestive of a power law dependence of width of the bistable zone on Strouhal number in the range of Strouhal numbers from 0.24 to 0.33. A vertical dashed line marks the end of the Strouhal number regime where power law dependence of width of the bistable zone is present.

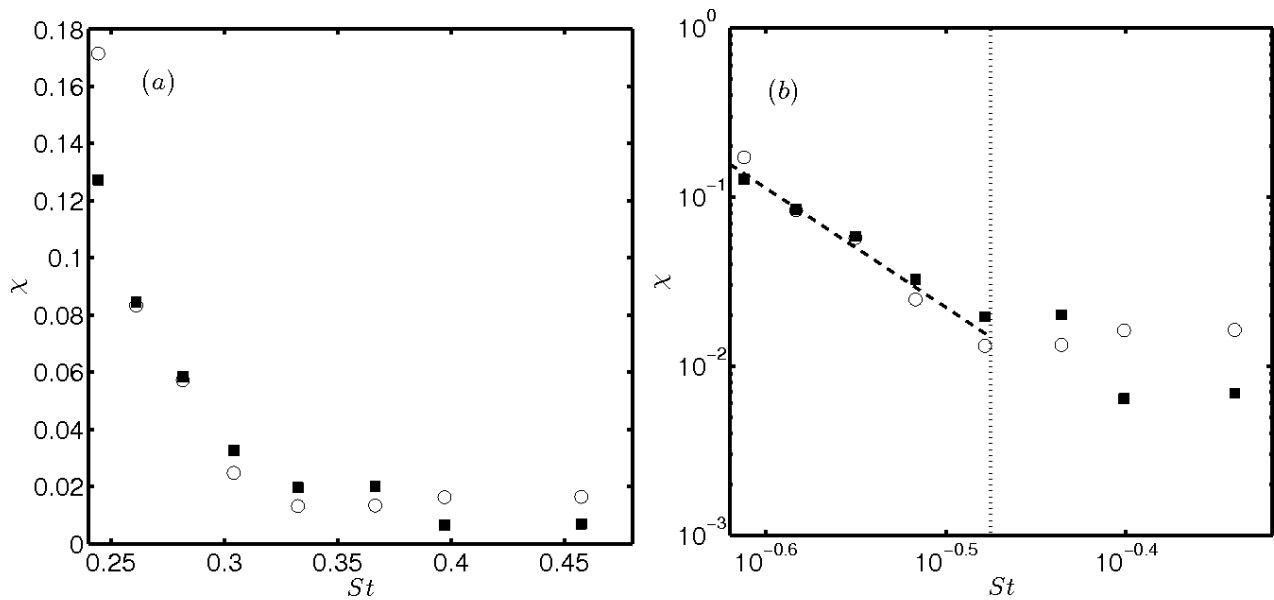


Figure: 5.13 Variation of non-dimensional width of the bistable zone χ with Strouhal number St shown in (a) Linear scale and in (b) Log-Log scale. It can be seen that the non-dimensional widths of the bistable zones are same for heater power and heater location for a range of Strouhal numbers and there exists a power law relation.
■-Heater power, ○-Heater location.

5.4 Concluding remarks

The heater power and the heater location were varied systematically, one at a time, in the present study. It is found that the width of the bistable zone decreases as the mass flow rate is decreased. The presence of the bistable zone along with a finite jump in the acoustic pressure near the transition point indicates that, irrespective of the value of mass flow rate, the transition is subcritical in all the experiments we performed. For low mass flow rates, although the bistable zone was observed only when the control parameter was varied in a fine manner a finite jump in acoustic pressure near the transition point is always present. Moreover a power law relation is established between non-dimensional width of the bistable zone and Strouhal number. It is extremely important to ensure that the variation in the parameter is fine enough before a bifurcation can be attributed as supercritical. However, the current results do not preclude the possibility of observing supercritical bifurcation in a horizontal Rijke tube.

We find that the non-dimensional widths of the bistable zone in the case of heater power and heater location are the same for a range of Strouhal numbers. This equivalence suggests a universal bifurcation behaviour which needs to be investigated in detail. When heater location was chosen as the control parameter, period-2 oscillations were observed for some specific values of heater power and mass flow rate. The presence of period-2 oscillations is suggestive of a period doubling route to chaos, however detailed experimental studies need to be performed in order to ensure the same. In summary, this work emphasises the need to thoroughly investigate the presence of bistable region before pronouncing a bifurcation as supercritical.

CHAPTER 6

EFFECT OF NOISE ON THE BISTABLE CHARACTERISTICS OF A HORIZONTAL RIJKE TUBE

The effect of noise on the bistable characteristics of a prototypical thermoacoustic system, a horizontal Rijke tube is presented in this chapter. We perform bifurcation experiments in the presence of noise to determine the influence of noise on the width of the bistable zone. We also study the effect of noise in a theoretical model perturbed with additive Gaussian white noise. We compare the results obtained from the experiments with that obtained from the theoretical model.

6.1. Reduction in the width of the bistable zone in the presence of external noise

The bifurcation diagram depicting the variation of the median value of the peak acoustic pressure with heater power for a mass flow rate of 2.34 g/s, in the absence of external noise is presented in figure 6.1(a). A clear bistable zone and an abrupt jump in the value of acoustic pressure can be observed in the bifurcation plot, which confirms that the bifurcation is subcritical under this condition. Furthermore, the amplitude spectra shows a prominent frequency (figure 6.1(b)) and the reconstructed phase portrait shows an isolated closed orbit which represents a limit cycle (figure 6.1(c)). The details of phase space reconstruction from an experimentally obtained time series data can be found in Abarbanel (1996) and its application to a thermoacoustic system is presented in Kabiraj & Sujith (2012). The subcritical bifurcation observed here is in agreement with the

experimental and numerical results reported in the past (Matveev, 2003; Balasuramanian & Sujith, 2008; Subramanian *et al.*, 2010; Juniper, 2011; Mariappan, 2011).

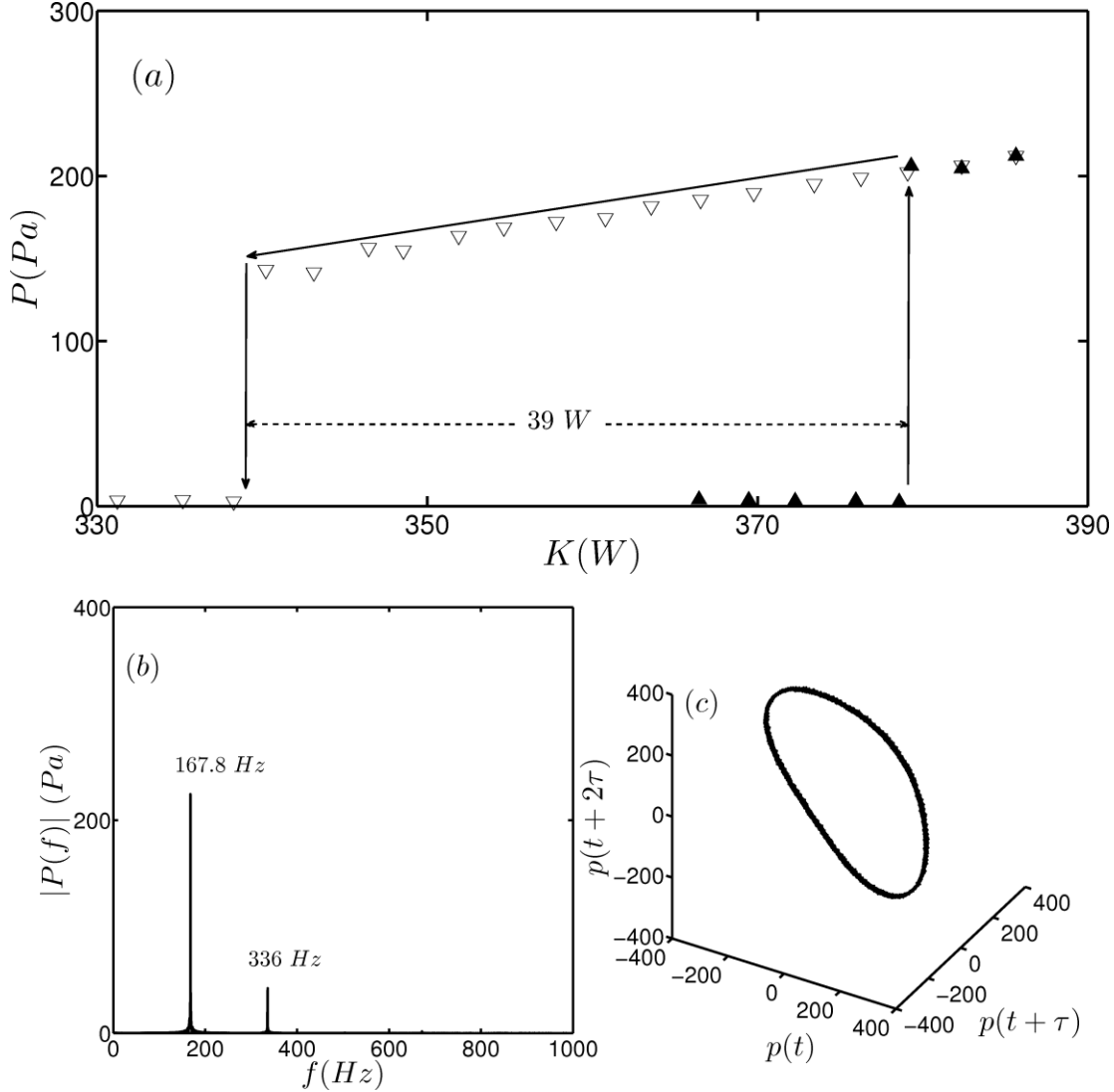


Figure 6.1 (a) Bifurcation diagram, obtained from experiments, depicting the variation of the median value of the peak acoustic pressure P with heater power K for mass flow rate $\dot{m} = 2.34$ g/s. Here, the transition to instability occurs via a subcritical Hopf bifurcation at the heater power $K = 380$ W. (b) The amplitude spectrum of the pressure time series, showing distinct peaks indicating limit cycle oscillations. The bin size used is 0.3 Hz. (c) Phase portrait reconstructed from pressure time series depicting an isolated closed orbit in the phase space. The experiment is conducted in the absence of external noise. ▲ - Forward path; ▽ - Reverse path.

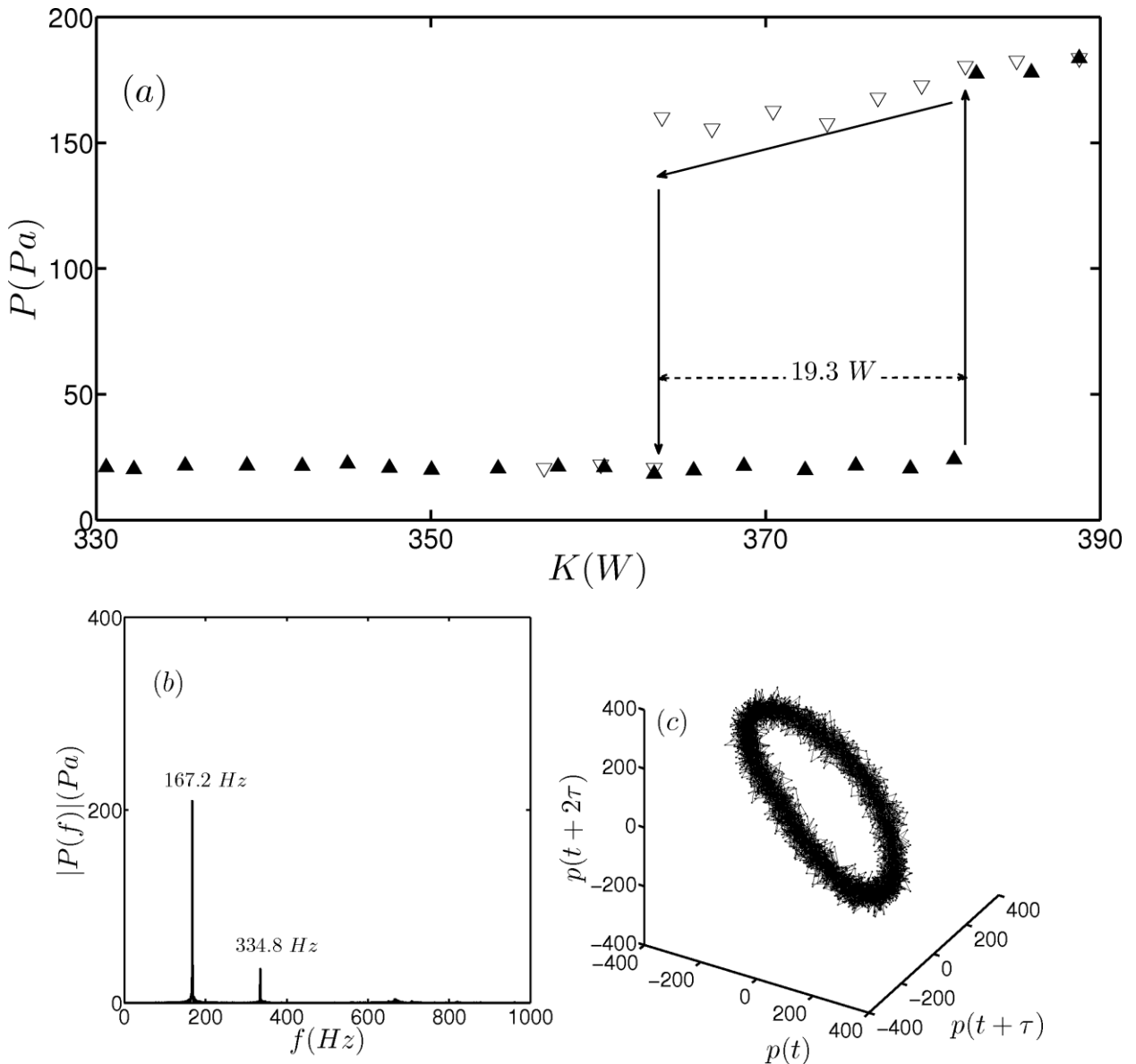


Figure: 6.2 (a) Bifurcation diagram, obtained from experiments, depicting the variation of the median value of the peak acoustic pressure P with heater power K , for a mass flow rate of $\dot{m} = 2.34$ g/s. Here, the transition to instability happens via a subcritical Hopf bifurcation at the heater power $K = 382$ W. (b) The amplitude spectrum of pressure time series, showing sharp peaks indicating limit cycle oscillations. (c) Phase portrait reconstructed from pressure time series, depicting an isolated closed orbit in the phase space. The experiment is performed in the presence of external noise of amplitude 10.5 Pa. ▲ - Forward path; ▽ - Reverse path.

Experiments were performed to investigate the effect of external noise on system dynamics. The bifurcation diagram, amplitude spectra and the reconstructed phase portrait in the presence of external noise of amplitude 10.5 Pa are shown in figures 6.2(a – c) respectively. It can be seen that the bifurcation remains subcritical in the presence of external noise of amplitude 10.5 Pa. Even in the presence of noise of 10.5 Pa, the change in frequency of oscillations is only 0.6 Hz which is of the order of the resolution of the FFT. Due to the presence of noise, the trajectories are spread out which is indicated by the increased thickness of the limit cycle (figure 6.2(c)). Further, we observe a reduction in the width of the bistable zone from 39 W to 19.3 W when external noise is applied.

It is worth mentioning that Waugh & Juniper (2011) in their numerical study reported that “*As the noise strength increases, the system becomes practically unstable further from the Hopf point, increasing the region where triggering may occur. As the noise strength increases further, the system can be dislodged from the stable periodic solution to the zero solution*”. Thus, from the work of Waugh & Juniper (2011) it can be inferred that the width of the bistable region decreases with increase in the intensity of the applied noise although they have not stated it explicitly or quantified it. Our observation of the reduction in the width of the bistable zone in the presence of Gaussian white noise is the first of its kind in experimental results reported in thermoacoustic literature. However, outside the context of thermoacoustics, a reduction in the width of the bistable zone in the presence of noise is observed in various dynamical systems (Sastry & Hijab, 1981; Coullet *et al.*, 1985; Geier *et al.*, 1985; Altares & Nicolis, 1988; Lekkas *et al.*, 1988; L’Heureux & Kapral, 1989; Fedotov *et al.*, 2002; Berthet *et al.*, 2003).

Experiments were performed at various noise levels for different mass flow rates to confirm the reduction in the width of the bistable zone. The noise level is increased with a step size of 1 Pa. Similarly, the variation of non-dimensional width of the bistable zone with the intensity of additive

Gaussian white noise is calculated from the theoretical model for different values of time lag τ . The time lag τ can be related to the mean flow using Lighthill's estimate of $0.2d_w/u_0$. Here, d_w refers to the diameter of the heater wire and u_0 refers to the mean flow velocity (Lighthill, 1954; Subramanian *et al.*, 2013).

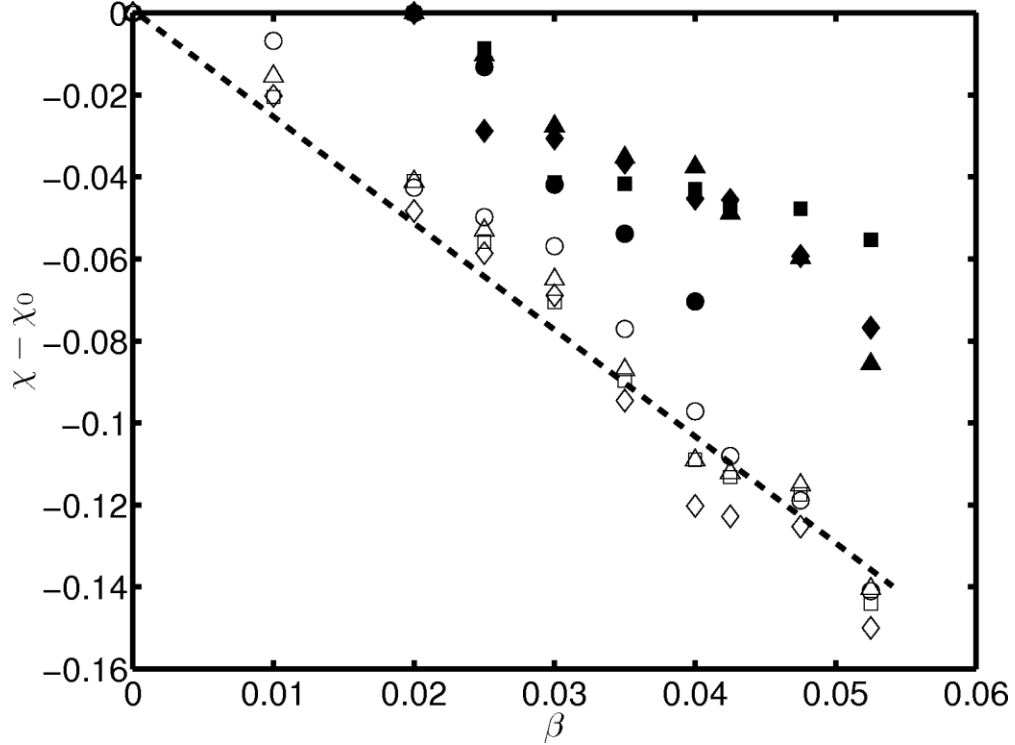


Figure: 6.3 Variation of non-dimensional width of the bistable zone ($\chi - \chi_0$) calculated from experimental and numerical results with non-dimensional noise intensity β for different mass flow rates \dot{m} and for different time lags τ . The width of the bistable zone decreases with increase in noise intensity in both experiments and in numerical simulations. The rate of decrease is constant for all mass flow rates and for all time lags. Nevertheless, for the noise levels mentioned here, the transition remains subcritical both in experiments and in numerical simulation. ● - $\dot{m} = 2.19$ g/s, ■ - $\dot{m} = 2.34$ g/s, ▲ - $\dot{m} = 2.50$ g/s, ♦ - $\dot{m} = 2.97$ g/s. ○ - $\tau = 0.2$, □ - $\tau = 0.175$, Δ - $\tau = 0.15$, ◇ - $\tau = 0.125$.

Figure 6.3 shows the variation of the non-dimensional width of the bistable zone with non-dimensional noise intensity calculated from the experiments and from the numerical model. The non-dimensional width of the bistable zone, in the absence of externally added noise, is denoted by χ_0 . The uncertainty in non-dimensional width of the bistable zone ($\chi - \chi_0$) is 0.008 and in the non-dimensional intensity of noise is 0.001. Inherent fluctuations are present in the experimental system even in the absence of external noise and these fluctuations correspond to a non-dimensional noise intensity of 0.02. As a consequence, in Fig. 6.3 there is no experimental data corresponding to zero noise intensity. For noise amplitudes up to a threshold, a definite bistable zone exists, indicating a subcritical Hopf bifurcation. Nevertheless the width of the bistable zone decreases as the noise intensity increases. A linear decrease in the width of the bistable zone with increase in the intensity of the applied noise is observed both in the results from experiments and from the numerical model. Further, the rate of decrease is independent of the values of mass flow rates and the values of the time lag.

6.2. Suppression of bistable zone in the presence of high amplitude noise

Here, the effect of high amplitude noise on the bistable characteristics is described. Figure 6.4 represents the variation of non-dimensional acoustic pressure with non-dimensional heater power for different values of non-dimensional noise intensity. Acoustic pressure is made non-dimensional by dividing it with the mean pressure both in case of experiments and in case of theoretical model.

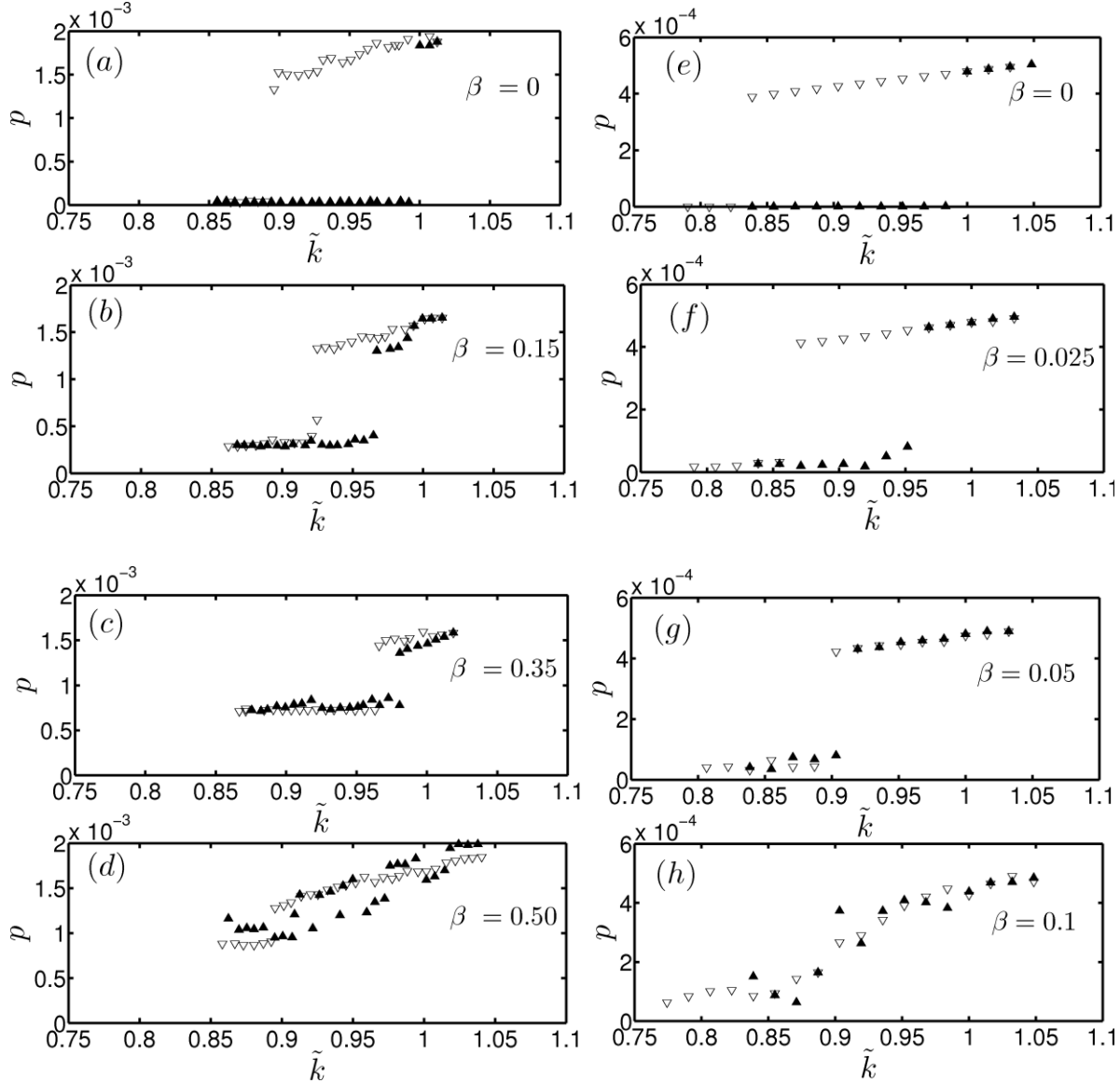


Figure: 6.4 Bifurcation diagrams, obtained from experiments (a-d) and from numerical model (e-h) depicting the variation of median value of peak non-dimensional acoustic pressure p with normalized non-dimensional heater power \tilde{k} (normalized by the value of heater power at the Hopf point in the absence of noise) for different values noise intensities. Here, β refers to the non-dimensional noise intensity. We can observe a change in the nature of transition and suppression of bistable region as the intensity of the external noise increases in experimental results. Although the pressure amplitudes differ in magnitude, a qualitatively similar behavior is observed in the case of numerical model. Note that the ordinates are different. ▲ - Increasing \tilde{k} ; ▽ - Decreasing \tilde{k} .

The heater power K , in experiments is made non-dimensional by dividing it with the value of heater power at the Hopf point in the absence of external noise. In case of numerical model, the heater power k is non-dimensional to begin with. The value of k is normalized by dividing it with the value of non-dimensional heater power at the Hopf point in the absence of noise.

Figures 6.4(a-d) represent the changes that happen with increasing noise intensity in experiments. The transition to instability is subcritical in the absence of external noise (figure 6.4(a)). When the non-dimensional noise intensity becomes 0.15, we observe a reduction in the width of the bistable zone (figure 6.4(b)). With further increase in the non-dimensional noise intensity to 0.35, there is a further reduction in the width of the bistable zone and the transition to instability becomes less abrupt (figure 6.4(c)). When the non-dimensional noise intensity is as high as 0.5, the bistable zone is no longer discernable and there is no jump in the value of acoustic pressure (figure 6.4(d)).

Figure 6.4 (e-h) shows the variation of non-dimensional acoustic pressure with non-dimensional heater power for the theoretical model for various values of noise intensity. Similar to the experimental results, in the absence of noise, the transition is subcritical (figure 6.4(e)). We observe that the width of the bistable zone decreases with increase in noise intensity (figure 6.4(f)). With further increase in noise intensity, the transition starts to become continuous (figure 6.4(g)) and once the noise intensity becomes high, there is no visible bistable zone (figure 6.4(h)). Transition to instability can no longer be termed subcritical as the bistable zone is no longer discernable. Even when the transition is continuous there is no perfect overlap between forward and reverse paths (figure 6.4f). This is due to the fact that each realization of a stochastic process will be different even when all the system parameters are maintained constant. It is to be noted that, in the case of numerical simulation, qualitatively similar trends with experiments are observed for lower values of non-dimensional noise intensities.

In the presence of high intensity noise, the system oscillates between a stable oscillatory state and a stable non-oscillatory state. This is referred to as *flickering* in the literature on the critical transitions observed in eco systems (Scheffer *et al.*, 2009; Dakos *et al.*, 2012). This flickering makes the transition continuous and the bistable region becomes indiscernible. The two features that help us to distinguish a subcritical transition are the presence of the bistable zone and an abrupt jump in the order parameter (acoustic pressure amplitude in the present case). As these two features become imperceptible beyond a critical noise threshold, we cannot attribute the transition as subcritical. This suppression of the subcritical nature of transition is in complete agreement with the earlier experimental and numerical observations on the effect of noise on nonlinear oscillator models (Sastry & Hijab, 1981; Juel *et al.*, 1997; Zakharova *et al.*, 2010).

The histograms of the pressure time series, both from experiments and from numerical model, just at the onset of instability for various values of external noise are shown in Fig.6.5 to understand the change in the nature of distribution of pressure values in a single time series of acoustic pressure. The histogram is constructed by determining the number of data points N in the pressure time series having a non-dimensional pressure amplitude $p \pm \Delta p$, where Δp refers to the width of the bin. In the absence of external noise, the distribution is bimodal with peaks situated away from the mean. When we increase the intensity of external noise, there is an increase in the spread of the distribution and a decrease in the height of the peaks. The values near the mean become more probable as the external noise amplitude is increased. Both experimental and numerical results depict the same behavior.

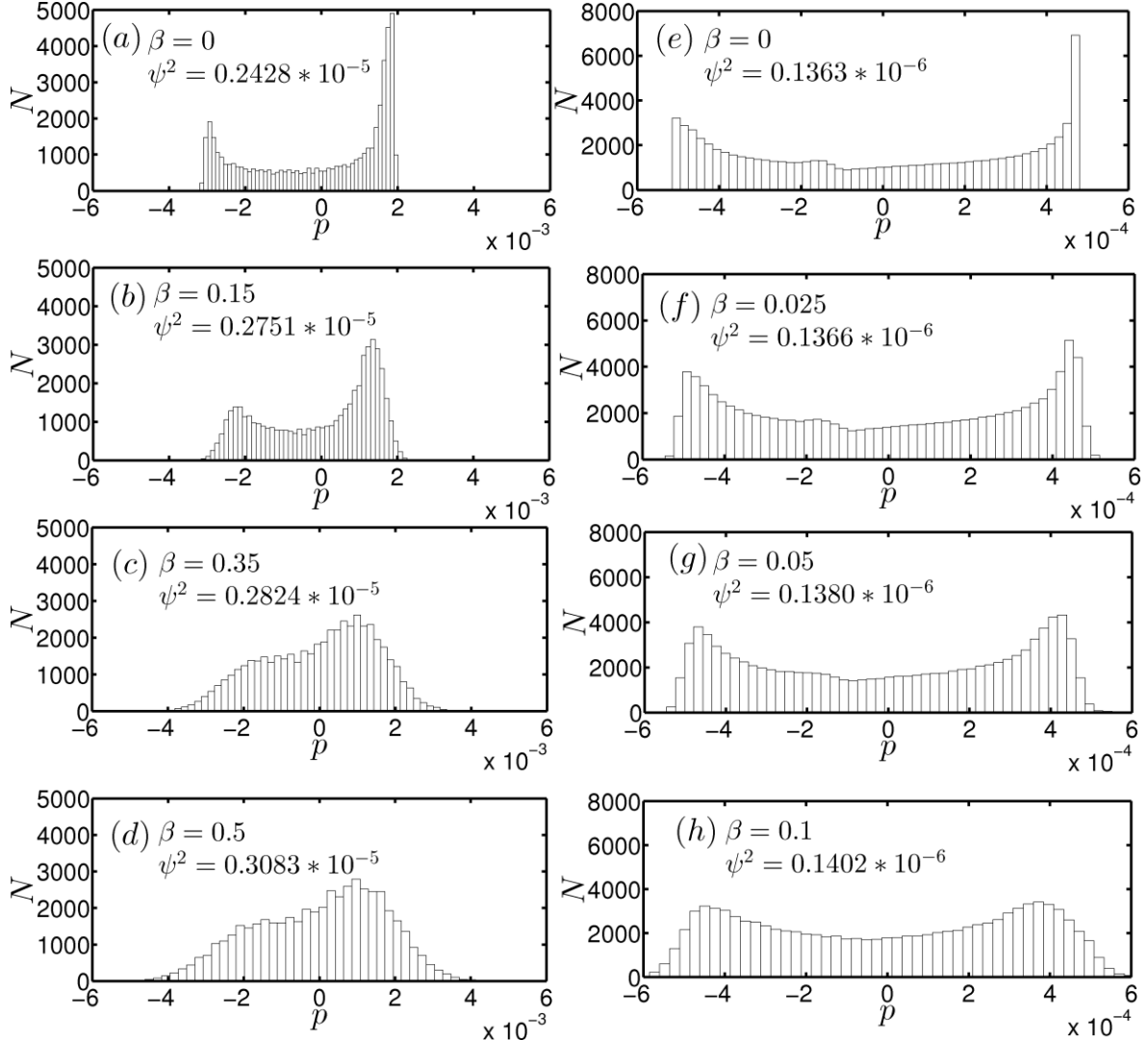


Figure: 6.5 Histogram of pressure time series at the onset of instability for experimental (a-d) and numerical (e-h) results for various values of noise amplitude. Here, β refers to the non-dimensional noise intensity. N represents the number of data points in the pressure time series with a non-dimensional pressure p . ψ^2 represents the variance of the pressure time series. We can see an increase in the spread of the distribution with increase in external noise amplitude, both in case of experimental and numerical results. The increase in the spread is confirmed by the increasing value of variance with increase in noise amplitude. The experimental and numerical results differ in magnitude; however, we intend a qualitative comparison rather than a quantitative one. Note that the abscissas are different by an order of magnitude.

This change in the distribution of the order parameter (acoustic pressure amplitude in our case) in the presence of high amplitude noise in bistable dynamical systems is reported outside the context of thermoacoustics (Juel *et al.*, 1997; Deco & Marti, 2007). The change from an abrupt transition to a continuous transition in the presence of high amplitude noise indicates that it will be difficult to identify subcritical transitions that happen in a practical thermoacoustic system working in an environment with turbulent fluctuations.

6.3. Concluding remarks

In the present chapter, noise induced transitions that can happen in a nonlinear system, in the context of a horizontal Rijke tube is presented. It is found that even an external noise of amplitude two orders of magnitude less than the limit cycle amplitude can significantly influence the dynamical features of a thermoacoustic system. The experimental and numerical investigations show that the presence of noise reduces the width of the bistable region. The rate of decrease in non-dimensional width of the bistable zone is linear with noise strength and it is nearly the same for both experimental and numerical results. We observed that the rate of decrease of non-dimensional width of the bistable zone with noise level is independent of the mass flow rate and the time lag. We found that in the presence of high intensity noise, the system exhibits the phenomenon of flickering. This flickering makes the transition continuous and there is a complete suppression of the bistable region.

CHAPTER 7

STOCHASTIC BIFURCATION OBSERVED IN A HORIZONTAL RIJKE TUBE

This chapter discusses the stochastic bifurcation that is observed in the horizontal Rijke tube. The stochastic bifurcation is characterized by analyzing the changes in the stationary probability distribution of acoustic pressure amplitude. The stationary probability distribution is obtained from the Fokker-Planck equation. A simple theoretical model which encompasses the essential features of a thermoacoustic system is considered to obtain Fokker-Planck equation.

7.1 Background

The addition of noise in the normal form equation of Hopf bifurcation changes the dynamics of the system and introduces novel dynamical states (Sastry & Hijab, 1981). The presence of additive or parametric noise can also induce global asymptotic stability in prototypical dynamical systems. The phenomenon of noise induced stability is observed for both supercritical and subcritical Hopf bifurcations (Mackey *et al.*, 1989). In the case of Hopf bifurcation, the presence of additive noise is found to smear out the sharp transition that is observed in a deterministic system (Juel *et al.*, 1997). Thus the determination of the Hopf point from experimental and numerical observations becomes impossible in the presence of additive noise. This difficulty in determining the bifurcation point is because the measured observable is no longer a deterministic quantity but a stochastic variable. Thus a single realization that we obtain in an experiment or from a mathematical model is incapable of providing the complete information about the state of the system. In the presence

of noise, stochastic differential equations (SDEs) are adopted instead of ordinary differential equations to describe the evolution of the system. Hence, we need to calculate the probability density function of the observable rather than its absolute value in the presence of noise. The probability density function of a stochastic variable can be obtained by solving the Fokker-Plank equation associated with the SDE (Stratonovich, 1963; Gardiner, 1997; Risken, 1989).

As against the deterministic bifurcation where we track the evolution of the absolute value of the observable, we track the change in the probability distribution of the observable in the presence of noise. The qualitative changes observed in the probability distribution of the observable are termed as phenomenological bifurcations (P-bifurcation). The bifurcation associated with the absolute value of the measured variable is known as dynamic bifurcation (D-bifurcation). In a stochastic system, both phenomenological and dynamical bifurcations are found. Both P and D-bifurcations are classified as stochastic bifurcations. There are studies on the effect of additive and multiplicative noise on stochastic bifurcations that happen in nonlinear systems. Additive noise does not change the location of the extrema of the stationary probability density function whereas multiplicative noise introduces novel dynamical states (Bashkirtseva *et al.*, 2015).

The phenomenon of stochastic bifurcation is very well studied both using models. The stochastic Hopf bifurcation is studied in the context of various nonlinear oscillators (Arnold *et al.*, 1999; Zakharova *et al.*, 2010; Xu *et al.*, 2011; Bashkirtseva *et al.*, 2015) and in biological systems including neuron models, synthetic gene oscillators (Zakharova *et al.*, 2010; Djeundam *et al.*, 2013) and cellular networks (Song *et al.*, 2010). The framework of stochastic bifurcation is also used to study the effect of noise in self-sustained bistable oscillators (Zakharova *et al.*, 2010). However, experimental studies on the concept of stochastic bifurcation are limited to driven laser systems (Billings *et al.*, 2004).

The literature on stochastic bifurcation in engineering systems is minimal. Many engineering systems are nonlinear and most engineering systems work in the presence of noise. Due to the nonlinear nature, they can undergo sudden transitions from a non-oscillatory state to an oscillatory state for an infinitesimal change in any of the system parameters. The oscillatory state following a Hopf bifurcation can cause a total collapse or decrease in performance of an engineering system (Fisher & Rahman, 2009). One such engineering system where the margins of safe operation are limited by Hopf bifurcation is a thermoacoustic system.

In Chapter 6, we find that the width of the bistable zone decreases with increase in the intensity of noise. Moreover, we also observe that there is a complete suppression of the bistable zone in the presence of high intensity noise. Therefore, it becomes impossible to ascertain the bifurcation point as evident from the results reported in Chapter 6. This difficulty in identifying the Hopf and fold points in the presence of high intensity noise brings in the need to calculate the stationary probability density function of the measured observable. As mentioned earlier, the stationary probability density function can be calculated by solving the Fokker-Planck (F-P) equation of the system.

Noiray & Schuermans (2013a, 2013b), in their pioneering work, introduced Fokker-Planck formalism in the thermoacoustic literature. They derived the F-P equation for a thermoacoustic system undergoing supercritical Hopf bifurcation. Their primary focus was to derive growth and decay rates of thermoacoustic oscillations for the unsteady pressure data obtained from a gas turbine engine and compare it with the numerical model.

In summary, the influence of noise characteristics on noise induced transitions has been studied in thermoacoustic systems. The F-P equation is derived for a thermoacoustic system depicting

supercritical Hopf bifurcation. The amplitude distribution obtained as a solution to the F-P equation is used to calculate the growth and decay rate of oscillations. The suppression of bistable zone in the presence of high intensity noise is also observed both in experimental and numerical frameworks. The issue of identifying the critical points of transition remains to be explored. It is necessary to adopt the amplitude distribution rather than the absolute value of the amplitude to determine the transition.

7.2 Fokker-Planck equation for a prototypical thermoacoustic system

From the results presented in Chapter 6, it is clear that the bifurcation points, Hopf point and fold point, cannot be determined in the presence of high intensity noise. In the presence of fluctuations, multiple realizations are required to describe the transition as any measured observable from the system is a stochastic variable. In this case, the peaks in the time series of acoustic pressure will follow a definite distribution rather than a single value. It will be more meaningful to describe the transition in terms of the nature of the amplitude distribution in such cases. Bifurcations in the system could be observed as changes in the distribution of the amplitude. To study this behavior of the probability distribution of amplitudes, the Fokker-Planck equation of the system needs to be derived. The probability distribution is a solution to the Fokker-Planck equation.

In order to derive the Fokker-Planck (FP) equation of a prototypical thermoacoustic system, a theoretical model very similar to the one described in Chapter 2 is used. However, the theoretical model used for the purpose of deriving FP equation differs from the one described in Chapter 2 in terms of the model used for heat release. Here for generality, a simple nonlinear model that depicts the bistable behavior observed in experiments on horizontal Rijke tube is used.

Instead of the Heckl's correlation (Heckl, 1988), a different model is used for heat release rate as described below

$$\dot{Q}' = -a_1(\eta - \tau\dot{\eta}) + a_2(\eta - \tau\dot{\eta})^3 + a_3(\eta - \tau\dot{\eta})^5 \quad (7.1)$$

where a_1 , a_2 and a_3 are constants. The constants are chosen such that the bistable behavior observed in experiments can be captured. The third and fifth order nonlinearity is required to capture the unstable and stable limit cycles. The generic heat release model is adopted in order to extend the analysis to any thermoacoustic system. The motivation for using such a model to describe the stochastic dynamics of a thermoacoustic system can be found in Noiray & Schuermans (2013a, 2013b). The model for heat release rate given in Eqn. (7.1) is similar to the functions adopted in earlier studies by Campa & Juniper (2012) and Subramanian *et al.* (2012). For simplicity, a single mode is considered for this analysis. The ordinary differential equations obtained after adopting Galerkin technique (Lores & Zinn, 1973) are given below.

$$\frac{d\eta}{dt} = \dot{\eta} \quad (7.2)$$

$$\frac{d\dot{\eta}}{dt} + 2\zeta\omega\dot{\eta} + \omega^2\eta = \dot{Q}' + \xi(t) \quad (7.3)$$

In Eqn. (7.3), a Gaussian white noise term $\xi(t)$ with $\langle \xi(t) \rangle = 0$ and $\langle \xi(t)\xi(t+\tau) \rangle = I\delta(\tau)$ is included to capture the influence of noise present in the system, where I is the noise intensity.

We write the state variables η and $\dot{\eta}$ (used in Eqns. (7.2) and (7.3)) in terms of slowly varying amplitude and phase (Kryloff & Bogoliuboff, 1949).

$$\eta(t) = a(t)\cos(\Theta(t)) \quad (7.4)$$

$$\dot{\eta}(t) = -\omega a(t)\sin(\Theta(t)) \quad (7.5)$$

where, $\Theta(t) = \omega t + \phi(t)$

We define a parameter $\kappa = 2\zeta\omega - c_1\tau$. Then, we transform Eqns. (7.2) and (7.3) in terms of the new variables $a(t)$ and $\varphi(t)$.

$$\frac{da}{dt} = f_1(a, \Theta) \sin \Theta + g_1(a, \Theta) \xi(t) \quad (7.6)$$

$$\frac{d\varphi}{dt} = f_2(a, \Theta) \cos \Theta + g_2(a, \Theta) \xi(t) \quad (7.7)$$

where,

$$f_1 = \frac{-a\omega\kappa \sin \Theta + c_1 a \cos \Theta - c_2 a^3 (\cos \Theta + \omega\tau \sin \Theta)^3 - c_3 a^5 (\cos \Theta + \omega\tau \sin \Theta)^5}{\omega} \quad (7.8)$$

$$f_2 = \frac{f_1}{a}, \quad g_1 = -\frac{\sin \Theta}{\omega}, \quad g_2 = -\frac{\cos \Theta}{a\omega} \quad (7.9)$$

In Eqn (7.8), c_1 , c_2 and c_3 represent constants and the values of these constants are selected such the probability distribution captures the distribution obtained from the experiments qualitatively. To derive the Ito's equation for a and φ , we perform averaging of (7.6) & (7.7) over one cycle of oscillation. More details on averaging can be found in Roberts & Spanos (1986).

$$da = F_1 dt + \frac{I}{4a\omega^2} dt + \sqrt{\frac{I}{2\omega^2}} dW_1(t) \quad (7.10)$$

$$d\varphi = \frac{F_2 dt}{a} + \frac{1}{a} \sqrt{\frac{I}{2\omega^2}} dW_2(t) \quad (7.11)$$

where $W_1(t)$ and $W_2(t)$ are independent Wiener processes and

$$F_1 = \frac{1}{2\pi} \int_0^{2\pi} f_1 \sin \Theta \, d\Theta \quad (7.12) \quad F_2 = \frac{1}{2\pi} \int_0^{2\pi} f_1 \cos \Theta \, d\Theta \quad (7.13)$$

Clearly, the equation for amplitude is independent of the phase. Therefore, it is not necessary to write the joint probability density for amplitude and phase. The transition probability density function $\Omega(a,t)$ for the amplitude can be obtained as a solution of the following Fokker-Planck equation.

$$\frac{\partial \Omega(a,t)}{\partial t} = -\kappa \frac{\partial}{\partial a} \left\{ \left[-\frac{a}{2} - \frac{3c_2 n a^3}{8\omega\kappa} - \frac{5c_3 m a^5}{16\omega\kappa} + \frac{I}{4a\kappa\omega^2} \right] \Omega(a,t) \right\} + \frac{\kappa}{2} \frac{\partial^2}{\partial a^2} \left\{ \frac{I}{2\kappa\omega^2} \Omega(a,t) \right\} \quad (7.14)$$

where, $n = \omega\tau + (\omega\tau)^3$ and $m = \omega\tau + (\omega\tau)^3 + (\omega\tau)^5$

The stationary probability density $\Omega(a)$ can be obtained from Eqn. (7.14) as given below.

$$\Omega(a) = Cae^{\left[-\frac{a^2\omega^2\kappa}{I} - \frac{3c_2 n \omega a^4}{8I} - \frac{5c_3 m \omega a^6}{24I} \right]} \quad (7.15)$$

where C is the normalization constant.

The extrema of the probability density function $\Omega(a)$ can be obtained from the roots of the equation given below.

$$8\kappa a^2 - \frac{6c_2 n a^4}{\omega} - \frac{5c_3 m a^6}{\omega} - \frac{4I}{\omega^2} = 0 \quad (7.16)$$

The extrema can be obtained for different values of κ and I , where I is the intensity of additive noise. The number of real roots of Eqn. (7.16) indicates the nature of the probability distribution. The distribution is unimodal if the number of real roots is 1 while the distribution is bimodal if the number of real roots is 3 (Zakharova *et al.*, 2010). Here, we define a normalized parameter,

$$\mu = 1 - \frac{\kappa}{\kappa_h},$$

where κ_h is the value of the control parameter at the Hopf point.

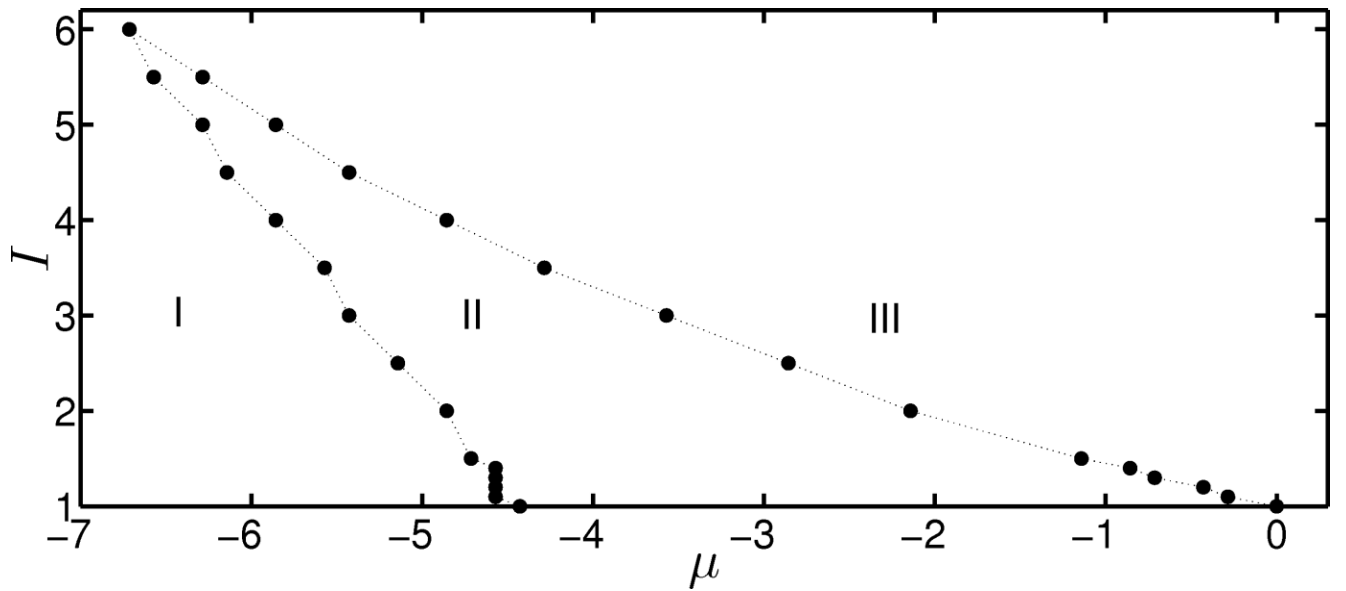


Figure 7.1: The regimes of unimodal and bimodal probability distribution in the (μ, I) plane, where μ is the control parameter and I is the intensity of the noise. Regions I and III correspond to the parameter regimes where the amplitude distribution is unimodal whereas region II corresponds to the parameter regime of bimodal amplitude distribution. The boundaries of the regions represent the locus of points where phenomenological bifurcation occurs. It can also be observed that above a noise intensity P-bifurcations are not observed.

The bifurcation diagram in the (μ, I) plane is shown in Fig. 7.1. Regions I and III correspond to unimodal probability distribution of amplitude while region II corresponds to bimodal amplitude distribution. For low intensities, P-bifurcations can be observed when the parameter μ is varied.

As the noise intensity is increased, the bimodality region reduces which corresponds to the reduction in width of the bistable zone in the experiments. Beyond a noise level (noise intensity $I = 6$ in the model), P-bifurcations are not observed. In this case, the probability distribution remains unimodal for changes in the parameter μ .

7.3 Concluding remarks

This study gains significance as most thermoacoustic systems work in noisy environments. Moreover, the bifurcation characteristics of a prototypical thermoacoustic system in the presence of high amplitude noise using experimental and numerical methods are identified. The Fokker-Planck equation associated with the governing differential equations of the system was derived. The suppression of the bistable zone is also identified with the help of probability distributions obtained by solving the Fokker-Planck equation.

CHAPTER 8

EARLY WARNING MEASURES FOR CRITICAL TRANSITIONS IN A HORIZONTAL RIJKE TUBE

In this chapter, a description of early warning measures based on the theory of critical slowing down to predict impending transitions in a prototypical thermoacoustic system is provided. It is found that the early warning measures such as variance increases well before the impending bifurcation and act as an effective precursor. The robustness of these early warning measures in the presence of noise is also established here. The viability of early warning measures are shown both in experiments and in a numerical model.

8.1 Early warning indicators based on critical slowing down

Many nonlinear systems such as eco systems, financial markets, and spiking neurons exhibit critical transitions (Lewontin, 1969; Holling, 1973; May, 1977; Carpenter *et al.*, 1999; Jackson *et al.*, 2001; Kéfi *et al.*, 2007; Dakos *et al.*, 2008; Lenton *et al.*, 2009). In a critical transition, the system moves from one stable state to another stable state and often this transition is not desirable. Most of these transitions are catastrophic in nature as they involve hysteresis, where the critical points for forward and reverse switching differ (Scheffer, 2009). In an eco-system, the critical transition may result in sudden extinction of certain species. In a financial market, a critical transition may result in a sudden collapse of the market (Scheffer *et al.*, 2001). The undesirable state following a critical transition creates the need to develop early warning measures to detect the proximity of the system to a critical point or tipping point.

Over the years, many early warning measures were developed to detect critical transitions in complex systems. A pioneering study on early warning signals was carried out by Scheffer *et al.* (2009). They proposed a plethora of early warning measures to predict the sudden change in eco systems, climatic shifts, collapse of financial markets and the onset of asthmatic attacks and epileptic seizures. We can find an extensive of use of these early warning measures to predict critical transitions in almost every field of science starting from ecology and extending up to medicine where these measures are used for prognosis (Dakos *et al.*, 2008; Meisel *et al.*, 2015; Livina *et al.*, 2015; Trefois *et al.*, 2015). Many studies applied these early warning measures to numerical models of complex systems. The viability of these measures are proved also with the help of experiments (Drake & Griffien, 2010; Kramer & Rose, 1985; Tredicce *et al.*, 2004; Carpenter *et al.*, 2011). Recent findings indicate that, even critical transitions that happen via subcritical Hopf bifurcation in spiking neurons can be predicted using these early warning measures (Meisel *et al.*, 2015). The applicability of early warning measures are not limited to low dimensional reduced order models but also extends to high dimensional complex systems (Kuehn *et al.*, 2015).

The early warning signals for critical transitions are obtained by exploiting the phenomenon of critical slowing down exhibited by dynamical systems near a transition. Critical slowing down results in increased autocorrelation and a rise in variance, before the onset of a critical transition. As a result of critical slowing down, the present state of the system resembles its past state and this increase in the ‘memory’ of the system results in the increase in the value of autocorrelation. Moreover, the rate at which the perturbations decay reduces due to critical slowing down and this results in the increase in variance as we approach the transition. Hence, autocorrelation and variance can be used as early warning measures in a real world system. Although enough literature

exist on the use of early warning signals for predicting the transitions in natural systems, the applicability of early warning signal to an engineering system is yet to be explored. Moreover, the robustness of the early warning indicators in the presence of fluctuations is not yet studied in the context of a physical system. In this study, the early warning measures to predict the critical transition is applied for the first time in an engineering system.

8.2 Early warning measures for subcritical Hopf bifurcation in a Rijke tube

Main aim here is to develop an early warning signal to enable the operator in the field to shut down the system before it reaches the oscillatory state. Unlike a laboratory experiment where we vary the control parameter in a quasi-static way, the control parameter is varied continuously in a practical environment. This prompted us to capture the time series depicting the transition from non-oscillatory state to oscillatory state. The heater power K is varied in every 20 s and the corresponding acoustic pressure is noted down using pressure sensors (Fig. 8.1a). The metric based methods suggested by Dakos *et al.* (2012) is used to calculate the early warning signals in the current study. A rolling window is used to calculate the autocorrelation and the variance (Dakos *et al.*, 2012). As we require precursors for an impending transition, time series prior to the transition is used to calculate the early warning measures. A significant increase in the value of variance well before the transition is observed, hence variance can clearly serve as an early warning signal (Fig. 8.1b). The trend is calculated by measuring the slope of a linear fit to the variation of autocorrelation and variance with respect to time. However, the lag-1 autocorrelation decreased before the transition rendering it as a less effective early warning signal (Fig. 8.1c).

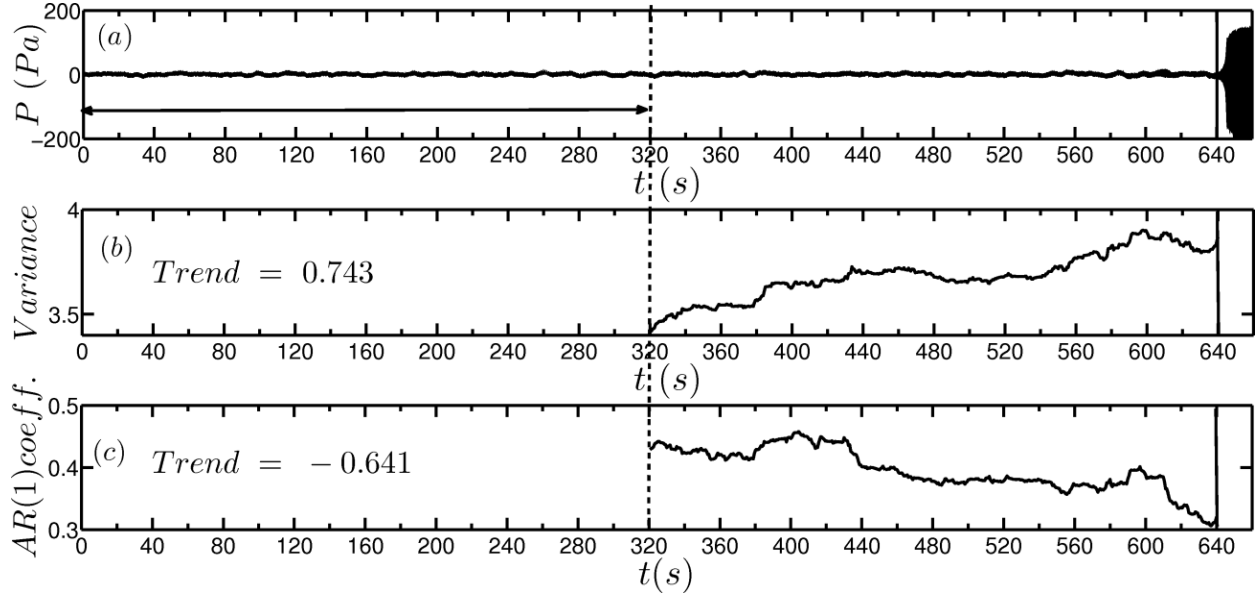


Figure: 8.1 Early warning signals for a subcritical bifurcation in a prototypical thermo-acoustic system using pressure time series generated from the experiments (a) Time series of acoustic pressure depicting transition from one stable to an alternate stable state. The control parameter is increased every 20 seconds. The system undergoes a critical transition from a non-oscillatory state to an oscillatory state via a subcritical Hopf bifurcation (b) Plot depicting the change in lag-1 autocorrelation as the system approaches the critical transition. (c) Plot depicting the change in variance as the system approaches the critical transition. The lag-1 autocorrelation and variance are calculated using a moving window of half the size of the time series. The black horizontal arrow represents the length of the moving window. We observe a clear increase in variance, well before the transition, whereas the autocorrelation shows a decrease. The thick black line indicates the time stamp up to which the data is used to generate the early warning indicators. Although, no external noise added to the system, the inherent fluctuations in the system correspond to a non-dimensional noise intensity $\beta = 0.02$.

The observation of variance being a more robust early warning measure than lag-1 autocorrelation is completely in conformity with Kuehn (2011). Although, no external noise is added, the system has inherent aperiodic fluctuations. The presence of inherent fluctuations makes autocorrelation a

less effective precursor and it is established that autocorrelation can increase or decrease in the presence of fluctuations. In order to use autocorrelation as a precursor, we need to have multiple realizations of the transition, which may not be feasible in a real time engineering system (Carpenter & Brock 2011). The amplitude of the inherent fluctuations is made non-dimensional by dividing it with the amplitude of periodic oscillations. This non-dimensional noise intensity is denoted by β .

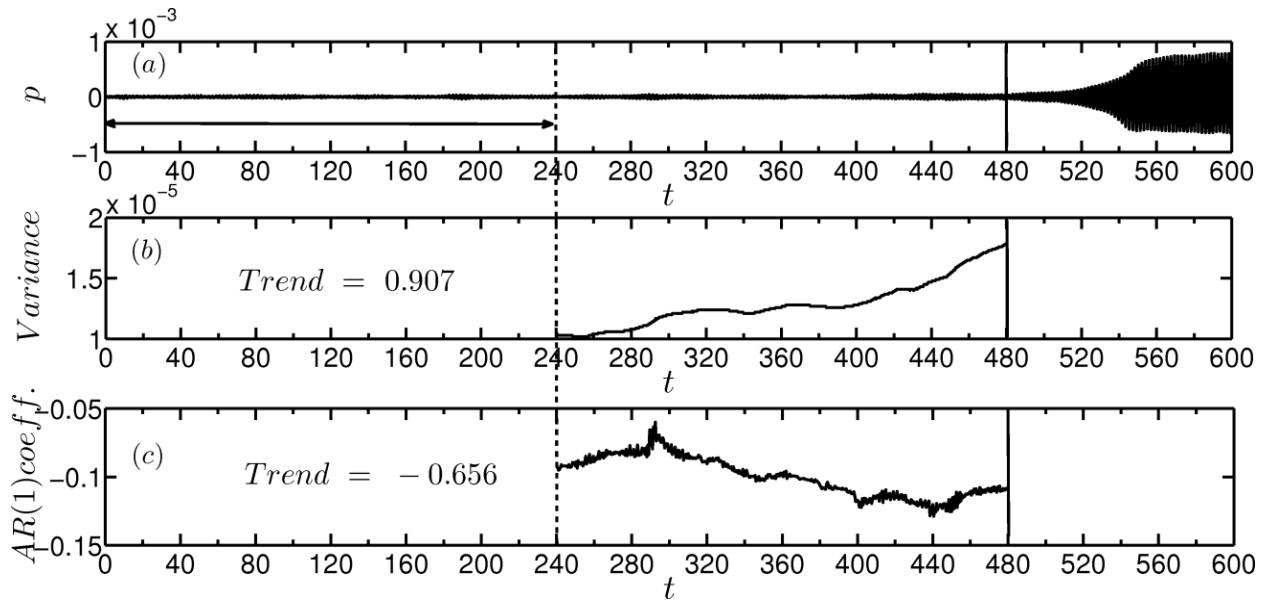


Figure: 8.2 Early warning signals for a subcritical bifurcation in a prototypical thermo-acoustic system using pressure time series generated from the numerical model (a) Time series of acoustic pressure depicting the transition from one stable to an alternate stable state. The control parameter is increased at every time step. The system undergoes a critical transition from a non-oscillatory state to an oscillatory state via a subcritical Hopf bifurcation (b) Plot depicting the change in variance as the system approaches the critical transition. (c) Plot depicting the change in lag-1 autocorrelation as the system approaches the critical transition. A clear increase in variance well before the transition can be observed. The non-dimensional noise intensity is maintained as $\beta = 0.02$ to match with the experimental conditions.

Further, the search for effective early warning signals for a thermo-acoustic system is extended in a numerical model. In order to simulate the experimental conditions, the numerical model is perturbed with additive Gaussian white noise such that the non-dimensional noise intensity is the same as that of the experiments. The control parameter is varied at each time step and the corresponding acoustic pressure is calculated. The lag-1 autocorrelation and variance were calculated using the same procedure as that followed for the time series obtained from experiments. Here also a significant increase in the variance and a decrease in the value of the lag- 1 autocorrelation are observed well before the transition (Fig. 8.2). The observation from the model makes it clear that variance is a robust early warning signal compared to lag -1 autocorrelation.

8.3 Robustness of early warning indicators in the presence of noise

As practical combustion systems work in a turbulent environment, the robustness of the early warning indicators in the presence of fluctuations needs to be verified. As the prototypical thermoacoustic system has a low amount of inherent fluctuations, external noise is added using loudspeakers. The detailed procedure of adding external noise to the system can be found in Chapter 2. We find that the early warning indicators work well even in the presence of external fluctuations. Here also, the control parameter is changed in every 20 s and the corresponding acoustic pressure is recorded. Robustness of the early warning indicators are tested in the presence of fluctuations of intensity 0.05, 0.1 and 0.2. We can see that both lag-1 autocorrelation and variance register an increase well before the transition even in the presence of external fluctuations (Figs. 8.3, 8.4 & 8.5). The current experimental results prove that early warning indicators perform very well even in the presence of high intensity external fluctuations.

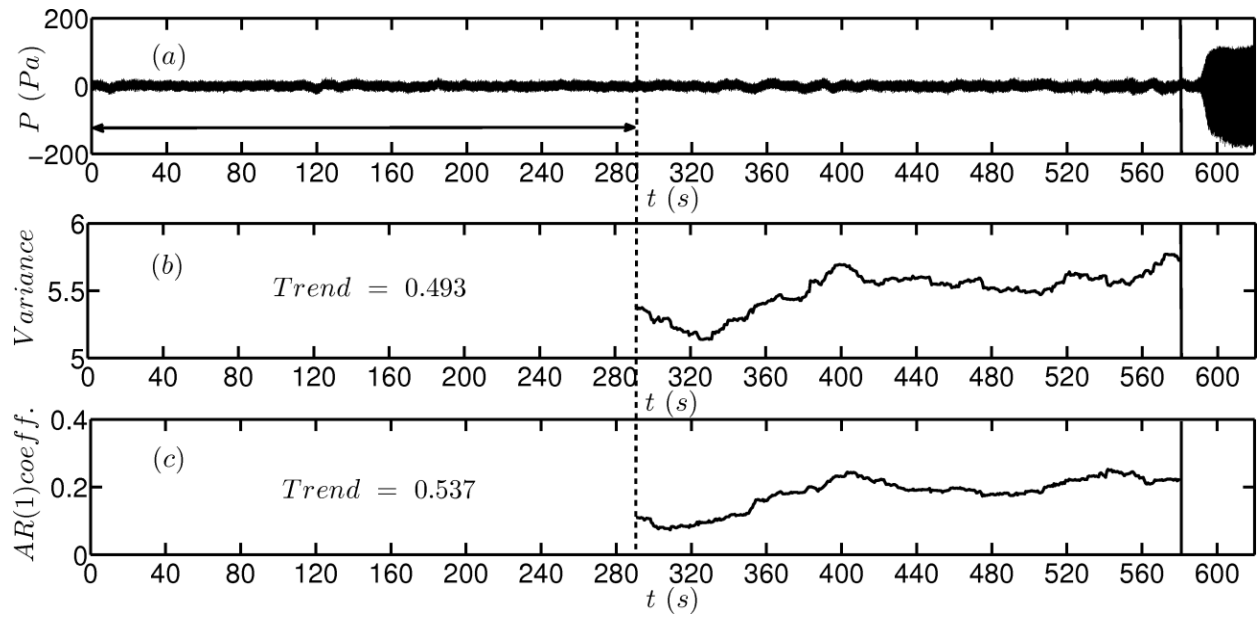


Figure: 8.3 Early warning signals for a subcritical bifurcation in a prototypical thermo-acoustic system in the presence of external fluctuations using pressure time series generated from the experiments (a) Time series of acoustic pressure depicting transition from one stable to an alternate stable state. The control parameter is increased every 20 seconds. The system undergoes a critical transition from a non-oscillatory state to an oscillatory state via a subcritical Hopf bifurcation (b) Plot depicting the change in variance as the system approaches the critical transition. (c) Plot depicting the change in lag-1 autocorrelation as the system approaches the critical transition. A clear increase in variance as well as autocorrelation can be observed well before the transition. External noise is added to the system such that the non-dimensional noise intensity is $\beta = 0.05$.

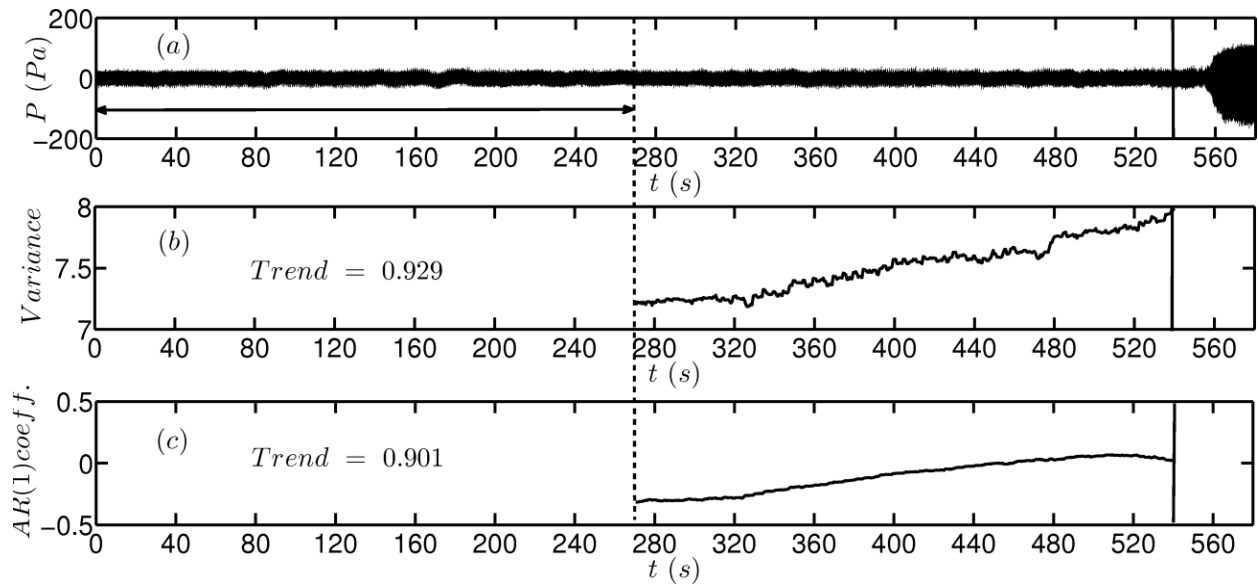


Figure: 8.4 Early warning signals for a subcritical bifurcation in a prototypical thermo-acoustic system in the presence of external fluctuations using pressure time series generated from the experiments (a) Time series of acoustic pressure depicting transition from one stable to an alternate stable state. The control parameter is increased every 20 seconds. The system undergoes a critical transition from a non-oscillatory state to an oscillatory state via a subcritical Hopf bifurcation (b) Plot depicting the change in variance as the system approaches the critical transition. (c) Plot depicting the change in lag-1 autocorrelation as the system approaches the critical transition. A clear increase in variance as well as autocorrelation can be observed well before the transition. External noise is added to the system such that the non-dimensional noise intensity is $\beta = 0.1$.

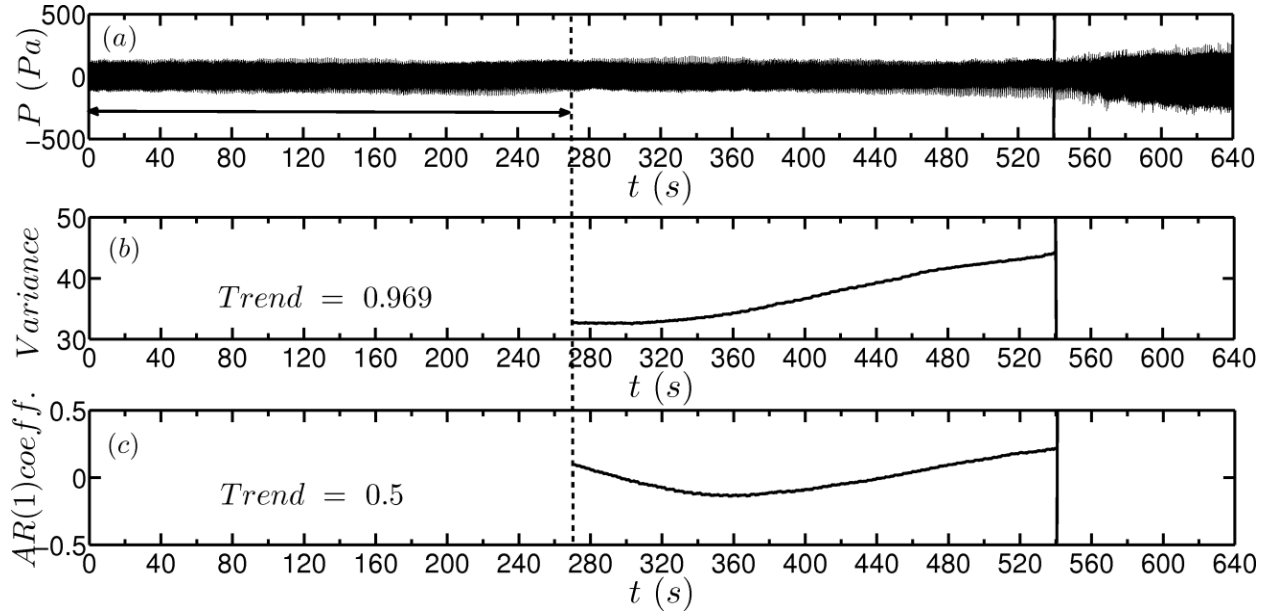


Figure: 8.5 Early warning signals for a subcritical bifurcation in a prototypical thermo-acoustic system in the presence of external fluctuations using pressure time series generated from the experiments (a) Time series of acoustic pressure depicting transition from one stable to an alternate stable state. The control parameter is increased every 20 seconds. The system undergoes a critical transition from a non-oscillatory state to an oscillatory state via a subcritical Hopf bifurcation (b) Plot depicting the change in variance as the system approaches the critical transition. (c) Plot depicting the change in lag-1 autocorrelation as the system approaches the critical transition. A clear increase in variance as well as autocorrelation can be observed well before the transition. External noise is added to the system such that the non-dimensional noise intensity is $\beta = 0.2$.

Further, the robustness of these early warning indicators is tested using the numerical model. In the numerical model, Gaussian white noise of high intensity is added to match with the experimental conditions. A trend similar to that of experiments is observed where both lag-1 autocorrelation and variance showed a significant increase well before the transition (Figs. 8.6, 8.7 & 8.8). The results from the present study show that irrespective of the presence of inherent or

external fluctuations, the early warning indicators perform well and forewarn us about an impending critical transition.

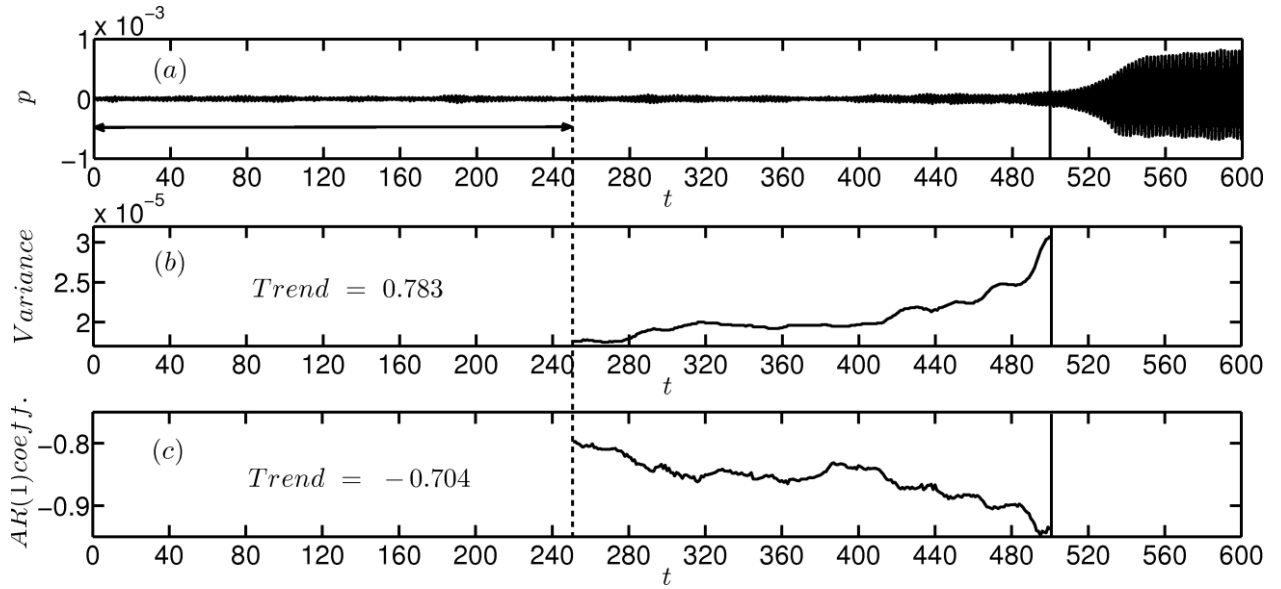


Figure: 8.6 Early warning signals for a subcritical bifurcation in a prototypical thermo-acoustic system using pressure time series generated from the numerical model (a) Time series of acoustic pressure depicting the transition from one stable to an alternate stable state. The control parameter is increased at every time step. The system undergoes a critical transition from a non-oscillatory state to an oscillatory state via a subcritical Hopf bifurcation (b) Plot depicting the change in variance as the system approaches the critical transition. (c) Plot depicting the change in lag-1 autocorrelation as the system approaches the critical transition. A clear increase in variance well before the transition can be observed. The non-dimensional noise intensity is maintained as $\beta = 0.05$ to match with the experimental conditions.

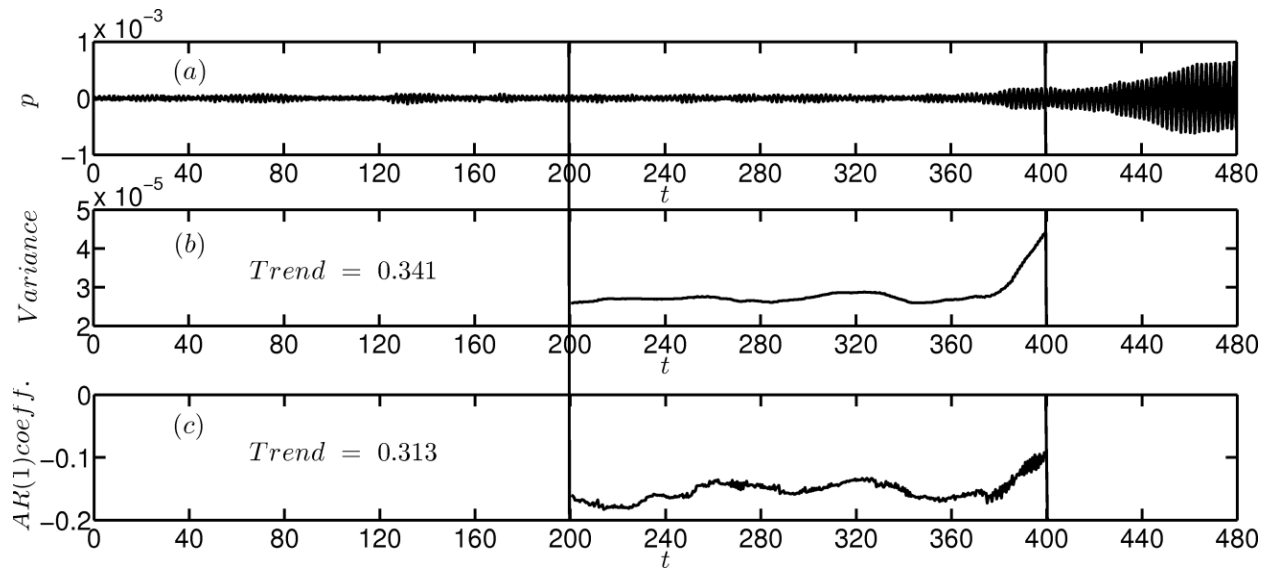


Figure: 8.7 Early warning signals for a subcritical bifurcation in a prototypical thermo-acoustic system using pressure time series generated from the numerical model (a) Time series of acoustic pressure depicting the transition from one stable to an alternate stable state. The control parameter is increased at every time step. The system undergoes a critical transition from a non-oscillatory state to an oscillatory state via a subcritical Hopf bifurcation (b) Plot depicting the change in variance as the system approaches the critical transition. (c) Plot depicting the change in lag-1 autocorrelation as the system approaches the critical transition. A clear increase in variance well before the transition can be observed. The non-dimensional noise intensity is maintained as $\beta = 0.1$ to match with the experimental conditions.

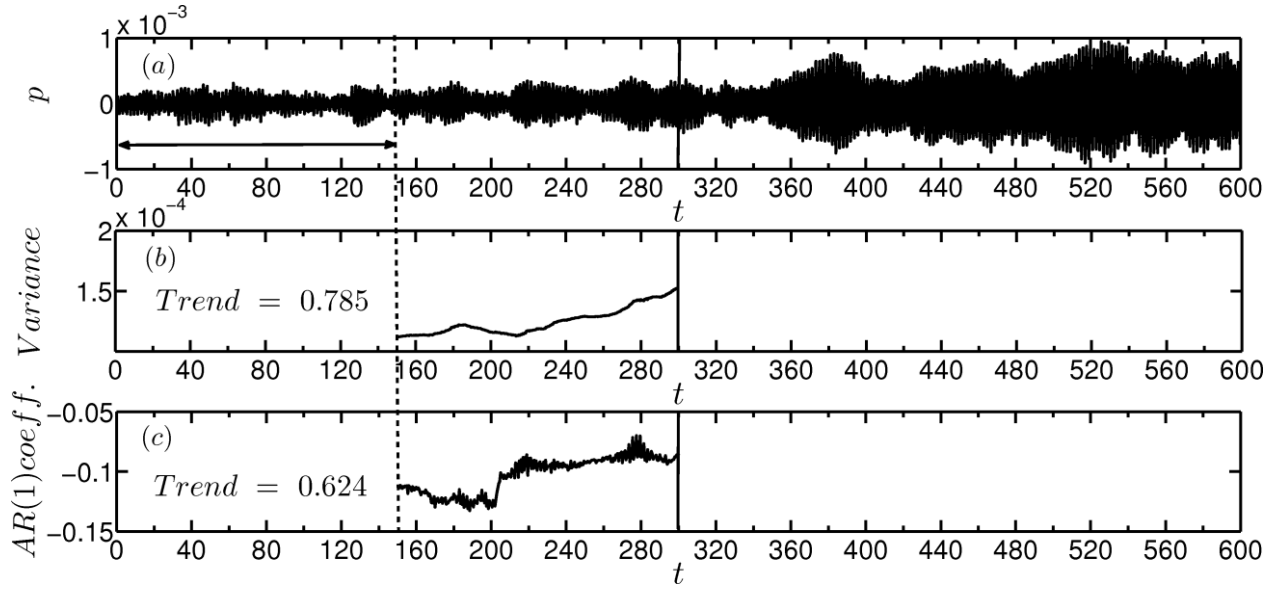


Figure: 8.8 Early warning signals for a subcritical bifurcation in a prototypical thermo-acoustic system in the presence of high intensity additive noise using pressure time series generated from the numerical model (a) Time series of acoustic pressure depicting the transition from one stable to an alternate stable state. The control parameter is increased in every time step. The system undergoes a critical transition from a non-oscillatory state to an oscillatory state via a subcritical Hopf bifurcation (b) Plot depicting the change in variance as the system approaches the critical transition. (c) Plot depicting the change in lag-1 autocorrelation as the system approaches the critical transition. A clear increase both in autocorrelation and in variance can be observed well before the transition. The thick black line indicates the time stamp up to which the data is used to generate the early warning measures. The non-dimensional noise intensity $\beta = 0.2$ to match with the experimental conditions.

8.4 Concluding remarks

We find that the early warning measures based on critical slowing down are able to predict catastrophic transitions in an engineering system. As we approach a subcritical Hopf bifurcation, the system dynamics can be projected in the eigenvector corresponding to the most unstable

eigenvalue (Ditlevsen & Johnsen, 2010). Since the real part of the dominant eigenvalue will become zero at the Hopf point, there will be an increase in autocorrelation and in variance (Scheffer *et al.*, 2009; Kuehn, 2011; Dakos *et al.*, 2012). However, variance acts as better precursor than autocorrelation in the presence of noise (Carpenter & Brock, 2011; Cecchi *et al.*, 2015). As the prototypical thermoacoustic system has inherent fluctuations, variance appears to be a more robust precursor than autocorrelation in predicting the critical transition. The ineffectiveness of the autocorrelation as an early warning signal is basically because we are using a single sample path or a single realization (Kuehn, 2011). The robustness of variance as an early warning signal opens up the possibility of applying this measure to predict critical transitions in engineering systems which work in the presence of noise. It is also established that the early warning measures are able to predict a subcritical Hopf bifurcation observed in a real system.

As many of the engineering systems exhibit catastrophic transitions, the findings from this study are highly pertinent. By implementing the early warning measures in systems such as the one considered in the present study, we can prevent catastrophic transitions in many engineering systems. The analysis employed in this investigation can be extended in future to turbulent reactive flows, aero-acoustic systems, aero-elastic systems and to any general system exhibiting oscillatory instability.

CHAPTER 9

CONCLUSIONS

The present thesis focuses on the effect of system parameters and noise on the bistable characteristics of a prototypical thermoacoustic system. The dependence of the width of the bistable zone with Strouhal number is established. Further, the reduction in the width of the bistable zone with increase in the intensity of noise is also investigated. The effect of high intensity noise on the bistable characteristics is analyzed by deriving the associated Fokker-Planck equation. Finally, precursors based on critical slowing down are shown to predict an impending bifurcation in a horizontal Rijke tube.

The effect of system parameters such as heater power and heater location on the bistable characteristics of a horizontal Rijke tube is understood by performing experiments. It is shown that for the experimental conditions employed in the present study, the transition to thermoacoustic instability happens always through subcritical Hopf bifurcation. A reduction in the width of the bistable zone with increase in Strouhal number is observed both in experiments and in mathematical model. Further, a power law relationship between the non-dimensional width of the bistable zone and Strouhal number is established. The present study reveals that the non-dimensional width of the bistable zone remains nearly the same irrespective of the choice of bifurcation parameter for the Strouhal numbers considered. Period-2 oscillations are found when heater location is chosen as a bifurcation parameter which is in conformity with numerical results reported in literature.

We establish that the width of the bistable zone decreases with increase in the noise intensity. The rate of decrease is found to be independent of the mass flow rate in case of experiments and time lag in case of numerical model. A complete suppression of the bistable zone is observed

in the presence of high intensity noise. Fokker-Planck formalism is used to study the stochastic bifurcations that happen in the presence of high intensity noise. The qualitative changes in the distribution of the pressure amplitude are studied and the regions of phenomenological bifurcation are identified.

Early warning measures such as autocorrelation and variance are developed for predicting the subcritical transitions observed in the horizontal Rijke tube. It is observed that there is a marked increase in the variance well before the subcritical Hopf bifurcation. This increase in variance well ahead of the transition makes variance a suitable precursor for predicting the impending transition. Unlike the marked increase in variance, such a trend is not observed in autocorrelation. This ineffectiveness of autocorrelation to act as a precursor can be attributed to the presence of noise in the system. However, variance is proved to be a robust precursor even in the presence of high intensity noise.

In summary, the present thesis brings out the dependence of the width of the bistable zone on Strouhal number and the intensity of the noise present in the system. Further, it is also established that the early warning measures based on the theory of critical slowing down can be used as robust precursors. Further studies can be conducted in order to understand the reason for the existence of bistable zone in a Rijke tube. Another aspect that can be analyzed is the possibility for observing a change of criticality in the transition from non-oscillatory to oscillatory state. In the current study, the control parameters are varied quasi-statically. It will be interesting to investigate the effect of variation of control parameters as a function of time on the dynamic characteristics of the proto typical thermoacoustic system. The possibility for detecting co-dimension 2 bifurcation in experiments can also be explored in future.

In the present study, the effect of additive noise on the dynamics of Rijke tube is explored. In future, experiments can be performed to analyze the influence of multiplicative and parametric noise. The possibility for observing noise induced intermittency can also be studied.

The findings in the current study can be extended to turbulent combustion systems. The effect of increasing turbulence on the transition to combustion instability can be investigated and can be compared with the effect of increasing noise intensity. Further, the early warning measures employed in the present study can be used in turbulent combustion systems to predict the transition to combustion instability and blow out. The tools and techniques used in the current thesis can be used for the analysis of not only engineering systems but also for eco systems, financial markets and physiological systems.

APPENDIX A

Stochastic Runge-Kutta method applied to a general stochastic differential equation

In this appendix, we describe the procedure to numerically integrate a general stochastic differential equation. We consider a general stochastic differential equation to show the application of stochastic Runge-Kutta method to integrate the differential equations in time (Richardson 2009).

Let us consider the general form of an autonomous stochastic differential equation

$$dX(t) = f(X(t))dt + g(X(t))dW(t) \quad (\text{A.1})$$

Here, X represents the dependent variable and t represents the independent variable say time. f and g correspond to the functions of the dependent variable X . The second term on the right hand side of Eqn. (A.1) represents the noise term, and the noise increment $dW(t)$ is generated from a Wiener process. The value of the dependent variable $X(t)$ at any time t is given by the expression

$$X(t) = X(0) + \int_0^t f(X(s))ds + \int_0^t g(X(s))dW(s) \quad (\text{A.2})$$

Let δt be the time step and let L be the total number of time steps that we use to numerically integrate Eqn. (A.2). The value of the dependent variable at any time $\tau_j = j \delta t$, where $j = 0, \dots, L$ is given by

$$X(\tau_j) = X(0) + \int_0^{\tau_j} f(X(s))ds + \int_0^{\tau_j} g(X(s))dW(s) \quad (\text{A.3})$$

Similarly

$$X(\tau_{j-1}) = X(0) + \int_0^{\tau_{j-1}} f(X(s))ds + \int_0^{\tau_{j-1}} g(X(s))dW(s) \quad (\text{A.4})$$

If we subtract Eqn. (A.4) from Eqn. (A.3), then we will get

$$X(\tau_j) = X(\tau_{j-1}) + \int_{\tau_{j-1}}^{\tau_j} f(X(s))ds + \int_{\tau_{j-1}}^{\tau_j} g(X(s))dW(s) \quad (\text{A.5})$$

The second term on the right hand side of Eqn. (A.5) can be integrated using the conventional deterministic Runge-Kutta method and we get

$$\int_{\tau_{j-1}}^{\tau_j} f(X(s))ds = \left\{ \frac{K_1 + 2K_2 + 2K_3 + K_4}{6} \right\} \quad (\text{A.6})$$

where K_1, K_2, K_3 and K_4 are the increments calculated using 4th order Runge-Kutta algorithm.

The third term on the right hand side of Eqn. (A.5), which is stochastic, can be obtained using the principles of stochastic calculus. We use Ito's formulation to integrate the stochastic integral.

$$\int_0^T g(X(t))dW(t) \approx \sum_{j=0}^{N-1} \{ g(X(t_j)) [W(t_{j+1}) - W(t_j)] + \frac{1}{2} g(X(t_j)) g'(X(t_j)) [W(t_{j+1}) - W(t_j)]^2 - \delta t \} \quad (\text{A.7})$$

If the coefficient of the noise term is independent of the state of the system such that $g(x) = \sigma$, i.e. when the noise term is additive in nature; Eqn. (A.7) changes to

$$\int_0^T \sigma dW(t) \approx \sum_{j=0}^{N-1} \sigma [W(t_{j+1}) - W(t_j)] \quad (\text{A.8})$$

If we substitute Eqns. (A 8) and (A 6) to Eqn. (A 5) then we get

$$X(\tau_j) = X(\tau_{j-1}) + \left\{ \frac{K_1 + 2K_2 + 2K_3 + K_4}{6} \right\} + \sigma [W(t_j) - W(t_{j-1})] \quad (\text{A.9})$$

Thus, we can numerically integrate Eqn. (A.2) in time to get $X(t)$.

APPENDIX B

Methods to calculate lag-1 autocorrelation and variance

The statistical analyses were performed using the “Early Warning Signals Tool Box” (<http://www.early-warning-signals.org/>). The time series up to the impending critical transition is used to calculate the early warning indicators. For variance and autocorrelation, the temporal trend is calculated by estimating the nonparametric Kendall rank correlation (τ_k). Kendall’s τ_k is a statistical tool used to measure the association between two measured quantities. Lag-1 autocorrelation is determined by the autocorrelation function (ACF) given below:

$$\rho_1 = \frac{E[(P(t) - P_m)(P(t + 1) - P_m)]}{\sigma^2}, \quad (\text{B.1})$$

where, $P(t)$ is the value of the state variable at time t , and P_m and σ^2 are the mean and variance of $P(t)$ within the time frame considered. Variance is calculated as:

$$\sigma^2 = \frac{1}{N} \sum_{t=1}^N (P(t) - P_m)^2, \quad (\text{B.2})$$

where N is the number of observations.

In the current study, the time required to compute the early warning measures for a moving window (of half the size of the time series) is around 0.03 seconds using a code written in R. The computing facility used has an Intel (R) Core (TM2 Quad CPU) processor with frequency 3 GHz, 16 GB RAM and 64 bit operating system.

REFERENCES

- Abarbanel, H. D. I.** (1996). *Analysis of Observed Chaotic Data*. Springer, New York.
- Altares, V. and G. Nicolis** (1988). Stochastically forced Hopf bifurcation: approximate Fokker-Planck equation in the limit of short correlation times. *Physical Review A* **37**, 3630-3633.
- Ananthakrishnan, N., S. Deo, and F. E. C. Culick** (2005). Reduced-order modeling and dynamics of nonlinear acoustic waves in a combustion chamber. *Combustion Science and Technology*, **177**, 221–248.
- Arnold, L., G. Bleckert and K. S. Schenk-Hoppe** (1999). *Stochastic Dynamics. The Stochastic Brusselator: Parametric Noise Destroys Hoft Bifurcation*. Springer, New York, 1999.
- Aumaitre, S., K. Mallick and F. Petrelis** (2007). Noise-induced bifurcations, multiscaling and on-off intermittency. *Journal of Statistical Mechanics: Theory and Experiment* **7**, P07016.
- Bake, F., C. Richter, B., Muhlbauer, N., Kings, I., Rohle, F., Thiele and B., Noll** (2009). The entropy wave generator (EWG): a reference case on entropy noise. *Journal of Sound and Vibration* **326**, 574-598.
- Balasubramanian, K. and R. I. Sujith** (2008). Thermoacoustic instability in a Rijke tube: non-normality and nonlinearity. *Physics of Fluids* **20**, 044103.
- Bashkirtseva, I., T. Ryazanova and L. Ryashko** (2015). Stochastic bifurcations caused by multiplicative noise in systems with hard excitement of auto-oscillations. *Physical Review E*, **92**, 042908.
- Bayly, B. J.** (1986). Onset and equilibration of oscillations in general Rijke devices, *Journal of the Acoustical Society of America*, **79**, 846-851.
- Berhet, R., A. Petrossian, S. Residori, B. Roman and S. Fauve** (2003). Effect of multiplicative noise on parametric instabilities. *Physica D* **174**, 84-99.

Bigongiari, A. and M. Heckl. Coupling of heat driven modes in the Rijke tube. *21st International Congress on Sound and Vibration*. Beijing, China, 2014.

Bigongiari, A. and M. Heckl. A Green's function approach to the study of hysteresis in a Rijke tube. *22nd International Congress on Sound and Vibration*. Florence, Italy, 2015.

Bigongiari, A. and M. Heckl. A Green's function approach to the rapid prediction of thermoacoustic instabilities in combustors. *Journal of Fluid Mechanics*, **798**, 970-996.

Billings, L., I. B. Schwartz, D. S. Morgan, E. M. Boltt, R. Meucci and E. Allaria (2004). Stochastic bifurcation in a driven laser system: Experiment and theory. *Physical Review E*, **70**, 026220.

Birbaud, A., S. Ducruix, D. Durox and S. Candel (2008). The nonlinear response of inverted V flames to equivalence ratio non-uniformities. *Combustion and Flame*, **154**(3), 356-367.

Brownlee, W. G. (1964). Nonlinear axial combustion instability in solid propellant rocket motors. *AIAA Journal*, **2**(2), 275-284.

Brownlee, W. G. and Kimbell, G. H. (1966) Shock propagation in solid-propellant rocket combustors. *AIAA Journal*, **4**(6), 1132-1134.

Burrage, P. M. (1999). *Runge-Kutta methods for stochastic differential equations*. Ph. D. thesis, The University of Queensland.

Campa, G. and M. P. Juniper (2012). Obtaining bifurcation diagrams with thermoacoustic network model. *Proceedings of ASME Turbo Expo*, GT2012-68241.

Cantrell, R. H., F. T. McClure and R. W. Hart (1965). Effects of thermal radiation on the acoustic response function of solid propellants. *AIAA Journal*, **3**(3), 418-426.

Carpenter, S. R., J. J. Cole, M. L. Pace, R. Batt and W. A. Brock (2011). Early warnings of regime shifts: a whole-ecosystem experiment. *Science*, **332**, 1079–1082.

Carpenter, S. R., D. Ludwig and W. A. Brock (1999). Management of eutrophication for lakes subject to potentially irreversible change. *Ecological Applications*, **9**, 751–771.

Collyer, A. A. and D. J. Ayres (1972). The generation of sound in a Rijke tube using two heating coils, *Journal of Physics D: Applied Physics* **5**(8), L73-L75.

Coullet, P. H., C. Elphick and **E. Tirapegui** (1985). Normal form of a Hopf bifurcation with noise. *Physics Letters* **111A** (6), 277-282.

Dakos, V., S. R. Carpenter, W. A. Brock, A. M. Ellison, V. Guttal, A. R. Ives, S. Kefi, V. Livina, D. A. Seekell, E. H. van Nes and **M. Scheffer** (2012). Methods for detecting early warning signals of critical transitions in time series illustrated using simulated ecological data. *PLoS ONE* **7**(7), e41010.

Dakos, V., M. Scheffer, E. H. van Nes, V. Brovkin, V. Petoukhov and H. Held (2008). Slowing down as an early warning signal for abrupt climate change. *Proceedings of National Academy of Sciences*, **105**, 14308–14312.

Deco, G. and **D. Martí** (2007). Deterministic analysis of stochastic bifurcations in multi-stable neurodynamical systems. *Biological Cybernetics* **96**, 487-496.

Dickinson, L. A. (1962). Command initiation of finite wave axial combustion instability in solid propellant rocket engines. *Journal of American Rocket Society* **32**, 643-644.

Djeundam, S. R. D., R. Yamapi, T. C. Kofane, and **M. A. Aziz-Alaoui** (2013). Deterministic and stochastic bifurcations in the Hindmarsh-Rose neuronal model. *Chaos*, **23**, 033125.

Domen, S., H. Gotoda, T. Kuriyama, Y. Okuno and **S. Tachibana** (2015). Detection and prevention of blowout in a lean premixed gas-turbine model combustor using the concept of dynamical system theory. *Proceedings of the Combustion Institute*, **35**, 3245-3253.

Drake, J. and **B. Griffen** (2010). Early warning signals of extinction in deteriorating environments. *Nature*, **467**, 456–459.

Fedotov, S., I. Bashkirtseva and **L. Ryashko** (2002). Stochastic analysis of a non-normal dynamical system mimicking a laminar-to-turbulent subcritical transition. *Physical Review E* **66**, 066310.

Fisher, S. C. and **Rahman, S. A** (2009). Remembering the giants: Apollo rocket propulsion development (NASA monographs in Aerospace History series) (NASA History Division, Washington, DC).

Gardiner, C. W. (1997). *Handbook of stochastic methods*. Springer, Berlin.

Geier, L. S., A. V. Tolstopjatenko and W. Ebeling (1985). Noise induced transitions due to external additive noise. *Physics Letters* **108A** (7), 329-332.

Goh, C. S. and A. S. Morgans (2013). The influence of entropy waves on the thermoacoustic stability of a model combustor. *Combustion Science and Technology* **185**, 249-268.

Gotoda, H., Y. Shinoda, M. Kobayashi and Y. Okuno (2014). Detection and control of combustion instability based on the concept of dynamical system theory. *Physical Review E*, **89**, 022910.

Guidi, G. M. and A. Goldbeter (1997). Bistability without hysteresis in chemical reaction systems: A theoretical analysis of irreversible transitions between multiple steady states. *Journal of Physical Chemistry A*, **101**, 9367-9376.

Hantschk, C., J. Hermann and D. Vortmeyer (1996). Active instability control with direct-drive servo valves in liquid-fueled combustion systems, *Proceedings of the Combustion Institute*, **26**, 2835-2841.

Hantschk, C. and D. Vortmeyer (1999). Numerical simulation of self-excited thermoacoustic instabilities in a Rijke tube, *Journal of Sound and Vibration*, **277**, 511-522.

Heckl, M. A. (1985). *Heat sources in acoustic resonators*. Ph. D. Thesis, Emmanuel College, Cambridge.

Heckl, M. A. (1988). Active control of the noise from a Rijke tube, *Journal of Sound and Vibration*, **124**, 117-133.

Heckl, M. A. (1990). Non-linear acoustic effects in the Rijke tube, *Acustica*, **72**, 63-71.

Heckl, M. and M. S. Howe (2007). Stability analysis of the Rijke tube with a Green's function approach. *Journal of Sound and Vibration*, **305**, 672-688.

Heckl, M. and B. Kosztin (2013). Analysis and control of an unstable mode in a combustor with tuneable end condition. *International Journal of Spray and Combustion Dynamics*, **5**, 243-272.

Hilborn, R. C. (2000). *Chaos and Nonlinear Dynamics: An Introduction for Scientists and Engineers*. Oxford University Press, New York.

Holling, C. S. S. (1973). Resilience and stability of ecological systems. *Annual Review on Ecological Systems*, **4**, 1–23.

Horsethemke, W. and **R. Lefever** (1984). *Noise Induced Transitions*. Springer-Verlag, New York.

Jackson, J. B., M. X. Kirby, W. H. Berger, K. A. Bjorndal, L. W. Botsford, B. J. Bourque, R. H. Bradbury, R. Cooke, J. Erlandson, J. A. Estes, T. P. Hughes, S. Kidwell, C. B. Lange, H. S. Lenihan, J. M. Pandolfi, C. H. Peterson, R. S. Steneck, M. J. Tegner and R. R. Warner (2001). Historical overfishing and the recent collapse of coastal ecosystems. *Science*, **293**, 629–637.

James, D. M. (2007). *Differential Dynamical Systems*, Society for Industrial Applied Mathematics, Philadelphia.

Jegadeesan, V. (2012). Experimental investigation of the noise induced transition in the thermoacoustic systems, M. S. thesis, Indian Institute of Technology Madras.

Jegadeesan, V. and R. I. Sujith (2013). Experimental investigation of noise induced triggering in thermoacoustic systems. *Proceedings of the Combustion Institute* **34**, 3175–3183.

Juel, A., A. G. Darbyshire and T. Mullin (1997). Effect of noise on pitchfork and Hopf bifurcations. *Proceedings of the Royal Society* **453**, 2627-2647.

Juniper, M. P. (2011). Triggering in the horizontal Rijke tube: non-normality, transient growth and bypass transition. *Journal of Fluid Mechanics* **667**, 272–308.

Kabiraj, L. (2012). *Intermittency and route to chaos in thermoacoustic oscillations*. Ph. D. Thesis, Indian Institute of Technology Madras.

Kabiraj, L. and R. I. Sujith (2012). Nonlinear self-excited thermoacoustic oscillations: intermittency and flame blowout. *Journal of Fluid Mechanics* **713**, 376-397.

Kabiraj, L., R. I. Sujith and P. Wahi. (2012). Bifurcations of self-excited ducted laminar premixed flames, *Journal of Engineering for Gas Turbines and Power*, **134**, 031502.

Kabiraj, L., A. Saurabh, P. Wahi and R. I. Sujith (2012). Route to chaos for combustion instability in ducted laminar premixed flames. *Chaos* **22**, 023129.

Kabiraj, L., R. Steinert, A. Saurabh and C. O. Paschereit (2015). Coherence resonance in a thermoacoustic system. *Physical Review E*, **92**, 042909.

Karimi, N., J. B. Michael, S. J. Brear and P. M. Jason (2009). Linear and non-linear forced response of a conical, ducted, laminar premixed flame. *Combustion and Flame*, **156**(11), 2201–2212.

Katto, Y. and A. Sajiki (1977). Onset of oscillation of a gas-column in a tube due to the existence of heat-conduction field, *Bulletin of the Japanese Society of Mechanical Engineers*, **20**, 1161-1168.

K'efi, S., M. Rietkerk, C. L. Alados, Y. Pueyo, V. P. Papanastasis, A. Elaich, P. C. de Ruiter, L. Alados and P. C. D. Ruiter (2007). Spatial vegetation patterns and imminent desertification in Mediterranean arid ecosystems. *Nature*, **449**, 213–217.

Komarek, T. and W. Polifke (2010). Impact of swirl fluctuations on the flame response of a perfectly premixed swirl burner. *Journal of Engineering for Gas Turbines and Power*, **132**(6), 061503.

Kopitz, J. and W. Polifke (2008). CFD-based application of the Nyquist criterion to thermo-acoustic instabilities. *Journal of Computational Physics*, **227**, 6754–6778.

Kramer, J. and J. Ross (1985). Stabilization of unstable states, relaxation, and critical slowing down in a bistable system. *Journal of Chemical Physics*, **83**, 6234–6241.

Krylo, N. and N. Bogoliubo (1949). *Introduction to Nonlinear Mechanics*. Princeton University Press, Princeton.

Kuehn, C. (2011). A mathematical framework for critical transitions: Bifurcations, fast–slow systems and stochastic dynamics. *Physica D*, **240**, 1020–1035.

Kuehn, C., G. Zschaler and T. Gross (2015). Early warning signs for saddle escape transitions in complex networks. *Scientific Reports*, **5**, 13190.

Kurtz, T. G. (2007). *Lectures on stochastic analysis*. University of Wisconsin-Madison.

L'Heureux, I. and R. Kapral (1989). White noise induced transitions between a limit cycle and a fixed point. *Physical Letters A* **136**(9), 472-476.

Laio, F. and **L. Ridolfi** (2008). Noise-induced transitions in state-dependent dichotomous processes. *Physical Review E* **78**, 031137.

Lee, K. E., M. A. Lopes, J. F. F. Mendes and **A. V. Goltsev** (2014). Critical phenomena and noise-induced phase transitions in neuronal networks. *Physical Review E* **89**, 012701.

Lehmann, K. O. (1937). Über die theory der netzzone, *Annalen der Physik*, **29**, 527-555.

Lekkas, K., L. Schimansky-Geier and **H. Engel-Herbert** (1988). Stochastic oscillations induced by colored noise. *Physica B* **70**, 517–520.

Lenton, T. M., R. J. Myerscough, R. Marsh, V. N. Livina, A. R. Price, S. J. Cox and **G. Team** (2009). Using GENIE to study a tipping point in the climate system. *Philosophical Transactions A*, **367**, 871–884.

Levine, J. N. and J. D. Baum (1982). Modeling of nonlinear combustion instability in solid propellant rocket motors. *19th International Symposium on Combustion, The Combustion Institute, Pittsburgh, PA*.

Lewontin, R. C. (1969). The meaning of stability. In: Woodwell GW, Smith HH (eds) Brookhaven symposia in biology. Brookhaven National Laboratory, Upton, 13–25.

Lieuwen, T. C. and B. T. Zinn (1998). The role of equivalence ratio fluctuations in driving combustion instabilities in low nox gas turbines. *Proceedings of Combustion Institute*, **27**, 1809-1816.

Lieuwen, T. C., H. Torres, C. Johnson and **B. T. Zinn** (2001). A mechanism of combustion instability in lean premixed gas turbine combustors. *Transactions of ASME*, **123**, 182-189.

Lieuwen, T. C. (2003). Modelling premixed combustion-acoustics wave interaction: A review. *Journal of Propulsion and Power*, **19**, 765-780.

Lieuwen, T. C. and A. Banaszuk (2005). Background noise effects on combustor stability. *Journal of Propulsion and Power*, **21**, 25-31.

Lieuwen, T. C. (2012). *Unsteady combustor physics*. Cambridge University Press.

Lighthill, M. J. (1954). The response of laminar skin friction and heat transfer to fluctuations in the stream velocity. *Proceedings of the Royal Society London A* **224**, 1–23.

Livina, V., T. Martins and A. Forbes (2015). Tipping point analysis of atmospheric oxygen concentration. *Chaos*, **25**(3), 036403.

Lores, E. M. and B. T. Zinn (1973). Nonlinear longitudinal instability in rocket motors, *Combustion Science and Technology*. **7**(6), 245-256.

Madarame, H. (1981). Thermally induced acoustic oscillations in a pipe, *Bulletin of the Japanese Society of Mechanical Engineers*, **24**, 1626-1633.

Marble, F. E. and S. Candel (1977). Acoustic disturbances from gas non-uniformities convected through a nozzle, *Journal of Sound and Vibration*, **55**, 225-243.

Mariappan, S. (2011). Theoretical and experimental investigation of the non-normal nature of thermoacoustic interactions. Ph. D. thesis, Indian Institute of Technology Madras.

Mariappan, S. and R. I. Sujith (2011). Modelling of nonlinear thermoacoustic instability in an electrically heated Rijke tube. *Journal of Fluid Mechanics*, **680**, 511-533.

Marxman, G. A. and C. E. Wooldridge (1969). Finite-amplitude axial instability in solid-rocket combustion. *Symposium (International) on Combustion* **12**(1), 115-127.

Matveev, K. I. (2003). Thermo-acoustic instabilities in the Rijke tube: Experiments and modeling. Ph. D. thesis, California Institute of Technology, Pasadena, CA.

May, R. M. (1977). Thresholds and breakpoints in ecosystems with a multiplicity of stable states. *Nature*, **269**, 471–477.

McManus, K. R., and C. T. Bowman (1991). Effects of controlling vortex dynamics on the performance of a dump combustor. *Symposium (International) on Combustion*, **23**, 1093-1099.

McManus, K. R., T. Poinsot and S. M. Candel (1993). A review of active control of combustion instabilities. *Progress in Energy and Combustion Science* **19**, 1 – 29.

Meisel, C., A. Klaus, C. Kuehn and D. Plenz (2015). Critical Slowing Down Governs the Transition to Neuron Spiking. *PLoS Computational Biology*, **11**(2), e1004097.

Merk, H. J. (1957). Analysis of heat-driven oscillations of gas flows, *Applied Scientific Research A*, **6**, 402-420.

Murugesan, M. and **R. I. Sujith** (2015a). Combustion noise is scale-free: transition from scale-free to order at the onset of thermoacoustic instability, *Journal of Fluid Mechanics*, **772**, 225-245.

Murugesan, M. and **R. I. Sujith** (2015b). Detecting the onset of an impending thermoacoustic instability in a turbulent combustor using complex networks, *Journal of Propulsion and Power*, 1-6.

Nair, V., G. Thampi, S. Karuppusamy, S. Gopalan and **R. I. Sujith** (2013). Loss of chaos in combustion noise as a precursor of impending combustion instability. *International Journal of Spray and Combustion Dynamics*, **5**, 273-290.

Nair, V. and **R. I. Sujith.** (2014). Multifractality in combustion noise: Predicting an impending instability. *Journal of Fluid Mechanics*, **747**, 635-655.

Nair, V., G. Thampi and **R. I. Sujith.** (2014). Intermittency route to thermoacoustic instability in turbulent combustors. *Journal of Fluid Mechanics*, **756**, 470-487.

Nair, V. (2014). *Role of intermittency in the onset of combustion instability*, Ph. D. thesis, IIT Madras.

Neuringer, J. L. and **G. E. Hudson** (1952). An investigation of sound vibrations in a tube containing a heat source, *Journal of the Acoustical Society of America*, **24**, 667-674.

Noiray, N. and **B. Schuermans** (2013). Deterministic quantities characterizing noise driven Hopf bifurcation in gas turbine combustors. *International Journal of Nonlinear Mechanics*, **50**, 152.

Noiray, N. and **B. Schuermans** (2013). On the dynamic nature of azimuthal thermoacoustic modes in annular gasturbine combustion chambers. *Proceedings of Royal Society A*, **469**, 20120535.

Ojalvo, A. G. and **J. M. Sancho** (1998). *Noise in Spatially Extended Systems*. Springer-Verlag, New York.

Pflaum, H. (1909). Versuche mit einer Elektrischen Pfeife, Dissertation, University of Rostok.

Picchini, U. (2007). *SDE tool box manual*, <http://sdetoolbox.sourceforge.net>

Polifke, W. (2004). *Combustion Instabilities, Advances in Acoustics and Applications*, Von Karman Institute, Brussels, Belgium.

Putnam, A. A. and W. R. Dennis (1954). Burner oscillations of the gauze-tone type, *Journal of the Acoustical Society of America*, **26**, 716-725.

Rayleigh, J. W. S. (1878). The explanation of certain acoustical phenomena. *Nature* **18**, 319–321.

Richardson, M. (2009). *Stochastic differential equations case study*. University of Oxford.

Rijke, P. L. (1859). The vibration of the air in a tube open at both ends. *Philosophical Magazine*, **17**, 419–422.

Risken, H. (1989). *The Fokker-Planck Equation: Methods of Solution and Applications*. Springer, Berlin.

Roberts, J. B. and P. D. Spanos (1986). Stochastic averaging: An approximate method of solving random vibration problems. *International Journal of Nonlinear Mechanics*, **21**, 111.

Ros, O. G. C., G. Platero and L. L. Bonilla (2013). Effects of noise on hysteresis and resonance width in graphene and nanotubes resonators. *Physical Review B* **87**, 235424.

Saito, T. (1965). Vibrations of air-columns excited by heat supply. *Bulletin of the Japanese Society of Mechanical Engineers*, **8**, 651-659.

Sastray, S. and O. Hijab (1981). Bifurcation in the presence of small noise. *Systems & Control Letters* **1**(3), 159-161.

Scheffer, M., J. Bascompte, W. A. Brock, V. Brovkin, S. R. Carpenter, V. Dakos, H. Held, E. H. van Nes, M. Rietkerk and G. Sugihara (2009). Early-warning signals for critical transitions. *Nature* **461**, 53–59.

Selimefendigil, F. and W. Polifke (2011). A nonlinear frequency domain model for limit cycles in thermoacoustic systems with modal coupling. *International Journal of Spray and Combustion Dynamics*, **3**, 303-330.

Selimefendigil, F., R. I. Sujith and W. Polifke (2011). Identification of heat transfer dynamics for non-modal analysis of thermoacoustic instability. *Applied Mathematics and Computation*, **217**, 5134-5150.

Shanbhogue, S. J., S. Husain and T. Lieuwen (2009). Lean blow-off of bluff body stabilized flames: Scaling and dynamics. *Progress in Energy and Combustion Science*, **35**, 98-120.

Song, C., H. Phenix, V. Abedi, M. Scott, B. P. Ingalls, M. Krn and T. J. Perkins (2010). Estimating the stochastic bifurcation structure of cellular networks. *PLoS Computational Biology*, **6**, e1000699.

Stratonovich, R. L. (1967). *Topics in the theory of random noise*, Volume 2. Gordon and Breach, New York.

Strogatz, S. H. (2000). *Nonlinear Dynamics and Chaos: with applications to Physics, Biology, Chemistry, and Engineering*. Westview Press, Colorado.

Subramanian, P. (2011) *Dynamical systems approach to the investigation of thermoacoustic instabilities*. Ph. D. thesis, Indian Institute of Technology Madras.

Subramanian, P., S. Mariappan, R. I. Sujith and P. Wahi (2010). Bifurcation analysis of thermoacoustic instability in a horizontal Rijke tube. *International Journal of Spray and Combustion Dynamics* **2**(4), 325–355.

Subramanian, P., R. I. Sujith and P. Wahi (2013). Subcritical bifurcation and bistability in thermoacoustic systems. *Journal of Fluid Mechanics* **715**, 210 – 238.

Surovyatkina, E. (2005). Prebifurcation noise amplification and noise-dependent hysteresis as indicators of bifurcations in nonlinear geophysical systems. *Nonlinear Processes in Geophysics* **12**, 25-29.

Takens, F. (1980) Detecting strange attractors in turbulence. in *D. Rand and L. S. Young*, editors, *Dynamical Systems and Turbulence*, **898**, 366–381.

Thampi, G. (2015). *Intermittency – A prior indicator of combustion instability and blowout in a turbulent combustor*, Ph. D. Thesis, Indian Institute of Technology Madras.

Tredicce, J. R., G. L. Lippi, P. Mandel, B. Charasse and A. Chevalier (2004) Critical slowing down at a bifurcation. *American Journal of Physics*, **72**, 799–809.

Trefois, C., P. Antony, J. Goncalves, A. Skupin and R. Balling (2015). Critical transitions in chronic disease: transferring concepts from ecology to systems medicine. *Current Opinion in Biotechnology*, **34**, 48–55.

Unni, V. R. and R. I. Sujith (2015). Multifractal characteristics of combustor dynamics close to turbulent combustors. *Journal of Fluid Mechanics*, **756**, 470-487.

Venkataraman, K. K., L. H. Preston, D. W. Simons, B. J. Lee, G. J. Lee and D. A. Santavicca (1999). Mechanism of combustion instability in a lean premixed dump combustor. *Journal of Propulsion and Power*, **15**, 909-918.

Veraart, A. J., E. J. Faassen, V. Dakos, E. H. van Nes, M. Lu'riling and M. Scheffer (2012). Recovery rates reflect distance to a tipping point in a living system. *Nature*, **481**, 357-359.

Waugh, I. C. and M. P. Juniper (2011). Triggering in a thermoacoustic system with stochastic noise. *International Journal of Spray and Combustion Dynamics* **3** (3 & 4), 225–242.

Waugh, I. C., M. Geuß and M. P. Juniper (2011). Triggering, bypass transition and the effect of noise on a linearly stable thermoacoustic system. *Proceedings of the Combustion Institute* **33**, 2945–2952.

Waugh, I. personal communication September, 6, 2012.

Wicker, J. M., W. D. Greene, S. I. Kim and V. Yang (1996). Triggering of longitudinal combustion instabilities in rocket motors: Nonlinear combustion response. *Journal of Propulsion and Power* **12**, 1148.

Wiesenfeld, K. (1985). Noisy precursors of nonlinear instabilities. *Journal of Statistical Physics*, **38**, 1071-1097.

Xu, Y., R. Gu, H. Zhang, W. Xu and J. Duan (2011). Stochastic bifurcations in a bistable Duffing--Van der Pol oscillator with colored noise. *Physical Review E*, **83**, 056215.

Yamapi, R., G. Filatrella, M. A. Aziz-Alaoui and H. A. Cerdeira (2012). Effective Fokker-Planck equation for birhythmic modified van der Pol oscillator, *Chaos*, **22**, 043114.

Zahringer, K., D. Durox and **F. Lacas** (2003). Helmholtz behavior and transfer function of an industrial fuel swirl burner used in heating systems. *International Journal of Heat and Mass Transfer*, **46**, 3539-3548.

Zakharova, A., T. Vadivasova, V. Anishchenko, A. Koseska, and **J. Kurths** (2010). Stochastic bifurcations and coherence like resonance in self-sustained bistable oscillator. *Physical Review E* **81**, 011106.

Zinn, B. T. and **Y. Neumeier**, An overview of active control of combustion instabilities. In *35th Aerospace Sciences Meeting & Exhibit*, AIAA, 1997. AIAA 97-0461.

Zinn, B. T. and **T. Lieuwen** (2005). Combustion instabilities: basic concepts. In *Combustion instabilities in Gasturbine Engines: Operational experience, Fundamental Mechanisms, Modeling* (edited by T. C. Lieuwen & V. Yang). AIAA.

LIST OF PAPERS BASED ON THESIS

Referred Journals:

1. Gopalakrishnan, E. A. and Sujith, R. I. Influence of system parameters on hysteresis characterisits of a horizontal Rijke tube. *International Journal of Spray and Combustion Dynamics*, 6 (3), 293-316, 2014.
2. Gopalakrishnan, E. A. and Sujith, R. I. Effect of external noise on the hysteresis characteristics of a thermoacoustic system. *Journal of Fluid Mechanics*, 776, 334-353, 2015.
3. Gopalakrishnan, E. A., Tony, J. and Sujith, R. I. Stochastic bifurcations in prototypical thermoacoustic system. *Physical Review E*, (2016 – Accepted).

International Conferences:

1. Gopalakrishnan, E. A. and Sujith, R. I. Influence of system parameters and external noise on hysteresis characteristics of a horizontal Rijke tube. n³l –Int'l Summer School and Workshop on Non-Normal and Nonlinear Effects in Aero- and Thermoacoustics, June 18-21, Munich, 2013.
2. Gopalakrishnan, E. A. and Sujith, R. I. Effect of noise on thermoacoustic systems in the context of a horizontal Rijke tube. European Fluid Mechanics Conference 10, September 17-18, Copenhagen, 2014.
3. Gopalakrishnan, E. A. and Sujith, R. I. “Influence of external noise on the nature of transition of a thermoacoustic system.” *Dynamic Days Asia Pacific-08*, July 21 – 24, 2014, Chennai, India.

